COUPLED DYNAMIC ANALYSIS OF LARGE-SCALE MONO-COLUMN OFFSHORE WIND TURBINE WITH A SINGLE TETHER HINGED IN SEABED

A Thesis

by

JIEYAN CHEN

Submitted to the Office of Graduate Studies of
Texas A&M University
in partial fulfillment of the requirements for the degree of

MASTER OF SCIENCE

August 2012

Major Subject: Ocean Engineering

Coupled Dynamic Analysis of Large-Scale Mono-Column Offshore Wind Turbine with

A Single Tether Hinged in Seabed

COUPLED DYNAMIC ANALYSIS OF LARGE-SCALE MONO-COLUMN OFFSHORE WIND TURBINE WITH A SINGLE TETHER HINGED IN SEABED

A Thesis

by

JIEYAN CHEN

Submitted to the Office of Graduate Studies of
Texas A&M University
in partial fulfillment of the requirements for the degree of

MASTER OF SCIENCE

Approved by:

Chair of Committee,	Moo-Hyun Kim
Committee Members,	Jun Zhang
	Jean-Luc Guermond
Head of Department,	John Niedzwecki

August 2012

Major Subject: Ocean Engineering

ABSTRACT

Coupled Dynamic Analysis of Large-Scale Mono-Column Offshore Wind Turbine with A Single Tether Hinged in Seabed. (August 2012)

Jieyan Chen, B.E., Shanghai Jiao Tong University

Chair of Advisory Committee: Dr. Moo-Hyun Kim

The increased interest in the offshore wind resource in both industry and academic and the extension of the wind field where offshore wind turbine can be deployed has stimulated quite a number of offshore wind turbines concepts. This thesis presents a design of mono-column platform supported for 5 MW baseline wind turbine developed by the National Renewable Energy Laboratory (NREL), with a single tether anchored to the seabed. The design, based on the pioneer concept SWAY®, results from parametric optimized design processes which account for important design considerations in the static and dynamic view, such as the stability, natural frequency, performance requirements as well as the economic feasibility. Fully coupled aero-hydro-servo-elastic model is established in the time-domain simulation tool FAST (Fatigue, Aerodynamics, Structures, and Turbulence) with the hydrodynamic coefficients from HydroGen, an indoor program providing same outputs as the commercial software WAMIT. The optimized model is verified by imitating the frequency-domain approach in FAST and thus comparing the results with the frequency-domain calculations.

A number of simulations with various wind and wave conditions are run to explore the effect of wind speed and wave significant height in various water depths. By modifying the optimized model to a downwind turbine with the nacelle rigidly mounted on the tower and the single tether connected to the platform by a subsea swivel, the modified models are more closed to the original SWAY®-concept wind turbine. These models are compared based on the platform motion, tether tension, displacement, nacelle velocity and acceleration, resonant behavior as well as the damping of the coupled systems. The results of these comparisons prove the advantage of the modified model in performance. The modified model has also clarified itself a good candidate for deep water deployment.

ACKNOWLEDGEMENTS

I would like to thank my committee chair, Dr. Kim, and my committee members, Dr. Zhang, Dr. Guermond, for their guidance and support throughout the course of this research.

Thanks also to the department faculty and staff for making my time at Texas A&M University a great experience. I also want to extend my gratitude to Mr. Bae, who has provided instructions and recommendations for me to master the research software programs.

Finally, thanks to my fiancé for his accompany and love, and to my mother and father for their encouragement.

NOMENCLATURE

BEM	Blade Element Momentum Method
CB	Center of Buoyancy
CG	Center of Gravity
CM	Center of Mass
DOF	Degree of Freedom
D/λ	Diameter to wavelength ratio, scatter parameter
FAST	Fatigue, Aerodynamics, Structures, and Turbulence
F-K	Froude-Kriloff force/pressure
F.S	Factor of Safety
FOWT	Floating Offshore Wind Turbine
HAWT	Horizontal-Axis Wind Turbine
JONSWAP	Joint North Sea Wave Project
KC	Keulegam-Carpenter number
1P	Revolution rotor frequency
NP	Internal tower flexibility frequency or blade passing frequency
NREL	National Renewable Engergy Laboratory
NWTC	National Wind Turbine Center
OC3	Offshore Code Comparison Collaboration
OWT	Offshore Wind Turbine
P-M	Pierson-Moskowitz spectrum

RAO		Response Amplitude Operator
Re		Oscillatory Reynolds Number
SDB		Shallow Draft Barge
SIMO		Simulation of Marine Operations
SWL		Still Water Level
TLP		Tension Leg Platform
WAMIT		Wave Analysis at MIT
WGN		White Gaussian Noise
WWEA		World Wind Energy Association
$a_1\|_{x=0}$	=	x-component fluid acceleration at location $x = 0$ for strip
A	=	rotor sweep area; or wave amplitude
A_{line}	=	cross-area of mooring lines
$A_{ij}(\omega)$	=	hydrodynamic added-mass matrices
$B_{ij}(\omega)$	=	hydrodynamic-damping matrix
C_D	=	drag coefficient
C_L	=	lift coefficient
C_M	=	normalized mass inertia coefficient in Morison’e equation
C_P	=	power coefficient of wind turbine
C_T	=	thrust coefficient
$C_{ij}^{hydrostatic}$	=	linear hydrostatic-restoring matrix
$C_{ij,\,H\&G}$	=	hydrostatical and gravitational restoring matrix
C_{ij}^{Lines}	=	linearized restoring matrix from mooring lines

C_{tether}	=	linearized restoring matrix from tether
D	=	submerged cylinder diameter; or draft
EA	=	mooring line extensional stiffness
fb	=	freeboard
$F_{ij}^{lines,0}$, T_0	=	mooring line load on platform in its undisplaced position
F_{thrust}	=	thrust force
h	=	water depth
H	=	wave height
H_s	=	significant wave height
k	=	wave number
K_{ij}	=	matrix wave-radiation-retardation kernels
L	=	total unstretched length; or characteristic length
m_0	=	zero spectral moment
M_{ij}	=	mass matrix
q_j	=	j^{th} DOF of the system
R	=	submerged cylinder radius
$S^{2\text{-}side}(\omega)$	=	two-side power spectral density of wave elevation per unit time
$S_\eta(\omega)$	=	wave spectrum
T	=	wave period
T_p	=	peak spectral period
$T_{tether,fairlead}$,	=	dynamic tether tension at the fairlead or anchor points
$T_{tether,\ anchor}$		

V	=	free-stream velocity; or fluid velocity amplitude
V_0	=	displacement
$V(z)$	=	wind speed at height z
$W(\omega)$	=	Fourier transform of white Gaussian noise time-series process
$X_i(\omega, \beta)$	=	hydrodynamic incident-wave-excitation vector
z	=	local water depth
Z_{hub}	=	hub height
Z_{ref}	=	reference height above ground
ρ_a	=	density of air
ρ	=	density of sea water
α	=	angle of attack; or power law exponent
β	=	local blade pitch angle; or wave heading
γ	=	peak shape parameter for JONSWAP spectrum
δ_{i3}	=	$(i,3)$ component of the Kronecker-Delta function
ε_j	=	random phase angles
η	=	wave amplitude
η_1, η_5	=	steady-state surge and pitch displacements
θ	=	angle the tether forms with the vertical axis
v	=	kinematic viscosity of fluid, 10^{-6} m^2/s
v_j , a_j	=	components of the fluid particle velocity and acceleration
ξ_j	=	non-dimensional definition of the structure motions

$\rho\pi R^2 dz$	=	mass of the displaced fluid of the cylinder strip
σ	=	standard deviation; or yield stress of mooring lines
ϕ	=	velocity potential
ϕ_D	=	diffraction potential
ϕ_I	=	velocity potential for incident wave
ϕ_S	=	scattered wave potential
φ	=	local inflow angle
ω_j	=	circular frequencies
ω_j^0	=	natural frequency of i^{th} mode at zero frequency
$\Delta\omega$	=	bandwidth of the spectrum
$\|.\|$	=	magnitude of the vector difference in Morison's equation

TABLE OF CONTENTS

Page

LIST OF FIGURES

Page

LIST OF TABLES

Page

1 INTRODUCTION

1.1 General Background

For many parts of the world, nonrenewable resources are still the main sources of energy nowadays, like the coal, natural gas, and oil. However, these fossil fuels continue to be depleted and are harmful to the environment. Therefore, the vast wind resource in deep water attract our sights to drive land-based wind turbines to ocean for electrical power generation which possess great potential since it is green, inexhaustible, and helpful to reduce the world's dependence on fossil fuels. Wind turbines at sea are also a good solution to avoid interfere with life on land, and achieve better energy efficiency due to steadier and higher annual mean wind velocity. According to WWEA the power capacity of worldwide installed wind turbines reached 215,000 MW at June 2011, 15% increase more than in the first half of 2010, and China still continues to dominate the world wind market with a total capacity of 52,800 MW (about 43% of the whole market), and United States follows the second with 42,432 MW. The stronger growth is also shown in most of the European markets this year.

Presently, most wind farms in European countries are built in relatively shallow water (<=30m) on piled or gravity-based foundations, considering the rare vacant land in Europe and great water wind resources in shallow water. In such shallow water and with small turbines of 2-3MW, monopile foundation is the best choice due to its low expenses

---

This thesis follows the style of *Journal of Fluid Mechanics*.

and simple construction when comparing with other bottom-fixed offshore wind turbines like jacket and tripod. However, if turbines are larger, the stiffness monopile foundations can provide become insufficient, and the dynamic coupling between the tower and rotor frequency (1P) may result in unacceptable vibrations. Besides, driving bottom-fixed offshore wind turbine into deeper water for larger turbine also turns out to be economically infeasible due to the increased steel cost and complicated installations. Thus, bottom-fixed platforms can operate with no major problems at depth under 30 m.

Globally, for countries such as the Unite States, China, Norway, etc., the offshore wind resource are mostly available in water deeper than 30m, which is also an initial drive behind the process of moving wind turbines from onshore to offshore, as illustrated in FIGURE 1.1. Besides, the 6 degree-of-freedom (6DOF) natural frequencies of floating offshore wind turbines (FOWTs) are designed much lower than those rotor- or tower-flexibility-induced excitations in most cases, such that the problem of dynamic resonance with blades and tower are avoided as much as possible (Jonkman *et al.* 2006).

However, the FOWTs also have possible disadvantages like the harsher ocean environments and the corresponding greater floater accelerations, the complicated problem for transmission and installation process including tower, turbine and the mooring systems. Potential challenges of the control system, such as the negative damping of the rotor thrust force above the rated wind speed, and the large-amplitude slowly-varying floater motions by low-frequency excitations from the blade-pitch control system are also mentioned in Skaare *et al*. (2006). All these problems would result in the significant reduction of the fatigue life of the floating wind turbines.

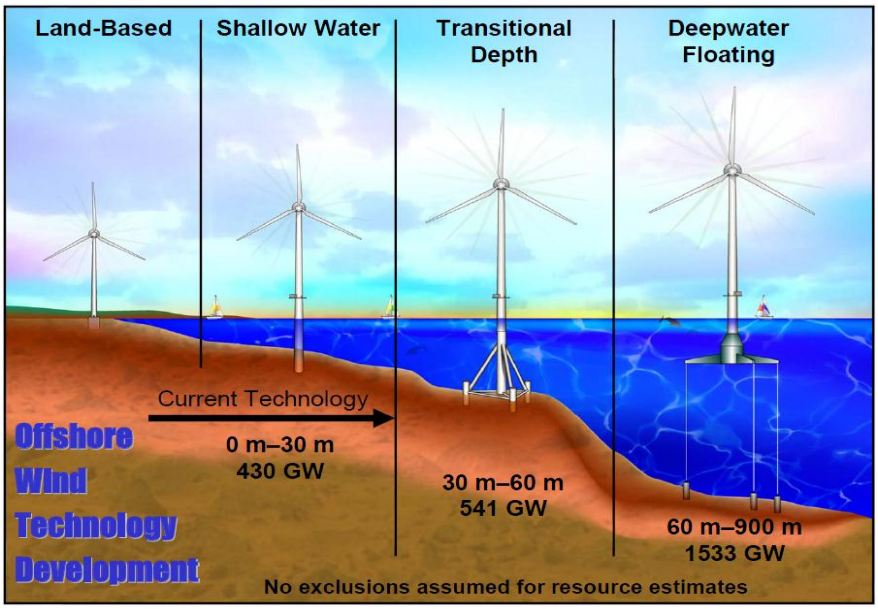

FIGURE 1.1 Deep water wind turbine development.

1.2 Previous and Ongoing Work

A great number of research organizations have been involved in the development of offshore wind turbine, whose work made it possible for the design and economic analysis of various wind farms using their reference designs, standards, computational simulation tools. The following section mainly introduces the major current state of FOWTs, their design challenges and the available simulation tools.

1.2.1 Floating Wind Turbine Concepts

The various choices of moorings, anchors, floaters, and ballast in the offshore industry make the vast number of possible offshore wind turbine concepts quite possible. Based on the classification of the National Renewable Energy Laboratory (NREL), floating supported platforms can be divided into three categories by the physical

principle used to achieve static stability: 1) ballast stabilization (as Spar-Buoys); 2) mooring line stabilization (e.g. TLP); 3) distributed-buoyancy stabilization (barge). See FIGURE 1.2 for these three typical concepts.

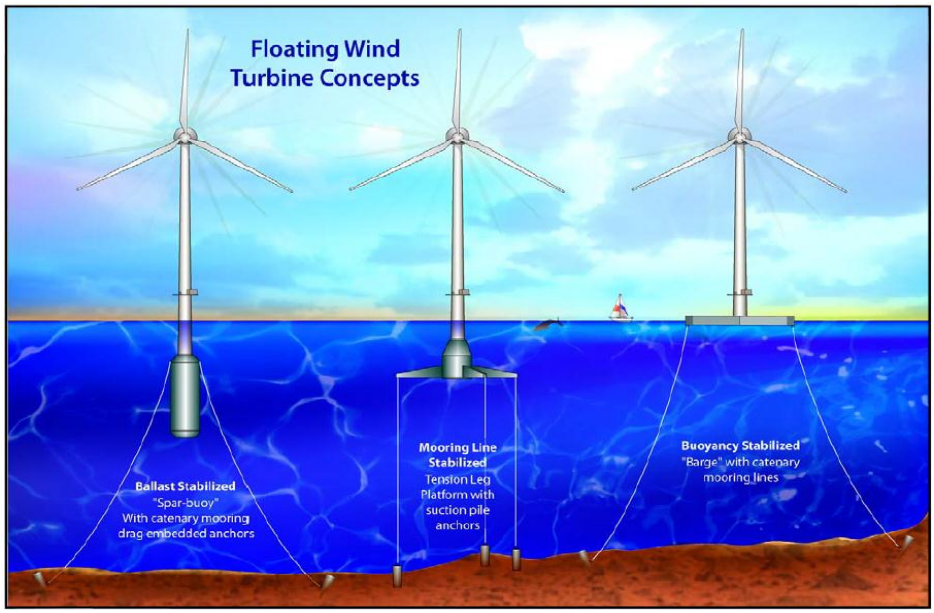

FIGURE 1.2 Typical floating platform static stability concepts.

Each of the idealized vessels using the above approaches to achieve stability has its limited properties. Therefore, in practice, the existed floating concepts are actually hybrid designs correlating the characteristics of the above three ways for stability. FIGURE 1.3 illustrates the "stability triangle" constructed by Butterfield *et al.* (2005), where each point represents a design of floating concept.

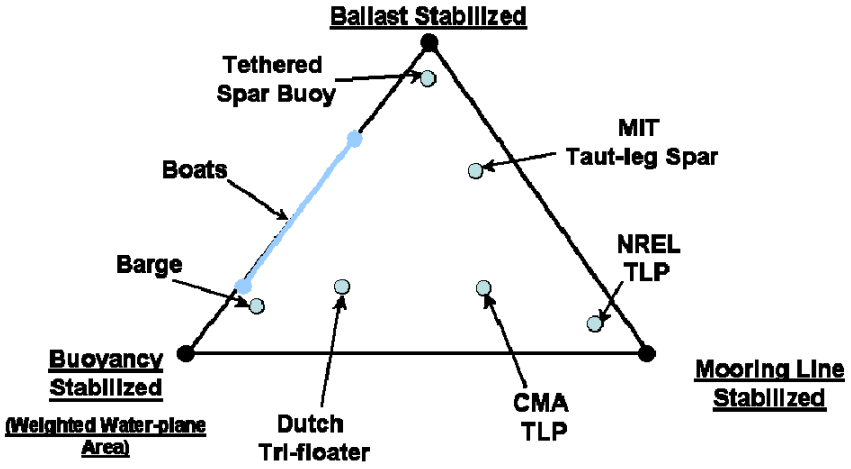

FIGURE 1.3 Floating platform stability triangle.

1.2.1.1 State-of-the-Art in Practice

The increased interest in the offshore wind resource in both industry and academic, and the extension of the wind field for FOWTs' deployment have stimulated quite a number of new concepts of offshore floating wind turbines.

NREL 5 MW baseline wind turbine is a design derived from onshore wind turbines and in accordance with the standards IEC 61400-3 for offshore wind turbine. See detail in Jonkman *et al*. (2009). Combining the mechanism of operating machines and theoretical designs, this is a realization of three-bladed upwind floating wind turbine with 5-MW power capacity. FIGURE 1.4 shows the NREL 5 MW wind turbine mounted on three concepts of platforms.

The MIT/NREL TLP is a modification of TLP concept adopting the parametric design optimization method in Tracy (2007) in linear frequency domain. The platform is cylindrical, ballasted with concrete and moored by four pairs of vertical. Another MIT

and NREL joint program is the MIT/NERL Shallow Draft Barge (SDB), which achieves its righting moment by high water plane area, and its mooring system is primary for station keeping, not the restoring stiffness for the system.

Hywind is one of the Norwegian concepts, which is a spar-buoy with catenary mooring systems. One example is the OC3-Hywind spar-buoy developed within the Offshore Code Comparison Collaboration (OC3), see Jonkman (2009). Its platform is adapted to support the large-scale NREL 5 MW reference wind turbine from the original Hywind concept, and the tower and control system of the 5 MW wind turbine are also modified to allow coupling and assure positive aerodynamic damping during operation.

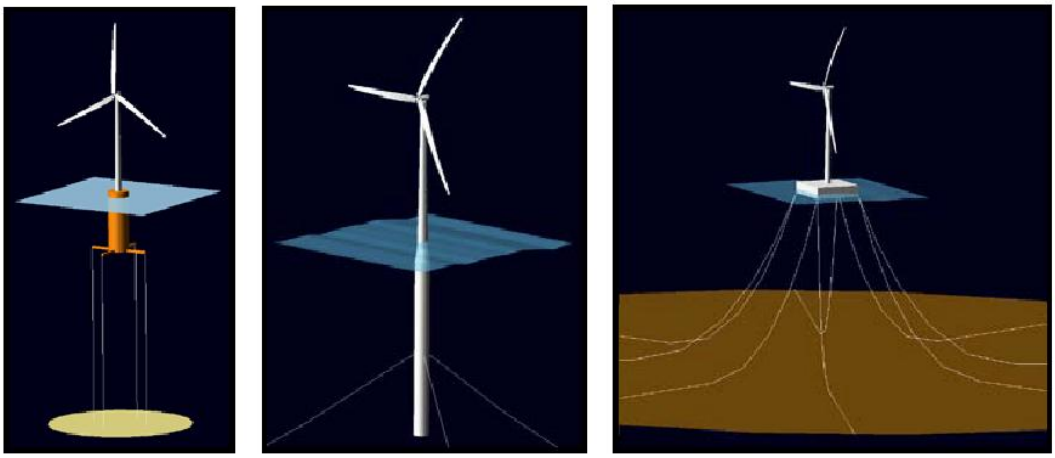

FIGURE 1.4 NREL 5 MW wind turbine on three concepts of platforms.

Another Norwegian concept is SWAY®, an advanced realization for large-scale FOWTs. The patented SWAY® system, shown in FIGURE 1.5 (a), consists of a floating tower which extends deep into water, and a single pipe anchored to seabed. With a floating ballast pole at the lower end, the tower has its center of gravity (CG) much

below the center of buoyancy (CB) for stability. The rotor is downwind-orientated with three blades. When the wind hits the rotor the system tilts 5 to 8 degrees, and when the inflow wind changes its direction, the entire tower turns around though a subsea swivel, which in turn reinforces the tower align with the wind. These properties not only improve the energy efficiency, but make it possible to add wire bracing on tower, which would enhance the tower stiffness. The tower is thereby capable to carry larger turbines.

Another two pioneers in offshore floating wind turbine is the WindFloat and Blue-H from the Netherlands. See FIGURE 1.5 (b) and (c). The WindFloat is also designed for large wind turbines up to 10 MW rated power, which is unique for its column-stabilized platform with closed loop active ballast system and an asymmetric mooring system. The Blue-H concept adopts a TLP design with gravity anchors.

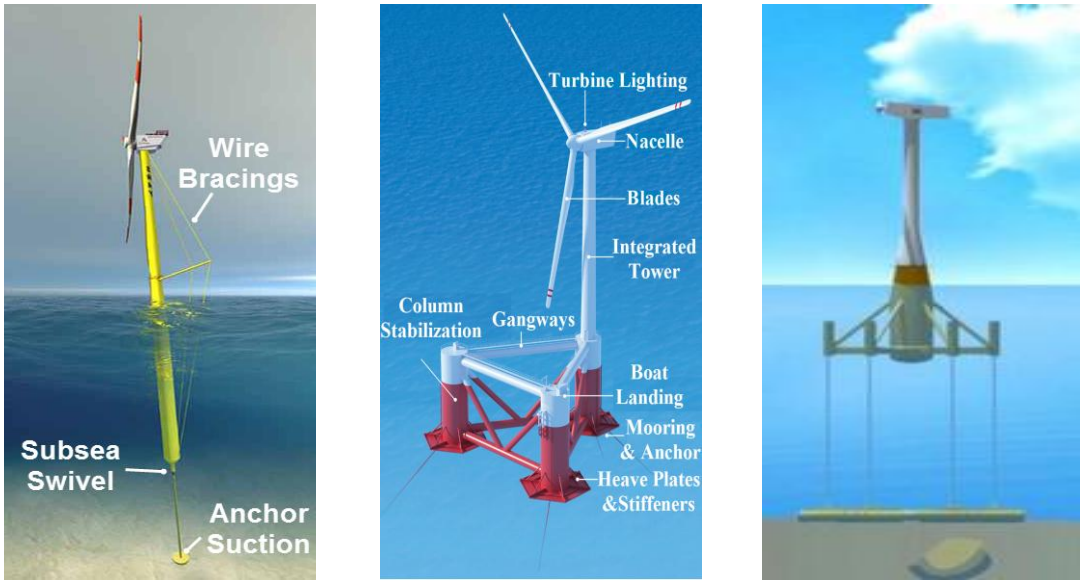

FIGURE 1.5 Prototype of floating concepts: (a) SWAY®; (b) WindFloat; (c) Blue-H.

1.2.1.2 Design Challenges

In order to achieve cost-effective systems with favorable performance while maintaining the structure integrity, there are still a number of interdisciplinary technical problems need to be solved, such as the challenges associated with the large aerodynamic loads high above the water, the resulted raised CG and large overturning moment, all of which has challenged the basic principle and criteria of naval architecture.

Take the three basic categories of FOWTs for instance. The barge-type is the worst for its significant angular motions. The spar-type has relatively good heave responses due to its deep draft and reduced vertical wave-exciting forces. However, the small water plane and less stiff catenary mooring lines result in larger angular motions. And It is also likely to be heavier and therefore more expensive to build. Both heave and angular motions of TLPs are very good, but the cost and complicacy of the mooring installation, the sudden change in tendon tension, and the dynamic coupling effects between the hull and the mooring system hinders its development.

1.2.2 Simulation Tools

For onshore wind turbine, the aero-elastic simulation tools are used, which employs sophisticated models of aerodynamics, inertial, and gravitational loading of the turbine; elastic effect in the components; and mechanical actuation and responses of the generator and control system. However, when in the offshore environment, additional dynamic behavior of the system including the dynamic characterization of mooring system is presented, and models of the hydrodynamic loading in regular and irregular

sea are necessary to be included. In recent years, the simulation tools capable of modeling the fully dynamic coupled FOWT systems have been improved a lot.

FAST (Fatigue, Aerodynamics, Structures, and Turbulence) is a publicly available program distributed by the National Wind Technology Center (NWTC) that employs a combined modal- and multibody structural-dynamics formulation in the time domain for analyses of horizontal-axis wind turbines (HAWT). AeroDyn, interfaced with FAST, is developed to model the coupled time-domain aero-servo-elastic wind turbine system. HydroDyn module is to include the additional hydrodynamic loads induced by wave, platforms and mooring systems, which allows for the fully coupled time-domain aero-hydro-servo-elastic simulations of FOWTs. The wave-platform interaction is solved by regular wave theory and input from the hydrodynamic computational program, such as WAMIT (Wave Analysis at MIT). The dynamics of the nonlinear moorings are invoked a quasi-static mooring system module. Further details on the theories employed in FAST will be presented later.

Choices are not limited as presented above. Charm3D, the finite element program for the time/frequency-domain coupled dynamic analyses of the platform-mooring (riser) system has been coupled to FAST by Texas A&M University. The software TimeFloat developed by Marine Innovation and Technology has also been coupled with FAST in order to model and analysis the WindFloat concept. SIMO (Simulation of Marine Operations), a time-domain program by MARINTEK, is coupled to the nonlinear finite element code, RIFLEX, as well as the aero-elastic code for bottom-fixed wind turbine, HAW2. The coupled SIMO/RIFLEX/HAWC2 has even been thoroughly verified by

Risø National Laboratory (Larsen & Hansen, 2007, Skaare *et al.* 2006). More recently, a FAST-OrcaFlex coupling code was developed in Masciola *et al.* (2011). Other codes, such as the 3Dfloat, developed by the Norweigian University of Life Sciences (UMB), Bladed by GL Garrad Hassan Stationed in the UK, and DeepC by DNV, can also be utilized for fully coupled time-domain dynamic analysis of FOWTs.

1.3 Objective

The major goal of the present paper is the design and analysis of a large-scale mono-column offshore wind turbine with a single taut tether hinged in seabed. The thesis would go through the static and fully dynamic analysis process, based on the comprehensive consideration of its stability, acceptable response motions, mooring system and low cost. The simulation tools adopted include the fully coupled time-domain aero-hydro-servo-elastic simulation tool FAST/HydroDyn, and HydroGen, an indoor program generating the same hydrodynamic coefficients as the preprocessor WAMIT. Two models are built in FAST and simulated in various loading cases: one with the single tether hinged joint to the floater, while the other with a swivel connection.

Outlines of the thesis:

- Preliminary design throughout an iterative parametric optimized design process is carried out to obtain an optimized model that satisfies the requirements for stability, natural frequency, and main cost drivers. The configuration of this optimized model includes three parts: the modified NREL 5 MW baseline wind turbine mounted on top; a mono-column

floating platform; a single tether with its both end hinged connected to the platform and the seabed.

- Verifying the optimized model by imitating the frequency-domain approach in FAST to obtain the platform 6DOFs, which are compared with the frequency-domain RAO calculations in HydroGen.
- Modifying the optimized model through setting the upwind 5 MW baseline wind turbine to downwind-orientation, and defining a swivel joint between the platform and the single tether in FAST. The influences of these modifications are also studied.
- Dynamic simulations and comparison between the modified downwind swivel model and the downwind hinged model (reference model) are performed based on the platform responses, tether tension, nacelle displacement, velocity and accelerations. Besides, the resonant behavior and damping of the two coupled systems are also detected.
- A number of simulations in certain water depth with various wind and wave load conditions are run to explore the effect of wind, wave and water depth on both modified and reference system performance.
- Conclusions are made for the modified model in the view of static, dynamic as well as its economic feasibility, and suggestions are drawn about the future work of this specific design of FOWT.

2 LOADS ON OFFSHORE WIND TURBINES

An offshore wind turbine is open to a variety of environmental loads, such as the wind, waves, currents and tides, icing, lightning, marine growth, scour, corrosion and earthquake, as illustrated in FIGURE 2.1. Among these common environmental impacts, wind and wave are the most significant, and all others are assumed to be relatively small and therefore ignored. It also in turn makes sense to the dynamic analysis of the coupled structure due to the coupled wind and wave loads.

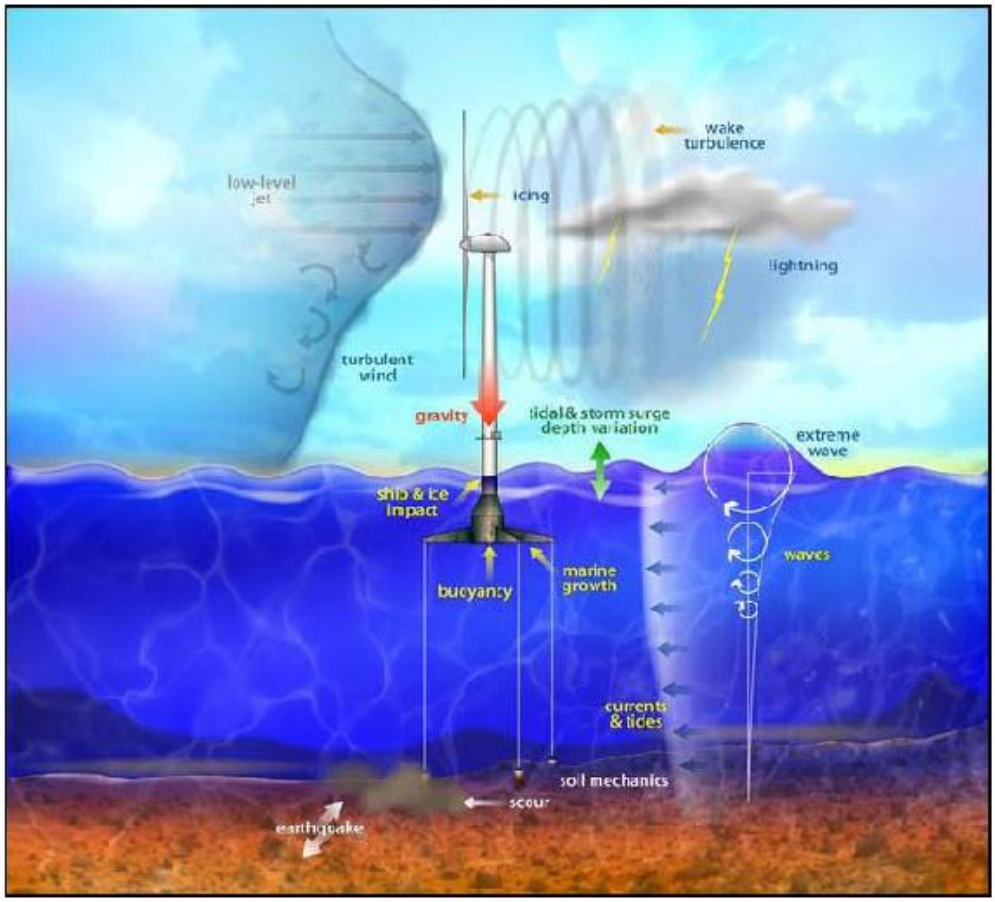

FIGURE 2.1 Overview of offshore wind turbine loads.

2.1 Aerodynamic Load

2.1.1 Aerodynamics

A wind turbine is a device that converts wind kinetic energy to useful output in the form of electrical power. Theoretically, there are two steps for this process. The first step is that the presence of turbines slows down the velocity of inflow air arriving at the rotor disk, resulting in the rise of static pressure to absorb the decreased wind kinetic energy. And the second step occurs in the downstream (wake with reduced wind velocity and static pressure), after the air passing through the rotor disk since there is a further drop in the static pressure. However, to achieve equilibrium, the static pressure in far downstream would return to the atmospheric value, and this increased static pressure is at the expense of wind kinetic energy as well. Therefore, between the far up- and down-streams, the static pressure keeps the same but a reduction in wind kinetic energy. This airflow affected by the turbine is assumed to remain separated from the outer free-stream air by a boundary surface, which generates an energy extracting stream-tube around the turbine.

The change of the pressure and the angular momentum during wind passing across the rotor blades produces lift force (normal to the inflow air) and drag force (parallel to the inflow air), which dictate the thrust and torque of the rotor, as well as a pitching moment, as presented in FIGURE 2.2. Drag arises from vortex shedding, viscous friction, and separated wakes. The pitching moment is the summation of the moments created by the individual forces acting on the airfoil. Lift and drag are commonly expressed as non-dimensional forces by coefficients C_L and C_D in equation

2.1 and 2.2 (Manwell *et al.* 2002), where ρ_a is the air density, A is the swept rotor area and V is the free-stream velocity. For ideal non-separated flow, these forces and moment act along the chord at a distance of approximately a quarter of the chord length from the leading edge (Manwell *et al.* 2002).

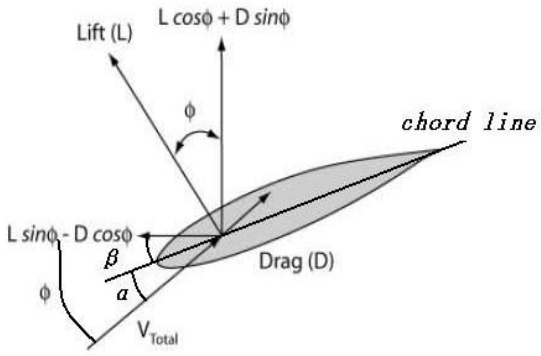

FIGURE 2.2 Forces and moments on a stationary airfoil.

α, the angle of attack, is a function of the local velocity vector and has a linear correlation to the lift force. It determines the point at which the effect of stall will occur for a fixed geometry and is also constrained by the inflow wind, rotor speed and blade element velocities. On a wind turbine, the rotation of the rotor increases the inflow into the airfoil, while at the same time changing the effective angle of attack. Another angle, β, is the pitch angle of the blade, determined by its static geometry, blade DOFs, and the pitch control system. This blade pitch angle is important since it changes the plane of rotor rotation directly and therefore influent the thrust force and even power outputs.

$$C_T = \frac{T}{1/2\rho_a V^2 A} \tag{2.1}$$

$$C_D = \frac{D}{1/2\rho_a V^2 A} \tag{2.2}$$

According to the Betz Limit, the maximum power coefficient C_P for an ideal wind turbine is 0.593.This limit is not caused in design, but the expansion of the upstream tube such that the cross-section of the tube where the air is at the free-stream velocity is smaller than the area of the disk. The corresponding thrust coefficient C_T is 8/9 and the torque coefficient can be expressed by the power coefficient divided by the tip speed ratio (Manwell *et al.* 2002).

The forces and moments generated by the rotor torque and the rotor thrust, as explained above, are the most significant aerodynamic loads acting with the moment arm of the tower. However, some other aerodynamic loads cannot be neglected as well for the resonant they may excite, even though the magnitudes of them are small compared to the torque and thrust. For instance, wind speed increases with elevation above the surface and is normally modeled using either the power law profile or the logarithmic profile in equation 2.3 and 2.4 (Manwell *et al.* 2002). This varying wind field causes a changing airflow field around the airfoil and therefore produces oscillating forces and moments, which may excite resonant motion of the floater and wind turbine and must therefore be considered.

$$V(z) = V(z_{ref}) \cdot (z / z_{ref})^{\alpha} \quad (\alpha=0.014 \text{ in IEC-61400-3 for OWT}) \tag{2.3}$$

$$V(z) = V(z_{ref}) \cdot \ln(z / z_0) / \ln(z_{ref} / z_0) \tag{2.4}$$

The aerodynamic loads and the gravitational force from the weight of the turbine are periodic due to the orientation of the rotor. The oscillation caused by these periodic

loads is proportional to the rotor speed. The rotor speed frequency is commonly denoted 1P. For a 1P periodic loading the turbine blade will experience a 1P periodic excitation force while passing through the swept rotor area, and the internal rotor-tower excitation force will have a NP periodic loading, where N equals blade numbers. This dynamic interactions induced by the periodic loads in turn induce loads in other parts of the wind turbine. For example, the changing plane of the rotation of the wind turbine rotor, driven from the shaft tilt of the wind speed angle to the rotor disk, the yaw and pitch motion of the floater, or the yaw error introduced by the time delay between the rapid change in wind direction and the inertia-dominated yaw mechanism of the nacelle and rotor, etc., will produce a gyroscopic moment for wind turbines. This precession torque acts about an axis perpendicular to both the rotor axis and the axis about which the plane of rotation is being changed. The gyroscopic moment is the cross product of the angular momentum vector and the angular velocity vector (Manwell *et al.* 2002).

In addition to the steady and periodic aerodynamic forces, the fluctuating aerodynamic forces induced by gust (wind speed increase in short duration of 2 ~ 30 sec), turbulence and dynamic effects, are also the main cause of fatigue and determine the lifetime estimation of a wind turbine.

2.1.2 AeroDyn Module in FAST

The AeroDyn subroutine package in FAST is to model and calculate the turbine aerodynamics through the classic blade-element/momentum (BEM) theory or a generalized dynamic-wake (GDW) model.

The BEM method is the most commonly used tool to calculate the steady contribution of the aerodynamic forces. The general idea of the BEM method is to find the steady-state lift and drag coefficients for uniform airflow, where the curves are produced by scale model testing, CFD or panel methods. Dynamic-stall behavior is also included to consider the important nonlinear effects like the stall phenomenon (Manwell *et al.* 2002).

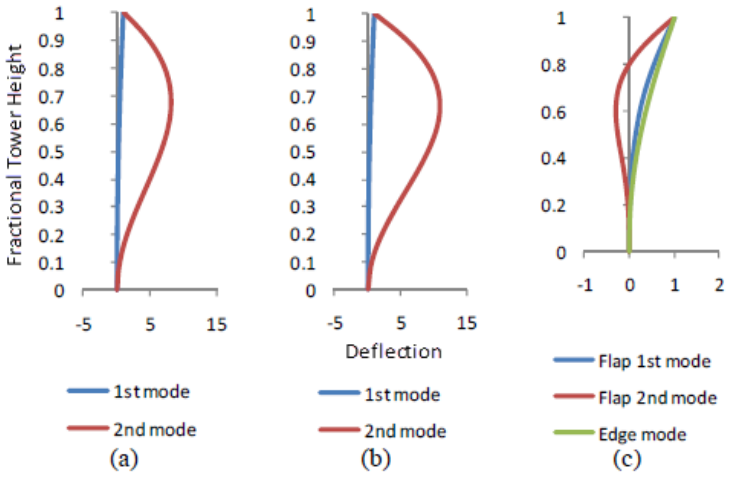

FIGURE 2.3 Normalized mode shapes.
(a) tower fore-aft; (b) tower side-to-side; (c) blades flapwise and edgewise mode

In FAST, the blades and tower flexibility is characterized by a linear model representation based on the small deflection assumption within each member. These elastic characteristics are defined by inputting distributed mass and stiffness factors for each member, and by prescribing their mode shapes as equivalent polynomials. The two flapwise and one edgewise mode of blade, two fore-aft and two side-to-side mode shapes of tower allowed in FAST is illustrated in FIGURE 2.3 (Bae & Kim 2009). The

torsional flexibility of the drivetrain is modeled as an equivalent single-DOF linear-spring and -damper model. The nacelle and hub are modeled in FAST as rigid bodies, same as the rigid platform. The tower is assumed to cantilever to the supported structure rigidly. See Jonkman (2007) for more detail.

2.1.3 NREL 5 MW Baseline Offshore Wind Turbine

The Horizontal Axis Wind Turbines (HAWT), with its output shaft parallel to the ground, is the most common wind turbine design. A wind turbine consists of several major subsystems: rotor, nacelle, tower, generator, drivetrain, control system, electrical output system, foundation and mooring system. Its general properties are given in TABLE 2.1. Detail information and FAST inputs for the NREL 5 MW wind turbine are available in Jonkman (2009, 2010).

Rating	5 MW
Rotor Orientation, Configuration	Upwind, 3 Blades
Control	Variable Speed, Collective Pitch
Drivetrain	High Speed, Multiple-Stage Gearbox
Rotor, Hub Diameter	126 m, 3 m
Hub Height	90 m
Cut-In, Rated, Cut-out Wind Speed	3 m/s, 11.4 m/s, 25 m/s
Cut-in, Rated Rotor Speed	6.9 m/s, 12.1 rpm
Rated Tip Speed	80 m/s
Overhang, Shaft Tilt, Precone	5 m, 5^o, 2.5^o
Rotor Mass	110,000 kg
Nacelle Mass	240,000 kg
Tower Mass	249,718 kg
Coordinate Location of Overall CM	(-0.2 m, 0.0 m, 70.4 m)

TABLE 2.1 General properties of the NREL 5MW baseline wind turbine.

The orientation of the rotor can be upwind or downwind. And the number of blades attached to the hub is normally two or three. The blade pitch can be constant or controllable. The rotor power can be controlled by aerodynamic- or variable-blades-pitch control strategies.

The nacelle of the wind turbine is a structure housing the generator and drivetrain, mounted on the tower top through a yaw bearing with certain yaw mechanism of spring and damping. For the adopted wind turbine, the hub, at 90 m above the mean sea level (MSL), is located 5 m upwind of the tower centerline when the system is undeflected. The vertical distance from the hub height to the tower top is specified as 2.4 m, such that the elevation of the yaw bearing point above MSL is 87.6 m. Since the yaw motion of a wind turbine would change the plane of rotor rotation, a gyroscopic moment would be generated. Therefore, the yaw rate of the nacelle must be limited.

In the nacelle, the drivetrain consists of gearbox, which is assumed to be typical multiple-stage with frictional losses, the journal and thrust bearings, which support the shafts and minimize the movement of the drivetrain. With the torque generated by the wind lift force, the gearbox is used to step up the rotor output shaft to spin the electric generator. Then generator converts the mechanical work input of the wind turbine into useful electrical output. The slip, difference between the generator rotor frequency and the rotating magnetic field, would determine the amount of power produced.

Since the speed of wind increases with height above ground, it is desirable to raise the wind turbine nacelle and rotor up to take advantage of this effect. However, the height of the tower is determined by the rotor stiffness, which should be restricted such

that there is no dynamic coupling between the rotor and tower. The present thesis adopts the modified tower of the 5 MW baseline wind turbine for Hywind-OC3 case. See TABLE 2.2 for the gross properties of its tower. The base of the tower is coincident with the top of the platform at an elevation of 10 m above the MSL, while the top of the tower is coincident with the yaw bearing at the elevation of 87.6 m. The actual height of the tower is 77.6 m. This adjustment is mainly for the coupling of the tower and the designed floating platform. See the following table for the geometry properties of the modified tower in the work.

Tower top elevation above MSL	[m]	87.6
Tower top diameter	[m]	3.87
Tower top thickness	[m]	0.019
Tower base elevation above MSL	[m]	10
Tower base diameter	[m]	6.5
Tower base thickness	[m]	0.027
Tower height	[m]	77.6
Tower center of mass (CM) above MSL	[m]	43.4
Effective steel density	[kg/m^3]	8500
Young's modulus	[GPa]	210
Shear modulus	[GPa]	80.8

TABLE 2.2 Gross tower properties

The effective density of the steel was 8,500 kg/m^3, which was meant to be larger than the typical steel density of 7,850 kg/m^3 accounting for the inner-tower welds, paint, bolts, and flanges which are not included in the tower thickness data. The tower CM shown above table is larger than the original design with 38.23 m.

The control system is to maximize the power output and fatigue life by changing the blade pitch, nacelle yaw, and generator loading of a wind turbine. The original NREL 5 MW wind turbine uses a conventional variable-speed, variable blade-pitch-to-feather control system. As pointed out by Skaare *et al.* 2006, a consequence of this conventional control system is that rotor thrust would reduce after the wind speed exceeds rated, which may cause negative aerodynamic damping and result in large-amplitude resonance of FOWTs. Thereby, the control system of the 5 MW wind turbine for Hywind-OC3 case is modified to eliminate the potential for negative damping of the platform-pitch mode and improve a floating turbine system's response. The detail information about this modified control system is available in Jonkman (2009).

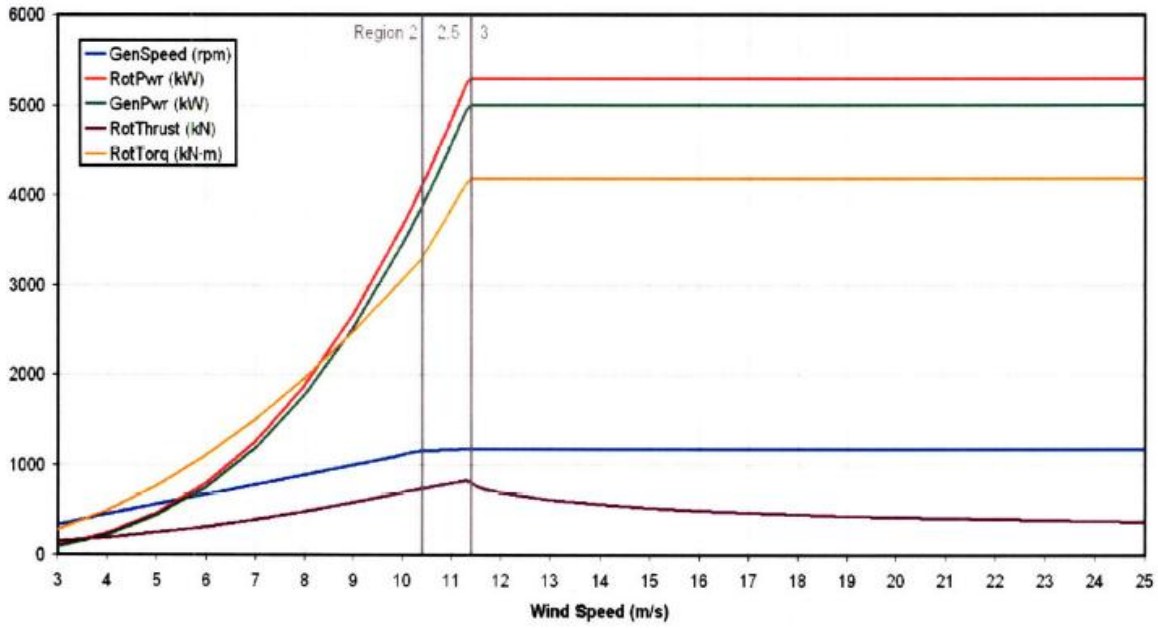

FIGURE 2.4 Performance regions of NREL 5 MW baseline wind turbine.

The power output generated by the torque is illustrated in FIGURE 2.4. When wind speed increased, the rotor torque increases without changing the rotational plane of the rotor. The generator starts to produce useful power output in Region 2 after the wind speed exceeds the cut-in speed (3 m/s), and achieves its maximum thrust load at the beginning of Region 3 at the rated power output of the wind turbine (11.4 m/s). Above the rate speed in Region 3, wind turbine power maintains a constant which is controlled by changing the blade pitch or by stalling a portion of the blade. When the speed exceeds the cut-out speed, 25 m/s, the wind turbine shuts down to avoid damage to the equipment.

2.2 Hydrodynamic Load

For wind turbines in the offshore environment, hydrodynamic loads are calculated by integrating of the dynamic pressure over the wetted surface, including contributions from linear hydrostatics, excitation from incident waves, diffraction (wave-induced) and radiation (platform-induced) hydrodynamic loads, as well as nonlinear effects. The fully coupled dynamic analysis of a FOWT must account for the dynamic coupling between the turbine, support platform motions, as well as the dynamic characterization of its mooring system.

The following sections briefly introduce the true linear hydrodynamic model in time domain in the HydroDyn hydrodynamic module, including the important assumptions for hydrodynamic linearization, the hydrostatic, diffraction and radiation problems, as well as the important nonlinear time-domain equation of motion for the fully coupled platform and wind turbine system.

2.2.1 Linear Hydrodynamics

At first, a six-DOF rigid body with small rotational motions is introduced in FIGURE 2.5 for the support platform kinematics. Modes 1-3 represent translational surge, sway, heave displacement, and the modes 4-5 represent angular motions about the *x*, *y* and *z* axes (roll, pitch and yaw). This inertial coordinate of the platform is fixed with respect to the mean location of the structure, with its $z = 0$ plane coincides with the SWL. The wind and wave direction are assumed to be in the positive *x*-direction throughout the static and dynamic analyses of the platform in the following thesis.

It is also worth mention here that the origin of the translational and rotational motions of the platform is defined at a reference point on the platform, which is as well the point external loadings are applied to. This platform reference point can be defined by setting the FAST input parameter "PtfmRef", which is at the central line of the platform on the SWL in the present work.

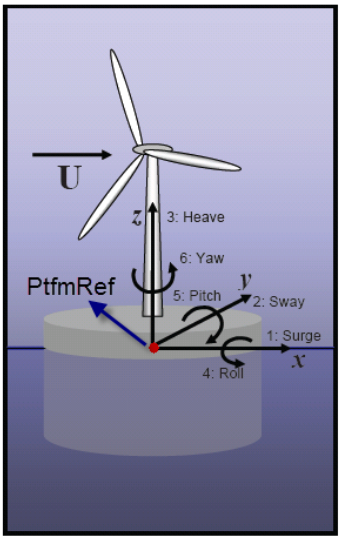

FIGURE 2.5 Support platform modes of motion.

For the linearization of HydroDyn hydrodynamic module, two fundamental assumptions are introduced: 1) small wave-amplitude assumption, which permits the use of regular wave theory (linear Airy wave theory) and the principle of superposition, together with appropriate wave representations (Pierson-Moskowitz and JONSWAP spectra) to determine the incident-wave kinematics for regular or irregular seas. Basic theories about the sea state presentation are shown in Appendix A.1. And more wave representations can be found in Faltinsen (1998); 2) small translational motions of the platform compared to its body size, which is the basic assumption for splitting the hydrodynamic problems into three separate and simpler problems: radiation, diffraction and hydrostatics. Based on the regular wave theory, when the platform is assumed to be fixed with no motion and the incident regular waves are existed, the diffraction loads are resulted from the undisturbed Froude-Kriloff (F-K) pressure field and wave scattering; while the platform is forced to oscillate and no incident waves presented, the radiation loads including contributions from added mass and radiation-damping are generated as it radiates waves away from itself.

2.2.1.1 Wave Excitation Load (Diffraction)

The F-K and diffraction forces and moments are the compositions of the wave excitation loads on the rigid body when it is restrained from oscillating and with incident regular waves presents. The F-K force is due to the unsteady pressure field induced by the corresponding undisturbed waves. The undisturbed F-K pressure for water depth *h* is written as equation 2.5, where ϕ_I is the velocity potential for incident wave.

$$p_{FK} = -\rho \frac{\partial \phi_I}{\partial t} = \rho g A \frac{\cosh k(z+h)}{\cosh kh} \sin(\omega t - kx) \tag{2.5}$$

From the expression above for the undisturbed pressure field, it is assumed that velocities and pressure around the structure are not changed by the presence of the structure, thus the force will be the same as on a water volume of the same shape. Therefore, the horizontal F-K force on a structure from Faltinsen (1998) combined with the strip theory is given in equation 2.6, where $\rho\pi R^2 dz$ is the mass of the displaced fluid of the cylinder strip and $a_1|_{x=0}$ is the x-component fluid acceleration at location $x = 0$ at the average z-coordinate for the strip.

$$dF = i\rho\pi R^2 dz\, a_1\big|_{x=0} \tag{2.6}$$

The undisturbed pressure field would exist only if the body was "transparent" to the wave motion such that a fluid can transport through the cylinder wall and suffer no effects from the existence of the body, which should be physically impossible. Therefore, there must be a force, wave-scattering force, accounting for the additional pressure distribution due to the presence of body. Since the summation of the incident wave potential ϕ_I and the scattered wave potential ϕ_S define the diffraction potential ϕ_D, the total wave excitation force can be found in the following equation, with the first term being the F-K force and the second term referring to the scattering wave force.

$$F_i^{exc}(t) = -\int_{SB} \rho \frac{\partial \phi_D}{\partial t} n_i ds = -\int_{SB} \rho \frac{\partial \phi_I}{\partial t} n_i ds - \int_{SB} \rho \frac{\partial \phi_S}{\partial t} n_i ds \tag{2.7}$$

where,

$$\phi_D = \phi_I + \phi_S; \qquad \frac{\partial \phi_S}{\partial n} = -\frac{\partial \phi_I}{\partial n} \tag{2.8}$$

When applying frequency domain analysis, the total excitation force is more conveniently presented in complex form as in equation 2.9 from Faltinsen (1998).

$$F_i^{exc}(t) = \mathrm{Re}\left\{-\int_{SB} j\omega e^{j\omega t}\rho(\phi_I + \phi_S)n_i ds\right\} = A\,\mathrm{Re}\left\{X_i(\omega)\right\} \tag{2.9}$$

2.2.1.2 Radiation

The added mass and damping loads are steady-state hydrodynamic forces and moments due to forced harmonic rigid body motions with the wave excitation frequency when there are no incident waves, which can be written as equation 2.10.

$$F_{i,rad}(t) = -A_{ij}\ddot{\eta}_j - B_{ij}\dot{\eta}_j \tag{2.10}$$

$$A_{ij} - \frac{i}{\omega}B_{ij} = \rho\iint_{SB} n_i\phi_j ds \tag{2.11}$$

where, A_{ij}, B_{ij} are the added mass and damping coefficient for the six by six matrix. If the structure has zero speed and no current present, half of the coefficients are zero for a structure whose submerged body has only on vertical symmetry plane. The symmetry leads to non-zero coefficients only for the diagonal elements. The equation 2.11 shows the relationship between the added mass and damping coefficients from Faltinsen (1998).

2.2.1.3 Hydrostatics

When a body is freely floating, the restoring forces will follow from hydrostatic and mass consideration. The hydrostatic load is the combined buoyancy force and restoring from water-plane area and CB, which are written as components:

$$F_i^{hydrostatic} = \rho g V_0 \delta_{i3} - C_{ij}^{hydrostatic} q_j \tag{2.12}$$

here, $\rho g V_0 \delta_{i3}$ is the buoyancy force from the displaced fluid in the platform's undisplaced position, which is only nonzero in the heave mode when $i = 3$. $C_{ij}^{hydrostatic}$ is the (i,j) component of the linear hydrostatic-restoring matrix, and q_j is the j^{th} DOF of the support platform. As one of the three independent hydrodynamic problems, the hydrostatic loads are separated from the incident and outgoing waves from the diffraction and radiation problems, respectively.

The hydrostatic restoring is expressed by a linear hydrostatic and gravitational restoring matrix, whose nonzero coefficients are given in TABLE 2.3. The result in table demonstrates that hydrostatics only provides restoring force in heave/roll/pitch modes; restoring in the other modes therefore should be from the mooring system.

$C_{33,H\&G}$	N/m	$\rho g A_0$
$C_{35,H\&G} = C_{53,H\&G}$	N	$-\rho g \iint_{A_0} x dA$
$C_{44,H\&G}$	Nm	$\rho g \iint_{A_0} y^2 dA + \rho g V_0 Z_{CB} - mgZ_{CG}$
$C_{55,H\&G}$	Nm	$\rho g \iint_{A_0} x^2 dA + \rho g V_0 Z_{CB} - mgZ_{CG}$

TABLE 2.3 Hydrostatic and gravitational restoring coefficients.

2.2.1.4 Linear Hydrodynamic Model in HydroDyn

In the true linear hydrodynamic model in time-domain, the total external load acting on the support platform not only include the above three separate problems, but also accounts for the restoring forces from mooring lines, the radiation-retardation effect by introducing the retardation kernel K_{ij}, and fully coupled the wind turbine and

supported platform through summing the mass matrix M_{ij} from the complete nonlinear equation of motion with the hydrodynamic-added-mass solutions A_{ij}. See the following equation 2.13. More introductions about this linear hydrodynamic model in HydroDyn are presented in Appendix B.

$$F_i^{platform} = -\left(M_{ij} + A_{ij}\right)\ddot{q}_j + F_i^{waves} + F_i^{hydrostatic} + F_i^{lines} - \int_0^t K_{ij}\left(t-\tau\right)\dot{q}_j\left(\tau\right)d\tau \qquad (2.13)$$

Besides, the linearization assumptions also allows for alternative time-domain hydrodynamic representations, such as the frequency-domain analysis of the response of the FOWTs in irregular seas. However, it is valid only when the platform oscillates at the incident wave frequency. A requirement for this is that all the loading presented in the system is linear in nature, which means only the steady-state situation can be analyzed, and not for nonlinear and transient events. Though the frequency-domain representation cannot be direct used in the analysis of FOWTs prevented by above reasons, its solutions such as $A_{ij}(\omega)$, $B_{ij}(\omega)$ and $X_i(\omega)$ are used in the time-domain true linear hydrodynamic-loading model in HydroDyn module to determine the parameters and the relationship between $A_{ij}(\omega)$, $B_{ij}(\omega)$ is valuable to find the wave-radiation-retardation kernel K_{ij}.

Another commonly used time-domain hydrodynamic formulations in offshore industry is the Morison's representation, which is most valid for slender vertical surface-piercing cylinders mounted on seabed. This makes Morison's representation widely apply to bottom-fixed offshore wind turbine. For FOWTs, it is valid only if the platform motions are very small since Morison's equation assumes viscous drag is the dominate damping in the system. A remarkable feature of Morison's representation is that the

hydrodynamic loading is written directly in terms of undisturbed water-particle velocity and accelerations, which allows Morison's equation and strip theory to adopt nonlinear wave kinematics model to account for the relative kinematics between the fluid and substructure motions, including nonlinear characteristics for real sea. However, it ignores the memory effects of free surface and a typical added-mass-induced coupling between modes of motion in the radiation problem. Tough the viscous drag is not shown in the equation 2.13, the nonlinear viscous-drag term from Morison's equation is still included in the HydroDyn module since it can be an important source of hydrodynamic damping and incorporate the influence of sea current as well (Jonkman 2007).

2.2.2 Nonlinear Time-domain Equation of Motion

The fully dynamic coupling between the motions of the supported platform and the wind turbine are very important in establishing the equation of motion for the whole system. Equation 2.14 gives the general form of the nonlinear time-domain equation of motion adopted in FAST for the coupled wind turbine and support platform system.

$$M_{ij}\left(q,u,t\right)\ddot{q}_j = f_i\left(q,\dot{q},u,t\right) \tag{2.14}$$

Here, M_{ij} is the (i,j) component of the inertia mass matrix nonlinearly relying on system DOFs, q, control input, u, and time, t. f_i is a forcing function of system DOFs, velocity ($\dot{q}$), control input and time, as well. It is defined positive in the support platform direction, and is also applied on the platform reference point. Since the FAST system has a great number of DOFs for all components, it was a tedious process deriving the equations of motion, can thereby would not be further discussed here. Find in Jonkman (2006) for more descriptions.

See the following FIGURE 2.6 for the calculations of the total external loads on supported platform. This flowchart has combined the steady-state frequency-domain solutions, the wave simulations, time-domain hydrodynamic-loading calculations and the nonlinear structural-dynamic-coupling module as well.

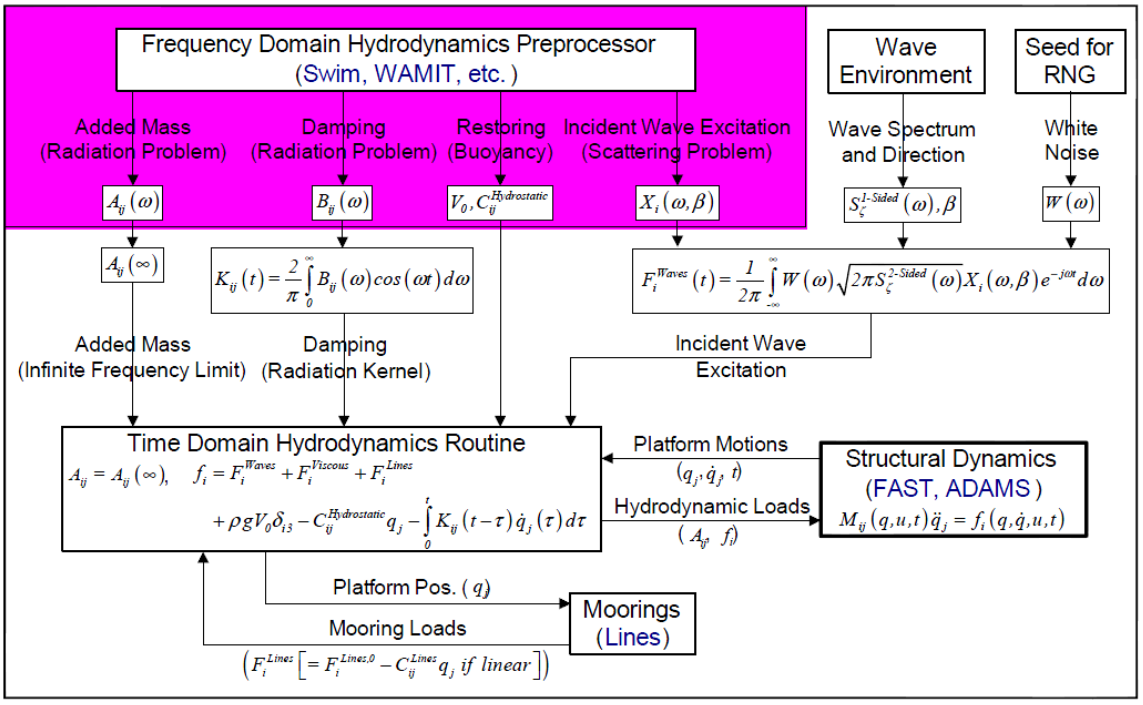

FIGURE 2.6 Summary of calculations for total external loads on support platform.

3 DESIGN METHODOLOGY

The preliminary model design in the thesis is illustrated in FIGURE 3.1. The large-scale 5 MW wind turbine is rigidly cantilevered to a mono-column supported platform. The mooring system includes only a single taut tether, with its both ends hinged to the hull and the sea floor. The structure achieves stability with an excess buoyancy giving rise to the pretension of the taut tether.

Actually, the design of this model is fairly complex and iterative due to the extensive amount of parameters and considerations, such as the design parameters' influence on natural frequency, satisfying system's response, damping mechanism and so on. A variety of articles in literature have been written for the parametric design of support platform structures. In 2004, the first work at MIT in developing a procedure for the design and analysis of support platforms was discussed by Withee (2004). A steady-state design optimization is presented by introducing certain requirements for FOWT performance in Wayman & Sclavounos (2006). A thorough parametric design process is further performed in the Master's thesis by Tracy (2007).

A presentation of important parametric design issues based on the results and discussions in the above mentioned theses are summarized in the following sections. The detailed description about the model, the static and dynamic analysis of the coupled wind turbine system, as well as the cost drives for the model are included in this chapter.

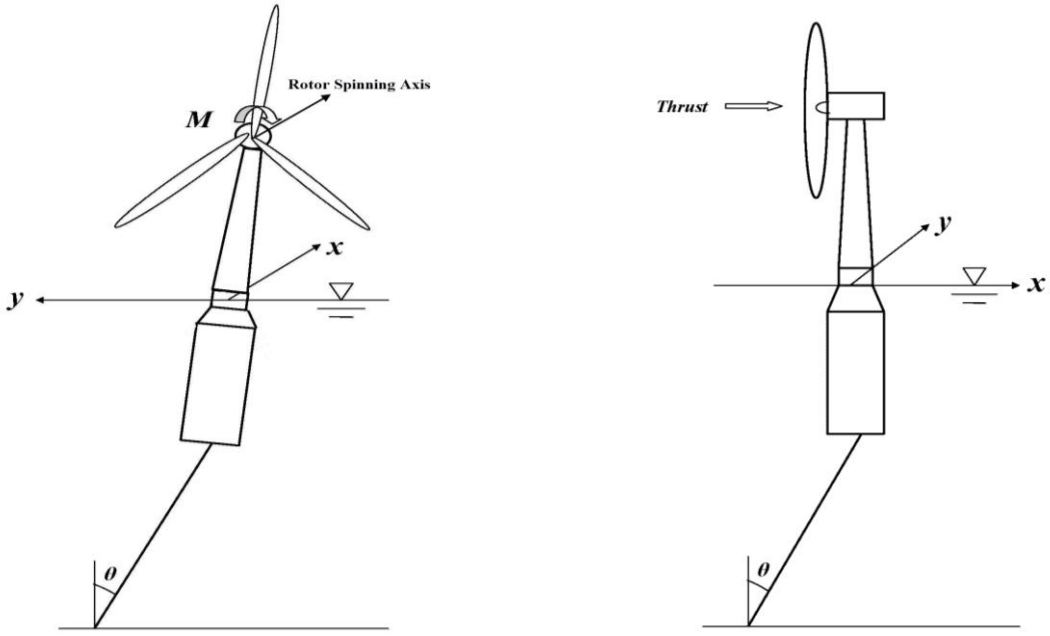

(a) **(b)**

FIGURE 3.1 Model diagram (a) downwind view; (b) side view.

3.1 Model Mechanics

The behavior of the FOWT is fairly complex because of the dynamic coupling between modes of motions of different parts of the system. For instance, a yaw moment can be produced due to the rotor blades spinning as well as the slightly tilting of the floating wind turbine. With both wind and waves aligned with *x*-axis, the generator torque produces a roll moment on the floater. This motion is resisted by the single tether. Roll of the floater also results in the nacelle moving off axis, which produces a moment arm along the *y*-axis. With wind into rotor, the rotor thrust in *x* direction acts on this *y*-axis moment arm results a yaw moment. Similarly, due to the gyroscopic effect, the

cross product of the rotor spinning and nacelle yaw would result in a pitch motion, which is also the reason that the yaw DOF of nacelle should be restricted.

Another important coupling example is the coupled surge/pitch, and surge/heave modes of motion. The coupling between the surge and pitch mode is mainly due to the definition of the reference point location on the platform. The coupling between surge/heave is nonlinear and determined by the length of the tethers. More coupling the shorter tethers have since set-down is large for the same amount of horizontal motion. Therefore, the displacement caused by the external loading on the floater is resisted by the restoring force produced by the tethers. For example, as the floater surges or sways away from the rest position its draft increases due to the fact that the tethers act as rods in tension. This increase in draft would cause an increase in the line tension.

$C_{11,tether} = C_{22,tether}$	N/m	T_0/L
$C_{33,tether}$	N/m	EA/L
$C_{44,tether} = C_{55,tether}$	Nm	T_0D^2/L
$C_{15,tether} = C_{51,tether}$	Nm	$-T_0D/L$
$C_{24,tether} = C_{42,tether}$	Nm	T_0D/L

TABLE 3.1 Restoring coefficient of the single tether.

By applying the small displacement approximation, the length of the draft and the tether tension can be considered constant, and the stiffness provided by the single tether in steady state operation can be written in TABLE 3.1 as following, where T_0 is the pretension provided by the excess buoyancy; L is the unstretched length of the single tether; D is the draft of the submerged body; and EA is the extensional stiffness.

An important design parameter in static analysis is the tether line stress. The line stress should not excess the yield stress to avoid the line material lose its elasticity characteristics. The yield stress for certain materials can be obtained by experiments. The relationship between strain and stress while the stress is under the yield stress limitation is as $\sigma = E\varepsilon$. The tension on the tether is provided by the excess buoyancy, and while the system is at rest the tension in the tether is the pretension, T_0. The following equation 3.1 is used to calculate the pretension stress of the tether with cross-area A_{line}.

$$\sigma_{line} = \frac{Buoy - Weight_{sys}}{A_{line}} = \frac{T_0}{A_{line}} \tag{3.1}$$

The estimation of the restoring coefficients is useful in predicting the natural periods of the system and verification of the time domain hydrodynamic analyses using linear theory, which will be discussed more fully in the following sections.

3.2 Frequency-Domain Approach

As described in section 2.2.1, the frequency-domain analysis can be applied in steady-static conditions and its solutions are helpful to determine the parameters for linear hydrodynamic equations in time domain. FAST itself has the capability of extracting a linear model by first determining an operating point to linearize the model about, and then numerically linearizes the complete nonlinear aeroelastic model about the operating point to form periodic state matrices.

Definition of an operating point is a set of values of the system DOF properties, control inputs and wind inputs that characterize a steady condition of the wind turbine. The steady-state operating point is calculated by adjusting the control system to obtain

the desired rotor speed. For the steady wind loading, this operating point is periodic driven by aerodynamic loads and the values of them depend on the rotor azimuth orientation. Since the operating point is periodic with the rotor orientation, the linearized representation of the model is also periodic.

The fully coupled governing equation of motion in 6x6 matrix in frequency-domain is given by equation 3.2, where all coefficient matrices are about the three system components: wind turbine (WT consisting of rotor, nacelle, tower), platform and mooring system.

$$F_{exc}(\omega)e^{i\omega t} = \left[A_{add}(\omega) + M_{sys}\right]\ddot{\eta} + \left[B_{rad}(\omega) + B_{external}\right]\dot{\eta} + \left[C_{H\&G} + C_{external}\right]\eta \quad (3.2)$$

Here, the hydrodynamic coefficients including the added mass matrix, $A_{add}(\omega)$, the platform radiation damping matrix, $B_{rad}(\omega)$, and the wave excitation force, $F_{exc}(\omega)$, are function of frequency. M_{sys} are the total mass of the system including the wind turbine and the platform. $B_{external}$ is the external damping contributions from wind turbine. $C_{H\&G}$ is the linear hydrostatic and gravitational matrix of the platform as shown in section 2.2.1.3. $C_{external}$ is the external stiffness matrix provided by the wind turbine as well as the mooring systems. η represents the response motion of the 6DOFs modes for the structure.

The non-dimensional form of the equation 3.2 is given in 3.3, where ξ_i is the non-dimensional definitions of the structure motions.

Generally, the solution to the frequency-domain problem is given in terms of an RAO. The following equation 3.3 is the non-dimensional form of the governing equation above, from which the RAO formulations are easily got in equation 3.4 for mode *i*.

$$X_i(\omega) = \sum_{i=1}^{6}\left[-\omega^2\left(A_{ij} + M_{ij}^{sys}\right) + i\omega\left(B_{ij}^{rad} + B_{ij}^{external}\right) + \left(C_{ij}^{H\&G} + C_{ij}^{external}\right)\right]\xi_j \tag{3.3}$$

$$RAO = \overline{\xi}_i = \frac{\xi_i}{A_{wave} / L^n} \tag{3.4}$$

where n = 0 for translational mode i = 1,2,3 and n = 1 for rotational mode i = 4,5,6; L is the characteristic length of the system, and A_{wave} is the incident wave amplitude. By setting the dimensional parameters to unity, the RAOs are equal to the transfer function $X_i(\omega)$ of equation 3.2, and the response spectrum can be found by its relationship between the wave spectrum in equation 3.5, and the mean square deviations is given in equation 3.6.

$$S_i(\omega) = \left|RAO_i(\omega)\right|^2 S_\eta(\omega) \tag{3.5}$$

$$\sigma_i^2 = \int_0^\infty \left|RAO_i(\omega)\right|^2 S_\eta(\omega)\, d\omega \tag{3.6}$$

The natural frequencies of the combined wind turbine and floating platform system therefore can be estimated by considering the system's restoring and inertial properties by equation 3.7:

$$\omega_i = \sqrt{\frac{C_{ii}}{M_{ii} + A_{ii}(\omega)}} \tag{3.7}$$

where the $A_{ii}(\omega)$ indicates the the added mass; M_{ii} is the total mass of the system, and C_{ii} is the total restoring stiffness consisted of the contributions from the wind turbine, the platform and the tether. For modes that restoring is weak (C_{ii} approaching zero), the natural frequency will go to zero. However, for such modes the natural frequency is

picked up through cross coupling to other modes of motion, which can be determined graphically by examining the frequency at which the peak of the RAO occurs.

All the hydrodynamic properties mentioned above as wave excitation force $X_i(\omega)$, added mass $A_{ij}(\omega)$ and damping $B_{ij}(\omega)$ matrix from wave radiation and the hydrostatics are computed in HydroGen and used later in the fully coupled time-domain model in FAST. The computation process for the frequency-domain solutions, the RAOs, has been outlined by the visualized flowchart in FIGURE 3.2.

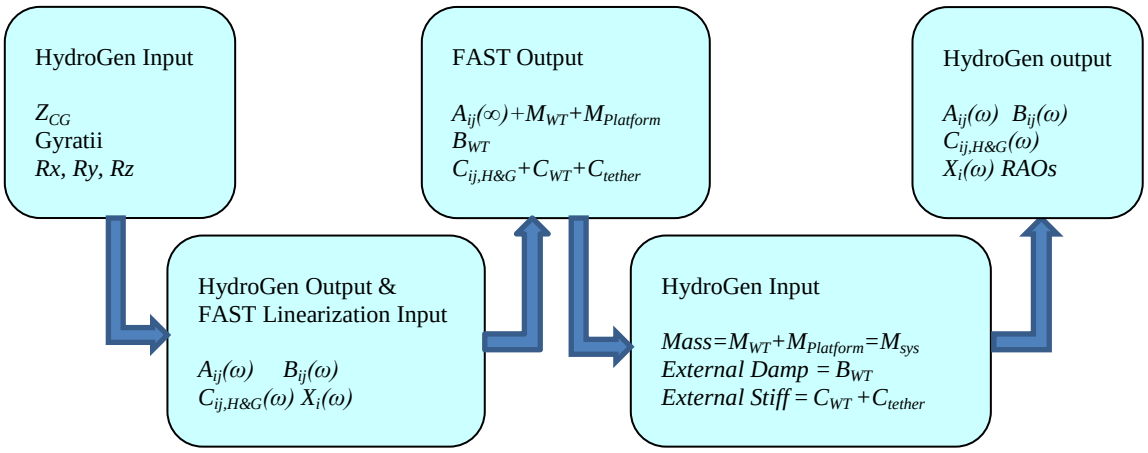

FIGURE 3.2 Flowchart of the computation process of HydroGen/FAST linearization.

3.3 Design Considerations

The design space for the model is quite large because of the variety of variables, such as the platform radius, draft, steel wall thickness (SWT), concrete height, water depth, mooring line properties, sea states, and so on. The platform radius and draft define the shape of the submerged body and directly give the displaced volume of sea

water. The platform radius, SWT, and the concrete heights are the dominant parameters determining the platform hull weight, CG as well as the cost. The sea state, such as the significant wave height, H_s, determines the worst environment that the floating structure will subject to: *6* m corresponding to an extreme design case in protected or near coastal waters while *10* m is an extreme design case in the open ocean. For the preliminary design of the model, however, certain inputs to the design process keep constant, as given in TABLE 3.2.

Constant Inputs	Value
Wind Turbine	*NREL 5 MW Baseline Wind Turbine*
Maximum Thrust	800 kN
Corresponding Wind Speed	11.2 m/s
Turbine Moment	72,000 kN·m
Freeboard	10 m

TABLE 3.2 Design constants.

The following sections present the important criteria for the design process, including the steady-state analysis, dynamic analysis and cost assessment. The static design aims to examine the mechanisms explained in section 3.1 that provide adequate restoring for the system to achieve a satisfying steady-state operating point once installed, while the dynamic analysis process is to elevate the systems RAOs, natural frequencies, and standard deviations of the system motions in various wind speeds and sea states. Finally, the economy-feasibility analysis is necessary to determine the most acceptable structure design.

3.3.1 Steady-state Design Criteria

Before the system can be considered for dynamic motion, the first criterion is to demonstrate the acceptable static performance in its installed state, about which the system oscillates in response to random waves. In steady-state, velocities and accelerations are zero, and only steady-state forces and moments exist. The governing equation of motion in equation 3.2 then reduces to the static equilibrium equation.

$$F_{steady-state} = \left[C_{H\&G} + C_{tether}\right]\eta_{steady-state}(\omega) \tag{3.8}$$

Therefore, the problem to achieve favorable steady-state performances in various modes is simplified by offering sufficient restoring stiffness to the system.

3.3.1.1 Pitch Displacement

The critical steady-state offset for floating wind turbine systems is the pitch displacement, which will not only lead the structure to capsize, but also change the rotation plane of the rotor blades.

Based the hydrostatic restoring matrix and mooring stiffness restoring matrix presented before, the system's steady-state pitch, η_5, is determined by the steady-state moment exerted on the system in pitch, F_5, in equation 3.9 and 3.10.

$$\eta_5 = M_5 / C_{55} \tag{3.9}$$

$$M_5 = F_{thrust} Z_{hub} \tag{3.10}$$

A minimum value of restoring in pitch can be calculated by limiting the structure's steady-state pitch to a certain threshold, *10* degree pitch angle, beyond which the wind turbine will lose substantial efficiency. The maximum turbine moment was

taken as *7200 kN*, which is the moment corresponding to the steady-state thrust *800 kN* at a wind speed of *11.2 m/s* acting on the turbine hub, at $Z_{hub} = 90\ m$.

$$C_{55,\lim it} = \frac{M_5}{\eta_5} = \frac{F_{thrust} Z_{hub}}{\eta_{5,\lim it}} = \frac{800 \times 90[kN \cdot m]}{10^o \pi / 180^o [-]} = 4.126E + 08[N \cdot m] \qquad (3.11)$$

The value calculated above serves as the preliminary design parameter for candidate structures. The pitch restoring coefficient C_{55} for the present model can be obtained through the following equation (R = cylinder radius; D = draft).

$$C_{55} = C_{55,H\&G} + C_{55,tether} = \rho g \frac{\pi}{4} R^4 + \rho g V_0 Z_{CB} - mg Z_{CG} + \frac{T_0 D^2}{L} \qquad (3.12)$$

3.3.1.2 Surge Displacement

The tether tension for this system should not only fulfill the required restoring for the restrained pitch angle, but also provide sufficient restoring force in surge to limit the steady-state surge displacement adequately. The criteria for surge displacement is that, the angle θ formed by the tether and the vertical axis as shown in the model diagram above should be limited to about 5 degrees in order to prevent the system from experiencing highly nonlinear restoring and displacement.

Surge restoring from the tether is related to pretension and tether length, as the given expression $C_{11} = T_0/L$. The steady-state surge displacement resulted from restoring can thereby be found through the following equation.

$$\eta_1 = \frac{F_1}{C_{11}} = \frac{F_{thrust}}{C_{11}} \qquad (3.13)$$

Meanwhile, in order to provide enough restoring force to achieve a satisfying steady-state surge displacement, the minimum surge restoring coefficient can be found through the above equation as well.

3.3.2 Dynamic Design Criteria

3.3.2.1 Natural Frequency

As the design process passes from the steady-state analysis to the dynamic phase, the most important step is to find out the natural frequencies of the coupled system in six modes of motion which should not coincide with the peak frequency of the dynamic loading. See Equation 3.7.

In the preliminary design process, C_{WT}, the restoring stiffness arisen from the tower deformation can be neglected comparing with the restoring force from the platform and tether. The non-zero mass matrix coefficients of the platform can be obtained following the expressions in TABLE 3.3 for the simplified submerged body in FIGURE 3.3. The added mass coefficients are determined by evaluating the reaction forces of the floater in mode *i*.

$$F_{1,react} = \int_{-D}^{0} m_{11} \cdot a_{strip} dz = A_{11}\ddot{\eta}_1 - A_{15}\ddot{\eta}_5 \tag{3.14}$$

$$F_{5,react} = \int_{-D}^{0} m_{11} \cdot a_{strip} \cdot z_{strip} dz = -A_{15}\ddot{\eta}_1 + A_{55}\ddot{\eta}_5 \tag{3.15}$$

The above two equations are the reaction forces due to forced oscillations in surge and pitch, where m_{11} in the expressions is the mass of displaced water by the cylinder per unit length. a_{strip} is the horizontal acceleration of the strip located at z_{strip}

from the SWL due to both translation and rotation. The relationship between them is as shown in equation 3.16.

$$a_{strip} = \ddot{\eta}_1 + z_{strip}\ddot{\eta}_5 \tag{3.16}$$

The added mass in heave is the mass of water under the hull that is accelerated by the vertical motion of the structure. This added mass can be approximated by the displacement of a half sphere of the water with a radius equal to that of the base of the hull. See TABLE 3.4 for the added mass coefficients in each mode.

$M_{11} = M_{22} = M_{33}$	kg	$M_{steel} + M_{concrete} = M_{platform}$
$M_{15} = M_{51}$	$kg{\cdot}m$	$M_{platform} CG_z$
$M_{24} = M_{42}$	$kg{\cdot}m$	$-M_{platform} CG_z$
$M_{44} = M_{55}$	$kg{\cdot}m^2$	$\sum_{j=s1,s2,concrete} \left(I_{x,j} + M_j CG_{z,j}^2 \right)$
M_{66}	$kg{\cdot}m^2$	$\sum_{j=s1,s2,concrete} I_{z,j}$

TABLE 3.3 Mass matrix coefficients of platform.

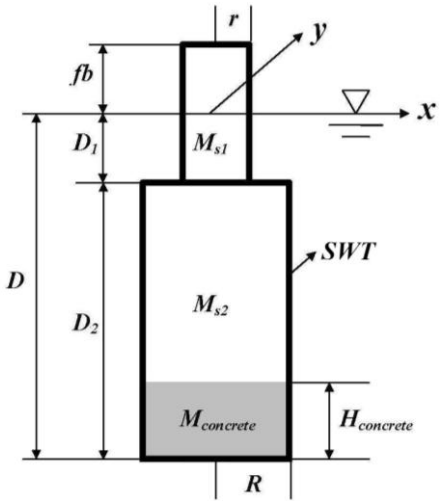

FIGURE 3.3 Simplified platform model without taper.

M_{s1}, M_{s2} = steel mass of cylinder 1 and 2 [kg];

$M_{concrete}$, $H_{concrete}$ = concrete ballast mass [kg] and height [m];

R, r = input exterior radius of the submerged cylinder and tower base [m];

D = input draft [m]

fb = constant freeboard [m]

SWT = steel wall thickness [m]

$$CG_x = CG_y = 0; \quad CG_z = \left[M_{steel} CG_{z,steel} + M_{concrete} CG_{z,concrete} \right] / M_{platform}$$

$$CG_{z,steel} = \left[M_{s1} \left(fb - D_1 \right) / 2 - M_{s2} \left(D_1 + D_2 / 2 \right) \right] / M_{steel}$$

$$CG_{z,concrete} = -D + \left(H_{concrete} / 2 + SWT \right)$$

$$\begin{aligned} M_{steel} &= \left(M_{s1,external} - M_{s1,inner} \right) + \left(M_{s2,external} - M_{s2,inner} \right) \\ &= \rho_{steel} \left\{ \pi r^2 \left(fb + D_1 \right) - \pi \left(r - SWT \right)^2 \left(fb + D_1 - 2SWT \right) \right\} \\ &+ \rho_{steel} \left\{ \pi R^2 D_2 - \pi \left(R - SWT \right)^2 \left(D_2 - 2SWT \right) \right\} \end{aligned}$$

$$M_{concrete} = \rho_{concrete} \pi \left(R - SWT \right)^2 H_{concrete}$$

$$I_x^j = I_y^j = \frac{m_j}{12} \left(3Radius_j^2 + Height_j^2 \right); \quad I_z^j = \frac{m_j}{2} Radius_j^2 \quad (j = \text{s1, s2, concrete}).$$

$A_{11} = A_{22}$	kg	$\rho\pi R^2 D$
A_{33}	kg	$2\rho\pi R^3/3$
$A_{44} = A_{55}$	$kg \cdot m^2$	$\rho\pi R^2 D^3/3$
$A_{15} = A_{51}$	$kg \cdot m$	$-\rho\pi R^2 D^2/2$
$A_{24} = A_{42}$	$kg \cdot m$	$\rho\pi R^2 D^2/2$

TABLE 3.4 Added mass matrix coefficients.

As explained in section 3.2, the wave excitation force is the only dynamic load considered in the frequency domain analysis. Therefore, the natural frequency of the modes of motion should be designed to avoid resonance by putting the natural frequencies beyond the range of dominant wave frequencies (*0.2 ~ 2.5 rad/s*). The wave excitation force in yaw is fairly low, and the natural frequency is therefore assumed to be not as important as for the other modes.

Besides, the resonance and second order effects from interaction with the time-varying loads on the wind turbine can also occur and is an important factor for the fully coupled dynamic analysis. To avoid this, the natural frequencies of the coupled system should not coincide with rotor frequency (1P) and the tower flexibility frequency or the blade passing frequency range (3P). For NREL 5 MW baseline wind turbine, the rotor speed is 12.1 rpm, such that the corresponding rotor frequency 1P equals 1.256 rad/s, and the blade passing frequency 3P is 3.801 rad/s.

Parameters	C				M				A				ω_0			
	1	3	5	6	1	3	5	6	1	3	5	6	1	3	5	6
↑ R	↑	-	-	-	↑	↑	↑	↑	↑	↑	↑	-	↑	↓	↓	↑
↑ D_1 or D_2	↑	↑	↑	-	↑	↑	↑	↑	↑	↑	↑	-	↑	↓	↓	↑
↑ EA Stiff	-	↑	-	-	-	-	-	-	-	-	-	-	-	↑	-	-

TABLE 3.5 Parameter variables' influence on natural frequency of TLP.
(↑ : increase; ↓ : decrease; - : unaffected or negligible effect)

In Withee (2004), a parameter study was conducted in order to determine the effect of design parameters on the system dynamic responses, especially the TLP case,

see TABLE 3.5. These results can also act as a reference for the modification of the parameter design of the model in this research.

3.3.2.2 Dynamic Tether Tension

An initial limit for the tether tension can be reached by limiting the system's steady-state displacement. For the model with only one taut tether in this case, it's especially worth attention to the variation of the tether tension during operation since the failure of the tether will directly lead the whole system to capsize. The dynamic tether tension should not excess the breaking load of the tether within a factor of safety, but also do not lose tension which may cause it fail via a buckling load. The expressions for the tether tension constraint in dynamic are given below.

$$\begin{aligned} \left(T_{tether,\,fairlead} + \sigma_{tether,\,fairlead}\right) F.S \le T_{\max} \\ \left(T_{tether,anchor} - \sigma_{tether,anchor}\right) F.S \ge 0 \end{aligned} \tag{3.14}$$

Here, $T_{tether,\,fairlead}$ and $T_{tether,\,anchor}$ are the dynamic tether tension at the fairlead and anchor point. And the tether tension at the anchor point is always smaller than the tension at the fairlead location considering the apparent weight the tether itself. σ represents the standard deviation of the tether tension at fairlead or anchor. F.S. is the factor of safety which is taken about 1.5 ~ 2.0 in the work.

3.3.3 Cost Drivers

The design of the support platform structure is the key factor which should be taken into account for the economic feasibility of the whole FOWT, and the total steel mass is the main cost driver behind the support structure. In order to ensure the floating

configurations to be competitive with bottom-fixed configurations at intermediate water depths (30 ~70 m), the steel mass must be less than 1000 metric tons. The cost of steel is set to be among the range between $600 and $800 per metric ton estimated by considering quotes from manufacturers.

The concrete ballast located at the bottom of the cylinder can also make significant contribution to the costs, the price of which is chosen from $50 to $150 per metric ton, based on the estimation in Wayman & Sclavounos (2006). The mooring system can take up a great part of the cost for the whole system especially when the tether tension is fairly high. The anchor cost per kilo-Newton tether tension is estimated $15 and $25, which was used in Wayman & Sclavounos (2006) for suction pile and vertical load anchor (VLA).

The estimated costs for steel, concrete and tether tension can be used to optimize the design by minimizing costs. As shown in TABLE 3.6, the design can be close to cost optimized when it fulfill the design limits that steel mass to vertical anchor load ratio is in the range of approximately 0.02 to 0.04, and the concrete mass to the vertical anchor load ratio in the range of 0.1 to 0.25, based on the price ranges discussed before. The cost for transmission, installation or maintenance are also important but are not considered here.

Property Ratio		Lower Limit	Upper Limit
Steel Mass/TetherTension	[metric ton/kN]	15/800 = 0.02	25/600 = 0.04
Concrete Mass/TetherTension	[metric ton/kN]	15/150 = 0.1	25/50 = 0.5

TABLE 3.6 Optimized property ratio ranges.

4 PRELIMINARY MODEL DESIGN

The actual design process of the model is an iterative process following the considerations discussed in section 3.3. The constant properties of the NREL 5 MW wind turbine mounted at the top, such as the rotor, nacelle and tower mass properties, thrust force, to which the design process should be sensitive, have already been determined as shown in TABLE 4.1. The preliminary design and verification process is then presented below considering the uncertainty of the parameters with the given constants.

Wind Turbine Mass (Rotor + Nacelle + Tower)	599718 kg
Wind Turbine CG above SWL	70.35 m
Maximum Thrust Operational Condition	800 kN
Hub Height	90 m
Deck Clearance	10 m
Steel Wall Thickness (SWT)	0.015m, 0.0253m, 0.045m
Draft	72 m
Depth	200 m
Number of Tether	1
Tether Axial Stiffness unit length *EA*	1.62E+10 Nm
Tether Mass Density μ_c	606.57 kg/m

TABLE 4.1 Input parametric constant for the NREL 5 MW wind turbine.

4.1 Design Uncertainty from Input Constant

First of all, the wind turbine mass given in the above table only accounts for the known weights of the main components—blades, rotor and tower, and ignores the

unknown weight contributions from other parts, which add great uncertainty to the design process.

Besides, the SWT is also a variable for different designs. For example, the SWT of the MIT TLP case adopts 0.015 m for the SWT in Matha (2010). However the necessary thickness will most likely be larger than 0.015 m since the sidewalls buckling may occur for such thickness, and the necessary steel thickness at the bottom of the model should also be larger otherwise additional stiffeners or concrete ballast will be needed. In this work, the design of the support platform is based on the concept of SWAY® 10 MW wind turbine, which is assumed to be the extension of the tower mounted on it, the SWT thereby has a choice to be set as the same value of the tower wall thickness at the tower base, 0.0253 m. However, the SWT should be further examined to ensure satisfying outcomes that fulfill all the requirements. The platform draft, 72 m, is defined based on the public available information about the SWAY® 10MW wind turbine concept.

The thrust force of the wind turbine can also provide uncertainties to the design process. However, since the given maximum thrust in the table is the steady-state operational thrust depended on the rated power which should not change much for various 5 MW wind turbines with same control, it is not emphasized here.

4.2 Iterative Design Process

The iterative design process is validated based on the properties of the wind turbine mounted on the top, and is conducted to determine the desirable parameters for

the model system. In the following sections, the design process for the variables of the model is presented step by step, as well as the influences of each variable on the design.

4.2.1 Step 1: Cost, Stability

Since the mass density of concrete is 2.56 times higher than water density, concrete requires a smaller volume to lower the CG. It is thereby much more efficiency to use concrete ballast to satisfy the stability requirements for the spar-buoy type platform—the CG is far below the CB and the total weight of the platform is equal to the buoyancy force. Besides, considering for the single tether mooring system, it is also necessary to make the platform hydrostatic coefficients positive to ensure its static stability in case of the collapse of the single tether. Therefore, with the top mass and platform draft known, the main work of the first step is to find out the acceptable platform diameter and the height of concrete ballast for three cases with different SWTs: 0.015 m, 0.0253 m, 0.045 m. The platform diameter is an important parameter determining the system buoyancy, steel mass, variables that influence the CG, pretension and cost directly. See the results in the following figures, where platform diameters are limited to the range from 11 m to 13 m. Therefore, the only variable remaining is the concrete ballast height.

FIGURE 4.1 shows that the minimum concrete height $H_{concrete}$ can be found for each case with certain diameter in order to obtain positive hydrostatic and gravitational restoring coefficients. For all cases, this restoring coefficient will increase with larger platform diameter and higher concrete ballast, which means better static stability at the same time.

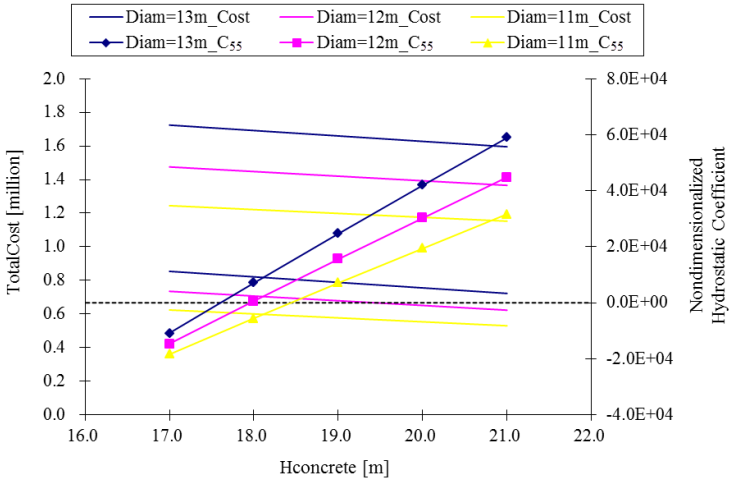

(a) Case 1: SWT = 0.015 m

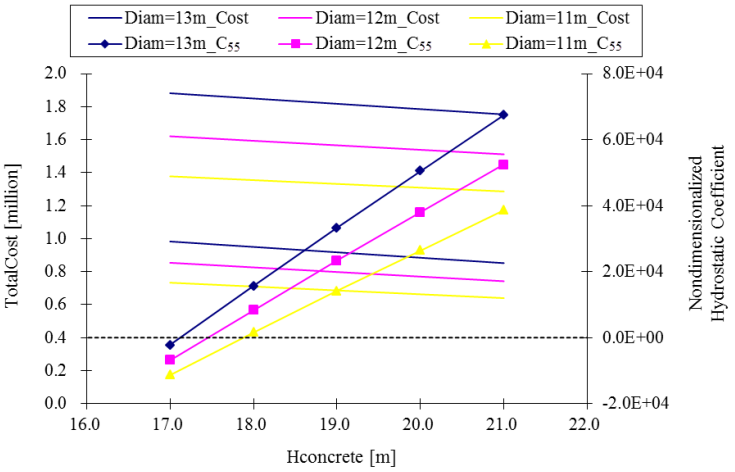

(b) Case 2: SWT = 0.0253 m

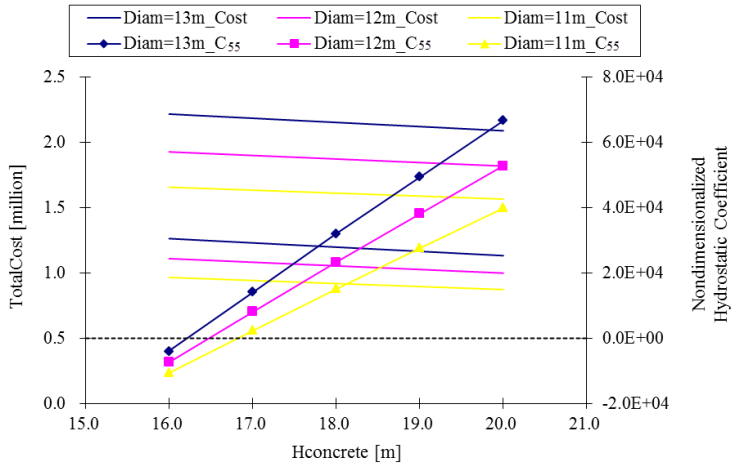

(c) Case 3: SWT = 0.045 m

FIGURE 4.1 Hydrostatic stiffness and total cost for three cases with SWT = 0.015 m, 0.0253 m, 0.045 m.

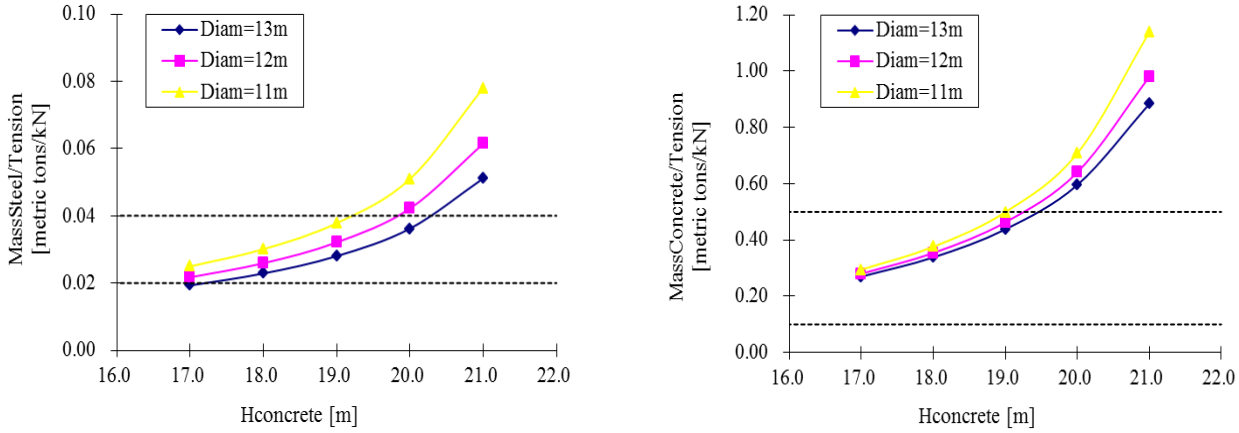

(a) Case 1: SWT = 0.015 m

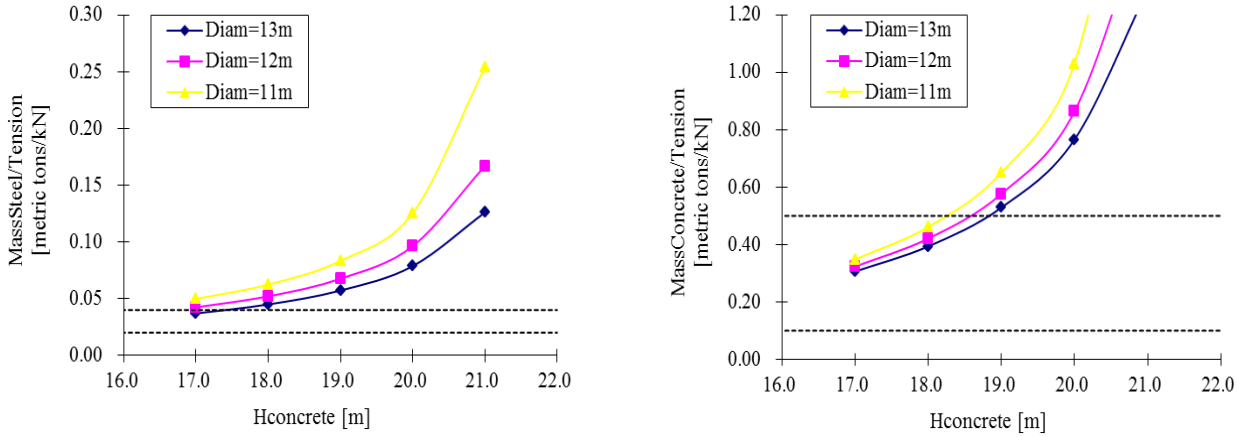

(b) Case 2: SWT = 0.0253 m

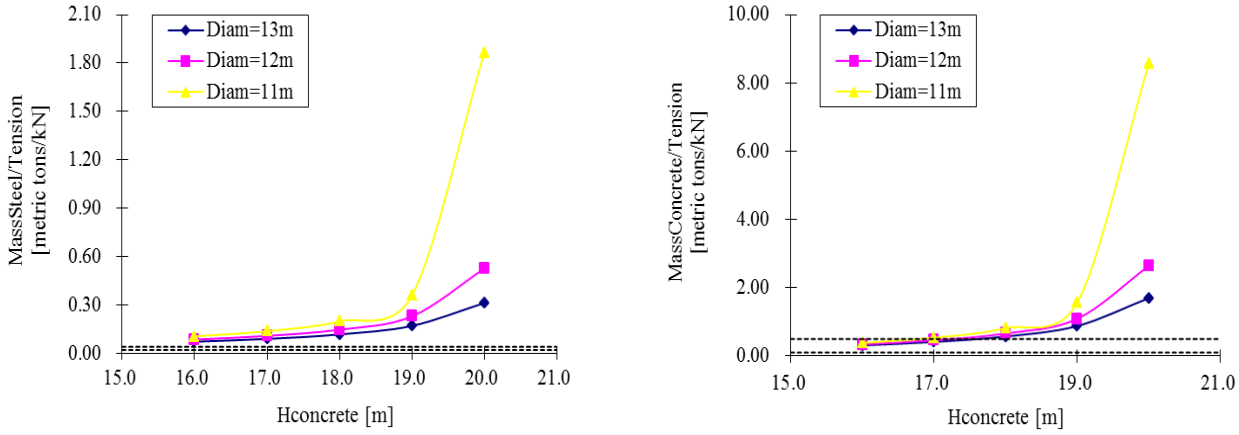

(c) Case 3: SWT = 0.045 m

FIGURE 4.2 Optimized mass property ratio for three cases with SWT = 0.015 m, 0.0253 m, 0.045 m.

In the same figures, the lower limit and upper limit of the total cost are also shown for each case. By comparing the total cost between the three cases, it's obvious that the system costs much more when SWT = 0.045 m, and its steel mass is also greater than 1000 metric tons limit, while the other two cases' are much below this limitation. But when observe the varying of the total cost within one case, it increases with larger diameter and decreases with the increase of concrete ballast height. These conclusions may be explained by the reason that steel mass is the main cost driver in the support platform design.

FIGURE 4.2 presents the results based on the economic optimized mass property ratio in section 3.3.3. It is obvious in the figure that the steel mass of case three has been greatly out of the economic optimized range. These figures also show that the mass property ratio decrease with larger platform diameter, while increase with more concrete ballast. In sum, the height of concrete ballast can be narrowed to certain range after step 1, considering both basic stability requirements and dominant cost drivers. See summary in TABLE 4.2. However, the cost oscillates accordance with the market, such that the following steps are very necessary to see whether these economic optimized designs also satisfy other considerations. Otherwise, this iterative process needs to be repeated, even enlarger these optimized mass property ratios if necessary to ensure a safe design.

Diameter [m]	Case 1: SWT = 0.015 m	Case 2: SWT = 0.0253 m
13	17.7~19.4	17.2~17.4
12	18.0~19.2	--
11	18.5~19.0	--

TABLE 4.2 Step 1 design result for concrete ballast height.

4.2.2 Step 2: Pitch, Surge Restoring

As presented above in the steady-state performance criteria, the minimum pitch restoring coefficient, $C_{55,Limit}$ equals 4.126E+08 Nm to ensure that the pitch angle is less than 10 degrees. As for the surge restoring coefficients, its limit value is related to water depth. For example, in 200 m water depth case, the unstretched length of the taut tether is assumed to be 128 m. In order to ensure the angle that the tether forms with the vertical is less than 5 degree, the maximum surge displacement and the minimum surge restoring coefficients are found to be 11.2 m and 71710 N/m, as shown in equation 4.1.

$$C_{11,\lim it} = \frac{F_{thrust}}{\eta_{1,\max}} = \frac{800\ [kN]}{L_{unstretched} \sin 5^{o}\ [m]} = \frac{800\ [kN]}{11.156\ [m]} = 71710.71\ [N/m] \qquad (4.1)$$

In this case, the minimum pretension corresponding to both $C_{11,limit}$ and $C_{55,limit}$ in 200 m water depth case is calculated to be 9.18E+06 N.

FIGURE 4.3 presents the restoring coefficient in surge and pitch case by case, from which the range of concrete ballast height can be further settled down. These figures show us that with the larger platform diameter, both surge and pitch restoring coefficients are larger, but when the concrete ballast height increases, the pitch restoring coefficients increase while the surge restoring coefficients decrease.

After the second step of the preliminary design, critical properties of each case are listed in TABLE 4.3 for a general picture of the designs achieved so far. The concrete heights in the table are chosen based on the step 1 results as well as the value corresponding to the intersection of surge and pitch restoring coefficients in the figures.

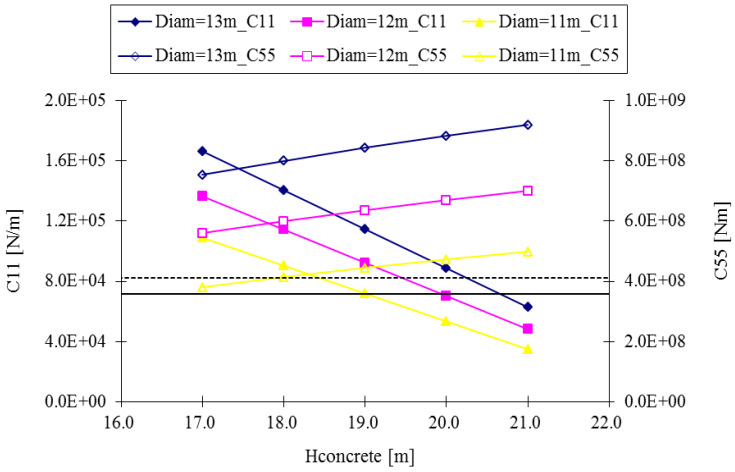

(a) Case 1: SWT = 0.015 m

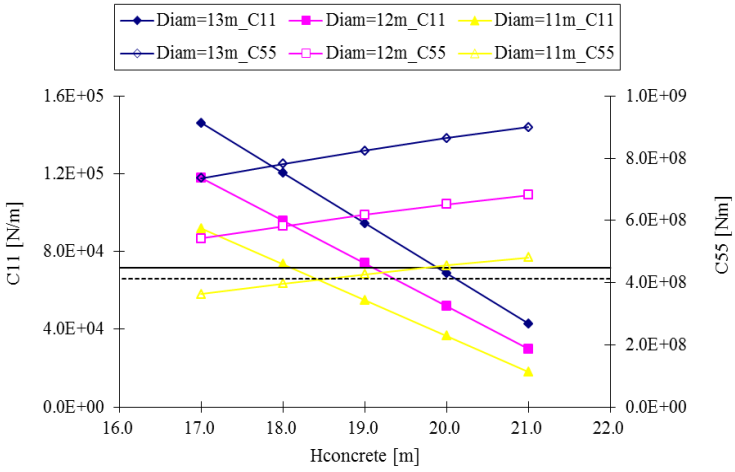

(b) Case 2: SWT = 0.0253 m

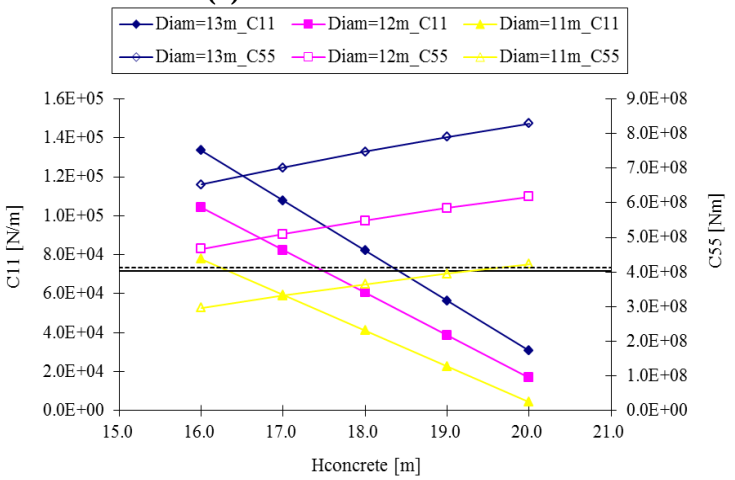

(c) Case 3: SWT = 0.045 m

FIGURE 4.3 Surge and pitch restoring stiffness for three cases with SWT =0.015 m, 0.0253 m, 0.045 m.

Properties	Case 1		Case 2	
	SWT= 0.015 m		SWT= 0.0253 m	
Diameter [m]	13	12	11	13
Hconcrete [m]	17.9	18.2	18.7	17.4
Hydrostatic Coefficient	5321.1	3572.8	3312.4	4944.5
Total Cost_Lower [million]	0.82441	0.70121	0.5841	0.97024
Total Cost_Upper [million]	1.69536	1.4423	1.20546	1.86954
Pretension [kN]	18324.5	14085.7	9922.1	17403.3
Surge Restoring Coefficient [kN/m]	143.16	110.04	77.52	135.96
Pitch Restoring Coefficient [kNm]	795629.3	606385.2	435140.4	754534.1
Surge Natural Frequency [rad/s]	0.09459	0.08904	0.08052	0.09192
Pitch Natural Frequency [rad/s]	0.13242	0.12397	0.11299	0.12908
Total Mass [metric tons]	7065.38	6222.45	5472.75	7159.32
Total Displacement [metric tons]	8933.99	7658.82	6484.54	8933.99

TABLE 4.3 Properties of the optimized design after Step 2.

4.2.3 Step 3: Natural Frequency, Tether Property

FIGURE 4.4 shows the results of natural frequencies in surge and pitch modes. The theoretical calculation of the mass matrix and the added mass coefficients are based on the equations explained in section 3.3.2.1. From the following pictures, the natural frequencies in surge and pitch are all below 0.14 rad/s, which is out of the energy-concentrated frequency domain.

Furthermore, before concerning the heave natural frequency, it is necessary to discuss the tether properties based on the results obtained from the frontier two steps. Accounting for the dynamic offset of the tether tension during time-domain simulation, the maximum tension of the chosen tether should be much larger than the pretension obtained from the optimized design, 1.83E+07 N for instant from TABLE 4.3. Based on

the API 5L steel pipe dimension and weight information as well as the steel hardness of various types of tubes in manufactory, the tether in this work is preliminary chosen with 603 mm diameter, 44 mm thickness, and the steel hardness type is API 5L X65, whose yield strength is 60200 psi (1 pound in square inch). In this case, the line mass per unit length is 606.57 kg/m, the *EA* stiffness is 1.62E+10 Nm, and the maximum tension can be calculated as 3.48E+07 N, much larger than the pretension.

With the tether properties defined, the heave natural frequency can thereby be found among the platform geometry ranges after step 1. The natural frequencies in heave motion shown in TABLE 4.4 are all much larger than 2.5 rad/s, the upper boundary of the power concentrated wave frequency domain.

Steel Wall Thickness (m)	Diameter (m)	Hconcrete (m)	ωn_33 (rad/sec)
Case 1 = 0.015 m	13	17.7	4.19561
		19.4	4.03792
	12	18.0	4.46077
		19.2	4.34475
	11	18.5	4.74421
		19.0	4.69420
Case 2 = 0.0253 m	13	17.2	4.16852
		17.4	4.14944

TABLE 4.4 Heave natural frequencies of optimized designs.

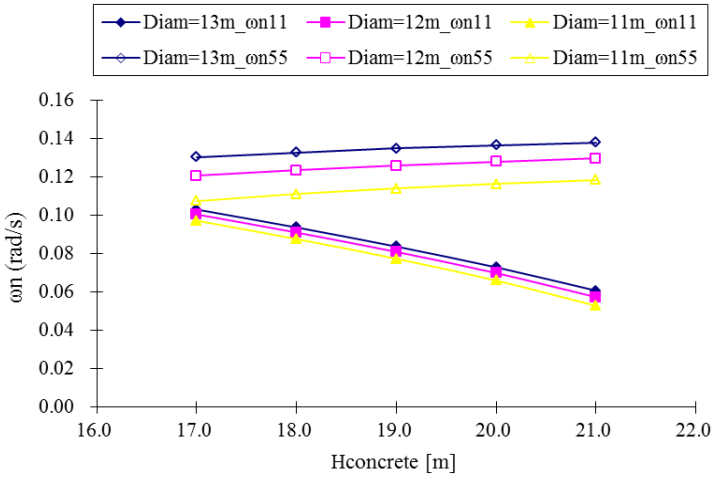

(a) Case 1: SWT = 0.015 m

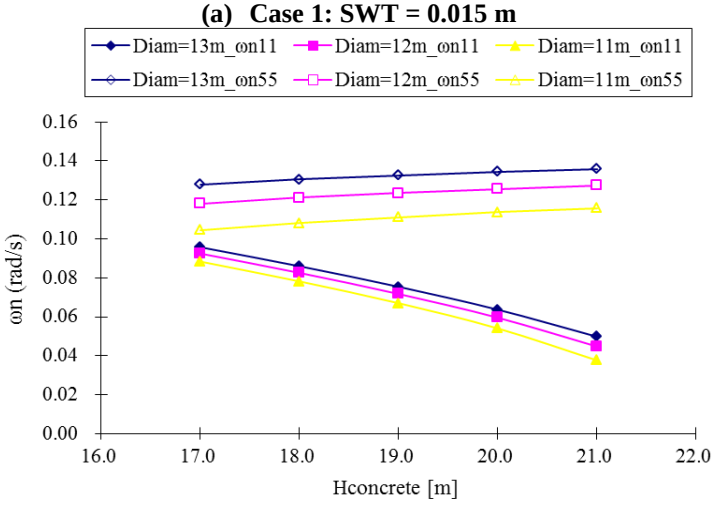

(b) Case 2: SWT = 0.0253 m

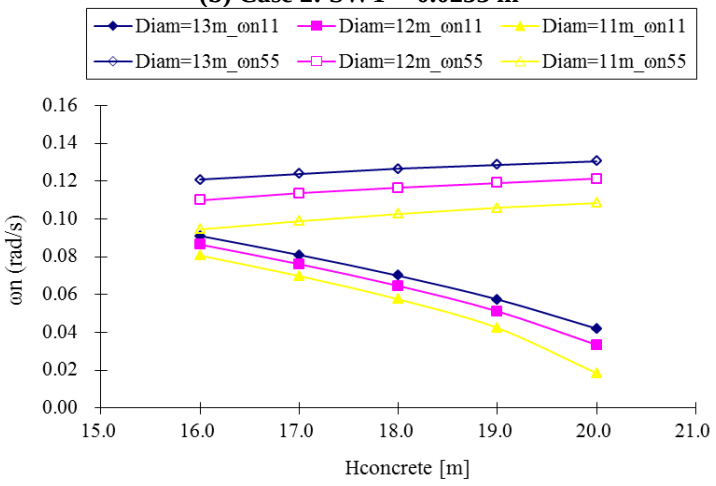

(c) Case 3: SWT = 0.045 m

FIGURE 4.4 Surge and pitch natural frequencies for three cases with SWT = 0.015 m, 0.0253 m, 0.045 m.

4.3 Preliminary Design Results

Based on the above iterative design process explained step by step and the synthetically considerations of all design criteria, the static operating point can be found for the optimized models through the linearization process in FAST (with rotor azimuth equals zero degree), see TABLE 4.5.

Case			SWT = 0.015 m		SWT = 0.0253 m
Diameter	[m]	13	12	11	13
Hconcrete	[m]	17.9	18.2	18.7	17.4
Surge	[m]	9.20	13.97	18.72	13.09
Sway	[m]	-0.1673	-0.1870	-0.1943	-0.1243
Heave	[m]	-0.1597	-0.5286	-1.0330	-0.3179
Roll	[deg]	0.0015	0.0034	0.0037	0.0035
Pitch	[deg]	0.0820	0.1065	0.1485	0.0926
Yaw	[deg]	-0.00053	0.00005	0.00108	0.00023

TABLE 4.5 Static operating points

In the steady linearization in FAST, the wind is giving in the *x*-direction with constant speed of 11 m/s, and no wave excitation is simulated. The control system is turned off as well. From the results shown in the above table, only the first case, which with 0.015m SWT and 13 m platform diameter, has its steady-state surge displacement less than the maximum allowable value of approximately 11.2 m in 200 m water depth to ensure that the angles the tether forms with the vertical plane does not exceed 5 degrees during operation.

In this way, the preliminary optimized model, that satisfies all the static, dynamic and economic requirements, is finally defined as presented in TABLE 4.6.

Specifications		Optimized Model
Platform draft	[m]	72
Elevation of taper top below SWL	[m]	4
Elevation of taper bottom below SWL	[m]	12
Platform diameter above taper	[m]	6.5
Platform diameter below taper	[m]	13
Concrete ballast height	[m]	18
Platform steel wall thickness (SWT)	[m]	0.015
Total cost	[million]	0.82~1.69
Steel mass	[metric tons]	411.376
System mass	[metric tons]	7099.20
Center of gravity (System)	[m]	-50.1373
Total displacement	[metric tons]	8934
Center of buoyancy	[m]	-39.0355
Platform roll/pitch inertia about SWL	[kg·m2]	2.5134E+10
Platform yaw inertia about centerline	[kg·m2]	1.4306E+08
Pretension	[kN]	17992.8
Surge restoring coefficient	[kN/m]	140.57
Pitch restoring coefficient	[kN·m]	800118.7
Max. line tension	[kN]	3.48E+04
Line cross-area	[m2]	0.0773
EA stiffness unit length	[Nm]	1.62E+10
Line mass density	[kg/m]	606.57
Surge/sway natural frequency	[rad/s]	0.098
Heave natural frequency	[rad/s]	4.166
Pitch/roll natural frequency	[rad/s]	0.112
Yaw natural frequency	[rad/s]	0.713

TABLE 4.6 Derived operational model properties for NREL 5 MW Wind Turbine.

4.4 Model Verification

4.4.1 KC number, Oscillatory Reynolds number, D/λ

Based on the theories explained in Appendix A, the Keulegan-Carpenter number, *KC*, the oscillatory Reynolds number, *Re*, and the diameter to wavelength ratio, D/λ, which are the main factors that the formulations for the hydrodynamic loads apply to separated and non-separated flows depend on, are as function of depth *z* along the spar by applying the equations A.3, A.4 and the dispassion relationship.

The water depth is taken to be 200 m. The external geometry of the floating platform has been defined above and the periodic sea states are given in the TABLE 4.7 as follows.

Sea State	Tp(s)	Hs(m)
1	2.00	0.09
2	4.80	0.67
3	6.50	1.40
4	8.10	2.44
5	9.70	3.66
6	11.30	5.49
7	13.60	9.14
8	17.00	15.24

TABLE 4.7 Sea state definitions.

FIGURE 4.5 shows that the *KC* number and oscillatory Reynolds number in the present research decrease with depth along the spar and increase with severity in the wave conditions.

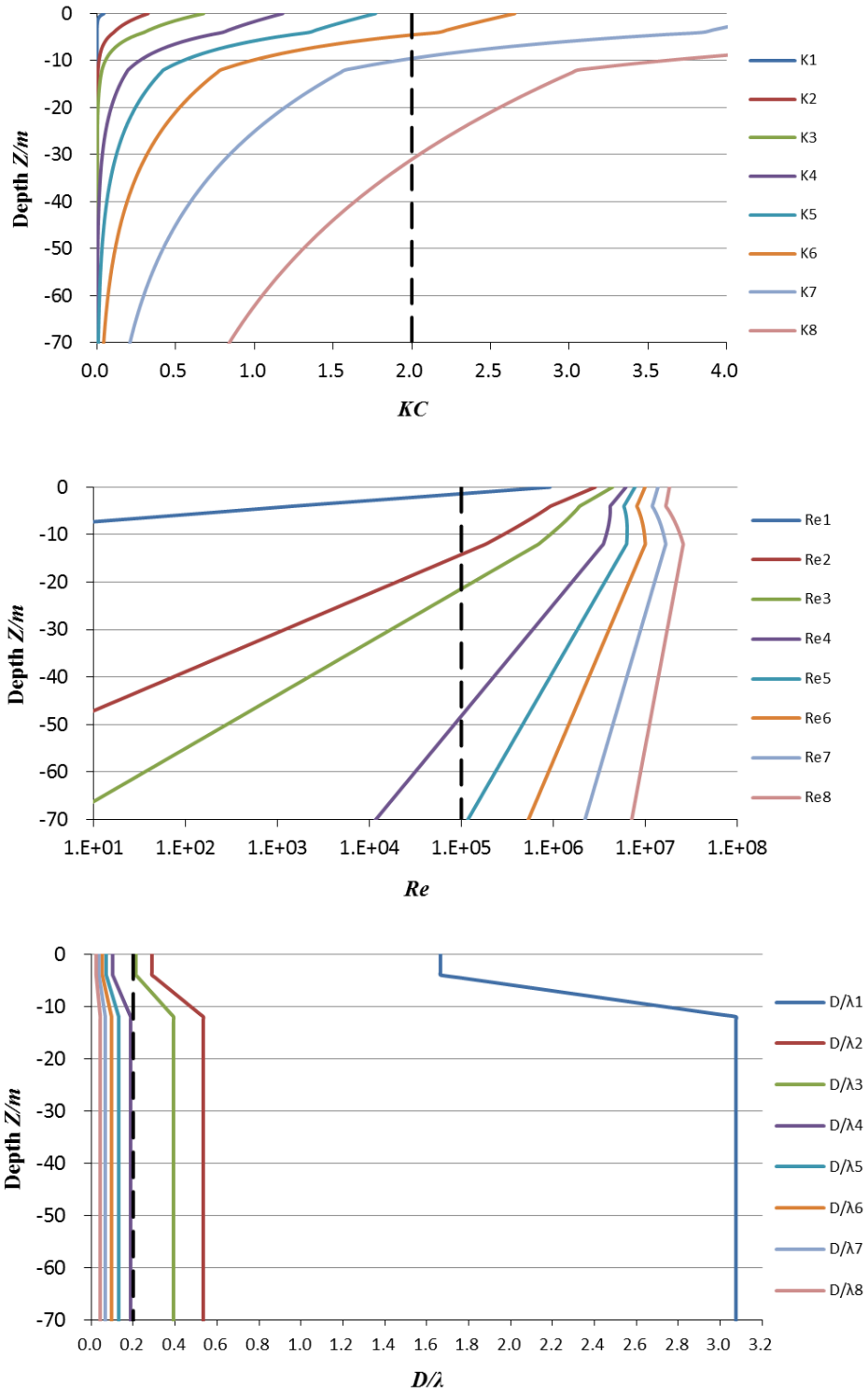

FIGURE 4.5 Dimensionless parameters for the optimized model.

Potential theory applied only for *KC* values lower than 2, since flow separation occurs when *KC* number exceeds 2. Consequently, from the first chart in FIGURE 4.5, except the extreme wave conditions where separation will occur along the upper portions of the platform, the potential-flow theory can be applied all along the spar. The bottom chart in FIGURE 4.5 shows that, for the optimized model, diameter to wavelength ratio decrease with severity of the wave conditions and its value is even lower above the taper. Since diffraction effects are important when D/λ exceeds 0.2, for this work, diffraction effects are only important when the wave conditions are mild, such as the sea state 1, 2, and 3 as defined above, where the hydrodynamic loads are small anyway.

Also, the middle chart of the FIGURE 4.5 shows that the optimized model in this work experiences oscillatory Reynolds numbers exceeding 10^5 in most important conditions from moderate to severe. Thus the viscous-drag coefficient, C_D, is taken to be 0.6, the same value as it is in Hywind-OC3 project, and it is also the typical coefficient for cylinder at high Reynolds numbers.

4.4.2 Hydrodynamic Properties

HydroGen, an indoor program, is able to generate the same hydrodynamic outputs as WAMIT, and act as the HydroDyn preprocessor for the linear frequency-domain analysis of the interaction between surface waves and offshore structures. The geometry of the structure in HydroGen is represented by the numerical panel method and the analysis is limited to rigid bodies. HydroGen, similar with WAMIT, uses a three-dimensional numerical-panel method in the frequency-domain to solve the linearized

potential-flow hydrodynamic radiation and diffraction problems for the interaction of surface waves with offshore platforms of arbitrary geometry.

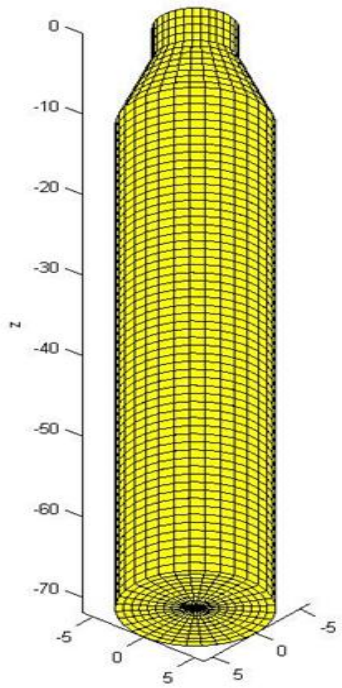

FIGURE 4.6 Model panel mesh.

The optimized platform in the thesis was modeled within two geometric planes ($x = 0$ and $y = 0$) of symmetry with 656 quadratic panels within a quarter of the body. See FIGURE 4.6 for the panel mesh with both symmetries. To improve the accuracy of the HydroGen results, the three default settings are followed by: (1) remove the effect of the irregular frequencies that program automatically discretizes the interior free surface, (2) integrate the logarithmic singularity in the Green function analytically, and (3) choose direct solver for the linear system of equations, considering for the infinite-frequency output.

FIGURE 4.7 and FIGURE 4.8 give the magnitude and phase of the calculated wave excitation force $X_i(\omega)$, added mass $A_{ij}(\omega)$ and damping $B_{ij}(\omega)$ matrix coefficients, as a function of wave frequency for incident waves with heading β equals 0 degree (that is along the positive x-axis). Due to the symmetries of the model, the loads in the direction of the sway, roll and yaw DOFs are zero. The magnitude of the wave excitation in the direction of surge, heave and pitch reach a peak around a wave frequency 0.6 rad/s and then drops at higher wave frequencies, except for the heave force which reverses sign at 0.2 rad/s.

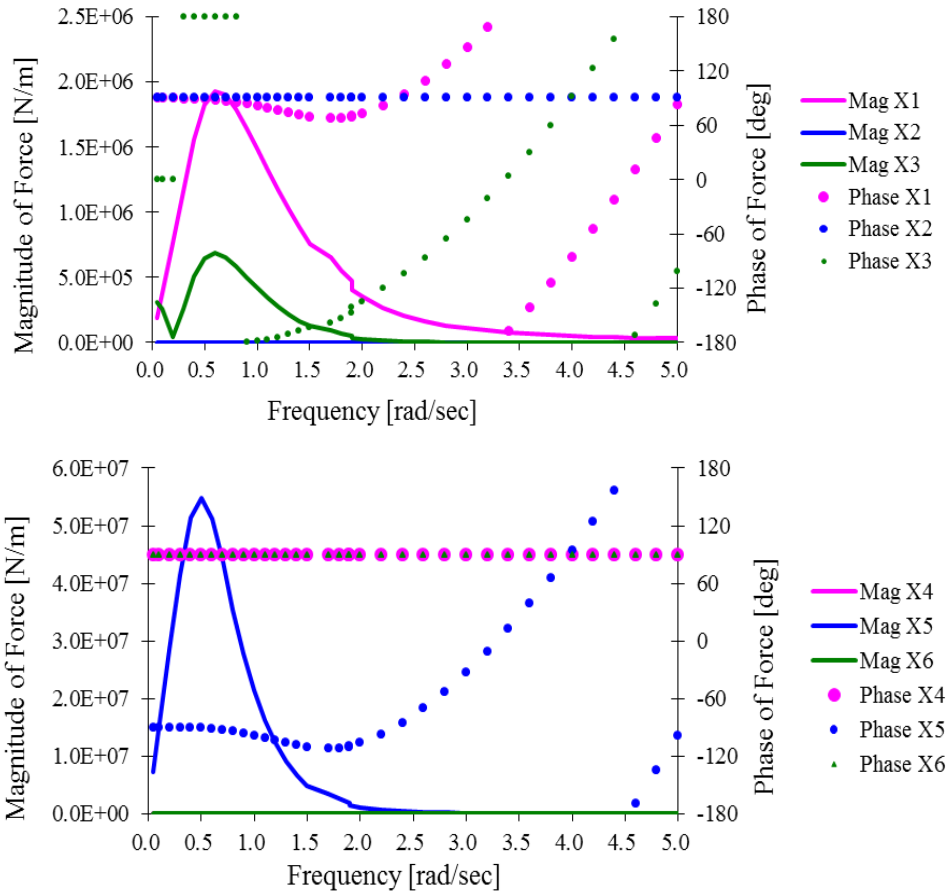

FIGURE 4.7 Hydrodynamic wave excitation per unit amplitude for optimized model.

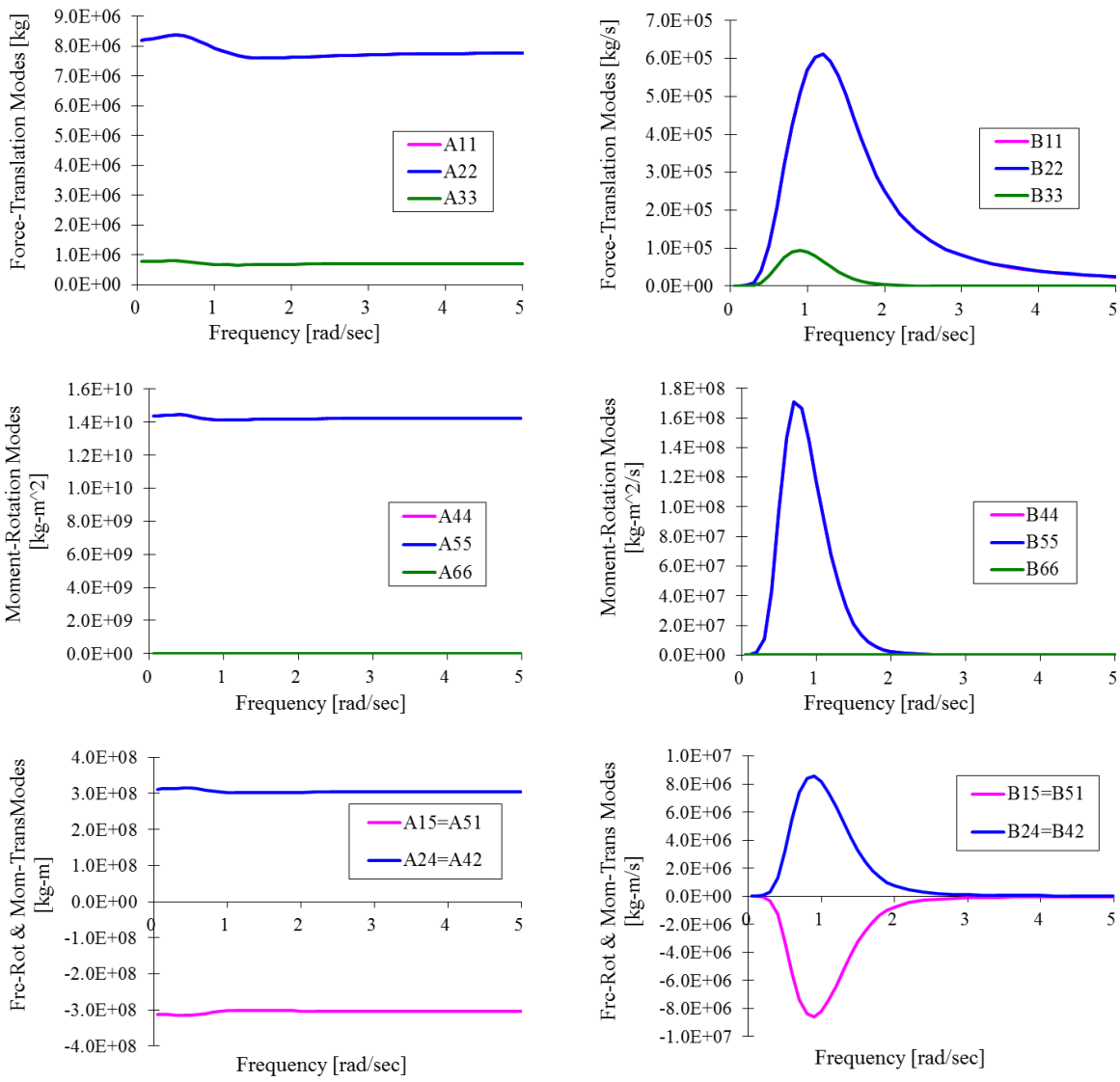

FIGURE 4.8 Hydrodynamic added mass and damping for the optimized model.

As shown in FIGURE 4.8, the values of the damping in the moment-rotation (i,j=4,5,6), force-rotation (i=1,2, j=4,5) and moment-translation (i=4,5,j=1,2) modes are considerably smaller than those of added mass, except in the force-translation modes (i,j=1,2,3), which imply the importance of the linear radiation damping. The added-mass coefficient, C_A, can also be determined according to the A_{11} value if it is assumed that C_A

is independent of depth and that the motion is of low-frequency so that the first term in Morison's equation $C_A\rho V_0$ is equal to zero-frequency limit of A_{11} (comparing equation A.18 with A.19). Therefore, C_A is taken to be 0.9.

4.4.3 Optimized Model Simulation in FAST

The HydroDyn model in FAST can be prepared based on the optimized design results under the environmental conditions as: 15 m/s steady wind with no shear in *x*-direction, incident waves generated by JONSWAP/Pierson-Moskowitz model with 6 m significant wave height, 10 s peak spectral period, heading 0-deg direction. TABLE 4.8 summaries the statistical analysis for the optimized models in time history after the whole system is stable and the transient effect has disappeared. See FIGURE 4.9 for the time-simulation results and their corresponding spectra of the platform response.

DOFs	Surge [m]	Sway [m]	Heave [m]	Roll [deg]	Pitch [deg]	Yaw [deg]	Tension [kN]
Average	6.706	-0.203	-0.258	0.152	2.872	-0.425	1.74E+04
Max.	11.142	-0.038	0.141	0.267	4.679	0.481	2.11E+04
Min.	1.867	-0.382	-0.254	0.062	0.963	-1.212	1.37E+04
SD	1.276	0.037	0.051	0.018	0.587	0.216	1178.54

TABLE 4.8 Statistic analysis of optimized model.

Overall, the 6DOF displacements are reasonable. Since the wind and waves are excited in *x*-direction only, the surge/pitch displacements are the dominant motion with greater magnitude than the sway/roll/yaw motions. In this single-tether system, the heave displacements are mostly caused by the set-down effects of the surge motions as the high

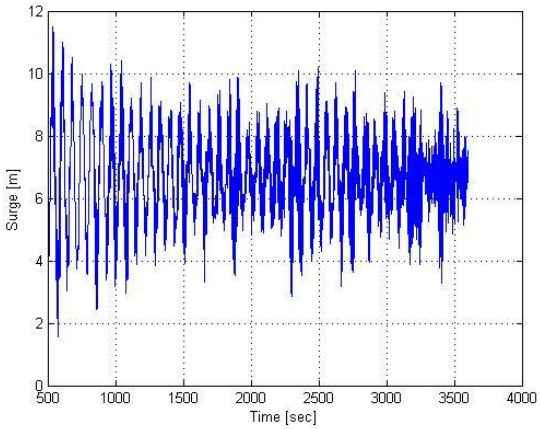

(b-1) Time-History of Platform Surge

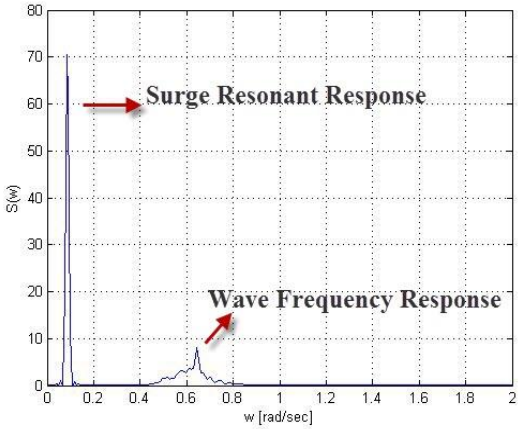

(b-2) Spectra of Platform Surge

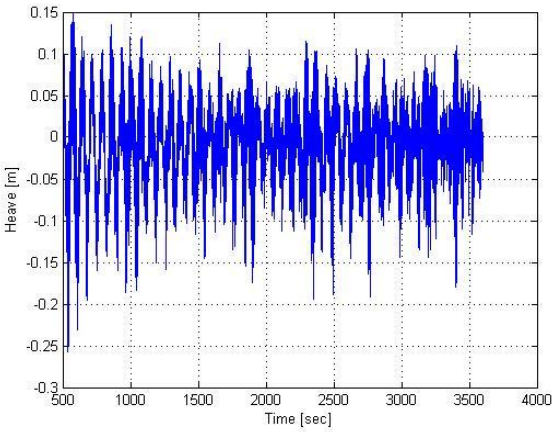

(c-1) Time-History of Platform Heave

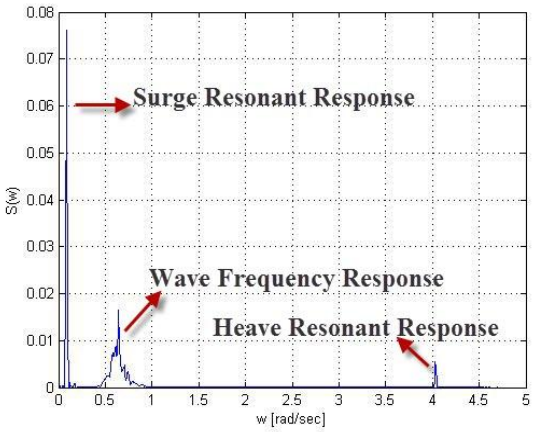

(c-2) Spectra of Platform Heave

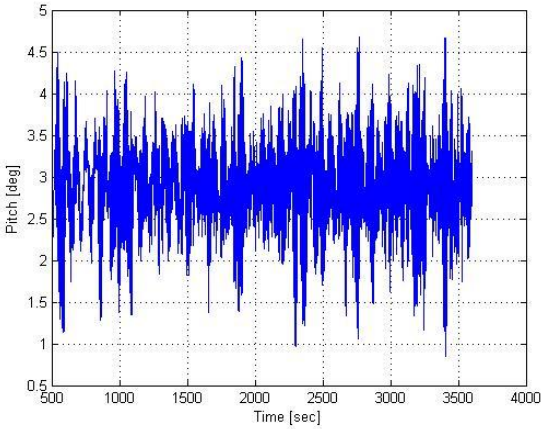

(d-1) Time-History of Platform Pitch

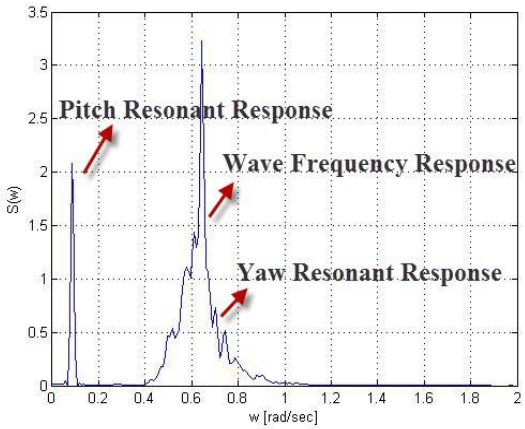

(d-2) Spectra of Platform Pitch

FIGURE 4.9 Time-history and spectra of the optimized model in FAST.
(wave heading = 0 deg, Hs = 6m, Tp = 10s, wind speed = 15m/s)

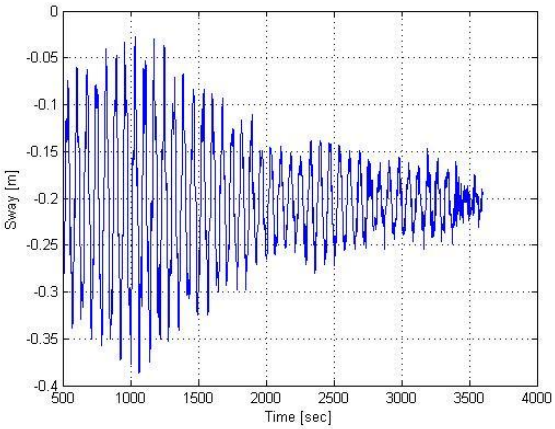

(e-1) Time-History of Platform Sway

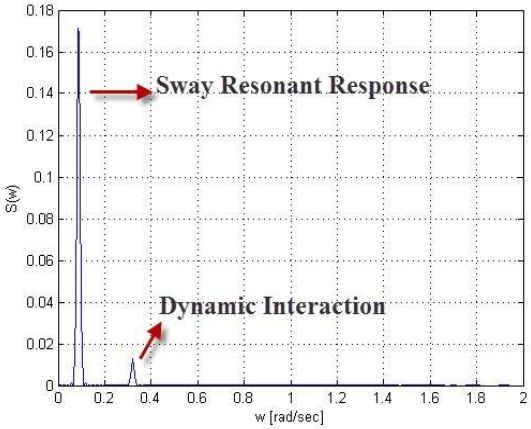

(e-2) Spectra of Platform Sway

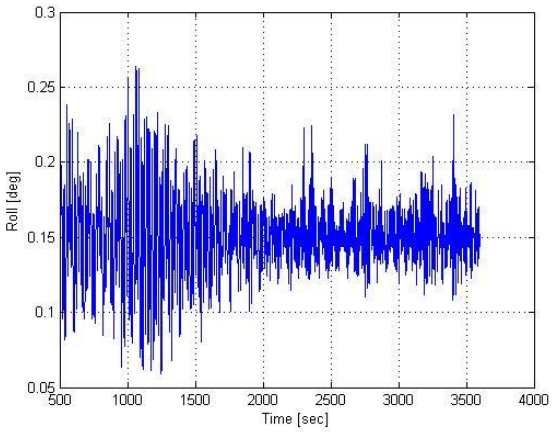

(f-1) Time-History of Platform Roll

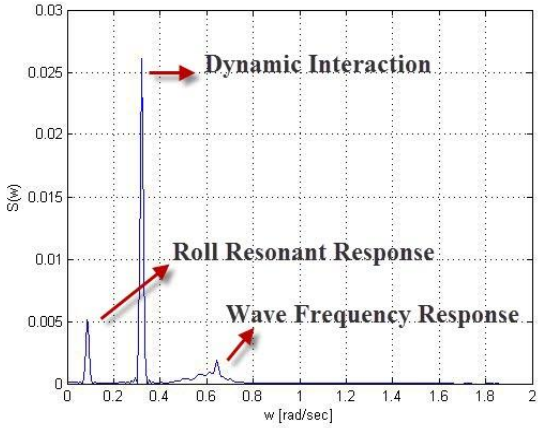

(f-2) Spectra of Platform Roll

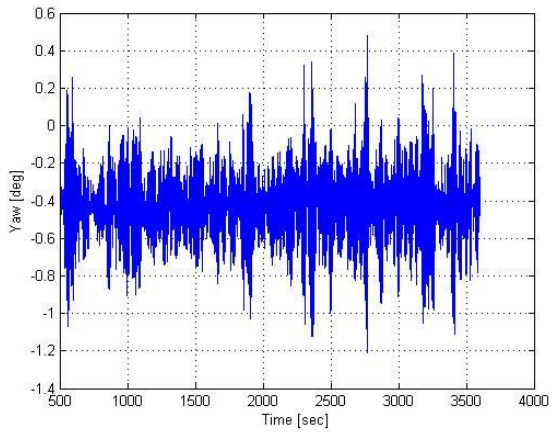

(g-1) Time-History of Platform Yaw

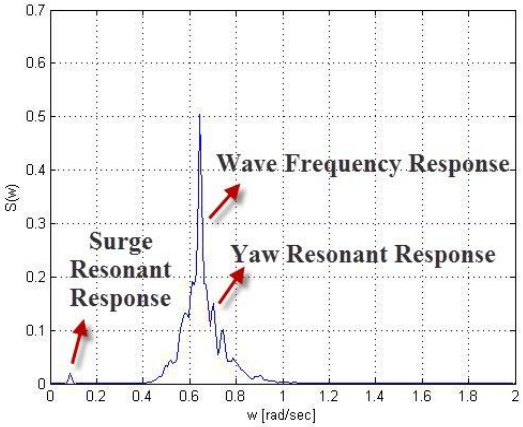

(g-2) Spectra of Platform Yaw

FIGURE 4.9 Continued.

peak shown in heave spectrum at the natural frequencies of surge. Since the roll/pitch and surge/sway natural frequency both around 0.1 rad/s, the responses there are quite significant. Considering the symmetry of the submerged hull, the sway-roll-yaw motion should be zero. However, in the fully dynamic coupled analysis case, they show nonzero displacement because of the dynamic interaction between the hull and turbine (aerodynamic loading, rotor rotation, gyroscopic effects, turbine flexibility, etc.), which can be easily recognized by the peak at the frequency about *0.32* rad/s in transverse sway-roll-yaw motion, but not shown in surge-heave-pitch.

The heave natural frequency (around 4.06 rad/sec) does not cause any resonance problems, since they are significantly larger than the excitation frequencies. And the wave excitation frequency can be clearly distinguished in FIGURE 4.9. Since the yaw natural frequency has coincided with the high-energy concentration of the wave spectrum, see FIGURE 4.9 (g-2), which was assumed not to cause significant problems in preliminary design processes, but would transfer significant motion through coupled mode such as pitch, as shown in FIGURE 4.9 (d-2). Further examination is therefore needed for this behavior. One consideration is to place the yaw natural frequency either below or above the high-energy concentration range. Besides, it is also obvious that the natural frequencies obtained through time-domain simulation have shifted from the original calculated values in the frequency domain. It is the reason that a time-domain simulation is necessary to find more appropriate natural frequencies.

FIGURE 4.10 presents the tether tension at fairlead and anchor position. As shown in the spectrum, the tether tensions are dependent on the pitch motion, and the pitch motion is also affected by motion in yaw mode. The tether tensions are greatly depended on the wave excitation. The anchor tension is a little smaller than the fairlead tension, and as the time-series shown, the tether does not go slack during the simulation. However, the tensions are also characterized by two frequencies, which is unfavorable considering fatigue.

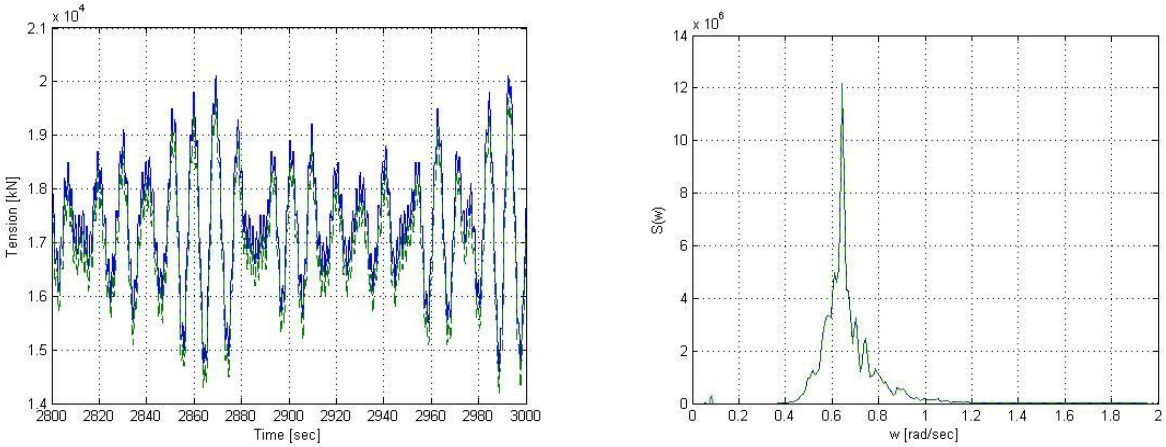

(a) Time-History of Tether Tension (200s) **(b) Spectra of Tether Tension**

FIGURE 4.10 Time-history and spectra of the tether tension.
(Solid Blue: fairlead tension; Dash Green: anchor tension)

4.4.4 Comparison of RAOs in HydroGen & FAST

Without former models for comparison, a code-by-code verification of the FAST model with the indoor code HydroGen has been conducted in this section. The frequency-domain approach was applied in FAST and its result was thus compared with

the frequency-domain RAOs calculations in HydroGen, as the detailed process flowchart shown in section 3.2.

The frequency-domain model only calculates the 6 DOFs of platform; the turbine is considered rigid; the mass, stiffness and damping matrices of them can be obtained by running a linearized model in FAST. Therefore, in this FAST model all DOFs of the wind turbine are disabled except for the platform DOFs. The control system is turned off, no waves are simulated, and the wind is steady with no shear at the speed of 11 m/s.

However, the results of the mass, stiffness and damping matrices from FAST linearization cannot be directly used as the external inputs in HydroGen. HydroGen automatically calculates the hydrostatic restoring matrix; therefore the stiffness matrix from the FAST linearization must be corrected for it. It is also important to exclude the gravity restoring terms, which can be easily realized by setting the CG position to zero.

The RAOs in FAST are obtained simply by running numerous simulations with 1-m amplitude waves at different wave periods. After certain seconds of simulation (around 1400 seconds), it is important to make sure that the transient effects have disappeared and the response fully converged to an oscillation solution of the constant amplitudes with the wave excitation periods. The resulting RAOs of the platform are presented in FIGURE 4.11. To imitate the frequency-domain approach in FAST, the turbine is also simulated as a completely rigid structure, and the wind condition is the same as it is in FAST linearization process. Since all the outputs from HydroGen are non-dimensionalized, and the rotational displacements from FAST time-simulation are in degrees, it is necessary to non-dimensionalize the RAOs for roll, pitch and yaw by

converting it to radians and multiplying by the characteristic length, which is taken as unit in this case.

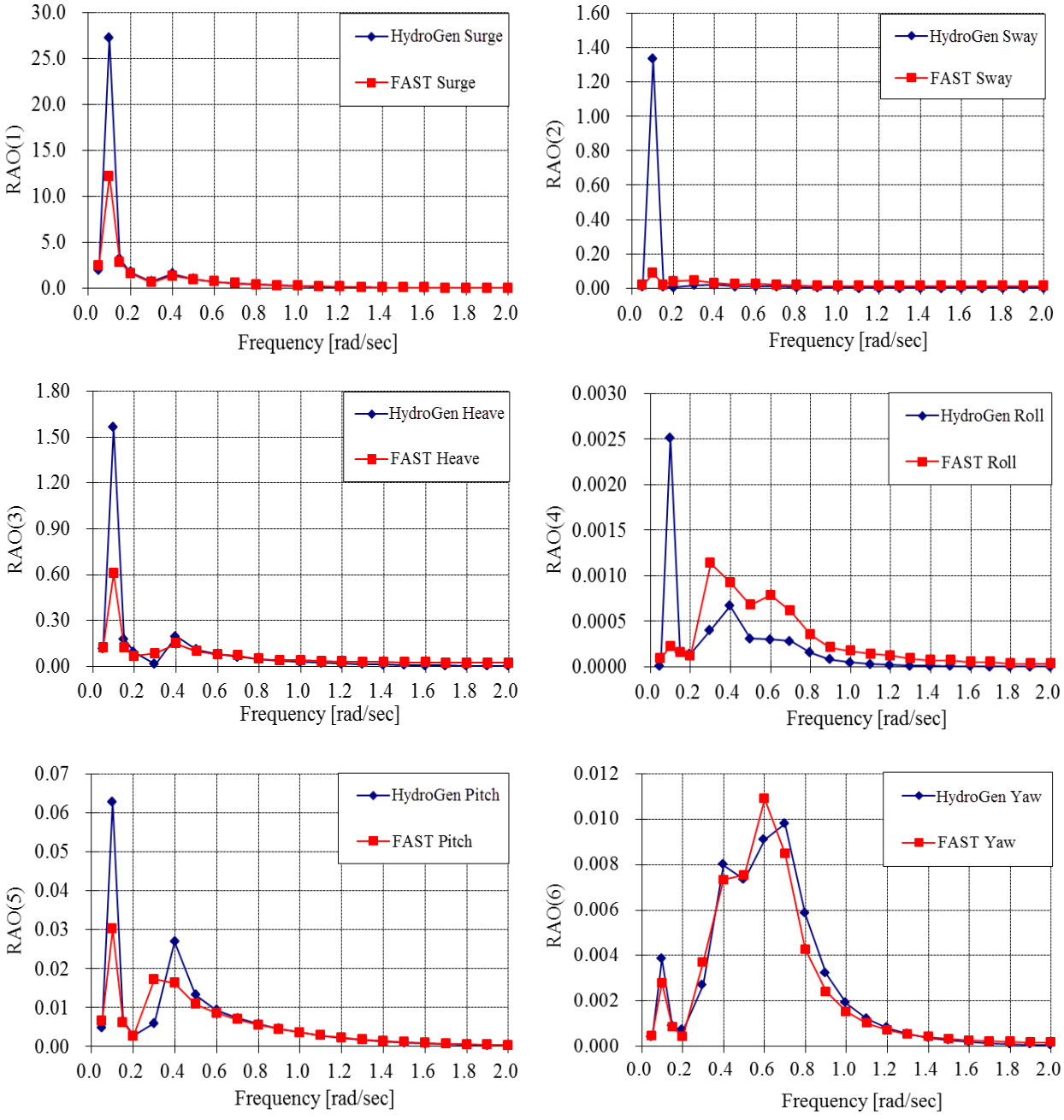

FIGURE 4.11 Platform RAOs of optimized model in HydroGen and FAST.

The experience show that the platform periodic response has the same period as the excited wave, except for the heave mode which has approximately half of the period. This may be explained that when the platform surges downwind it heaves downward and when it surges upwind it heaves downward as well. Therefore, the heave mode appears to have half the period as surge (same as the excited wave period).

As discussed by Matha (2010), the peak response in the time-domain computations is shifted compared to the natural frequencies obtained in frequency-domain calculations. In this case, the natural frequencies of surge/sway, roll/pitch modes in low frequency domain are consistent for both codes, while the yaw natural frequency has been shifted from 0.72 rad/s to 0.6 rad/s. These deviations in natural frequencies are due to turbine flexibility, the couplings between platform motions and the tower and blades— which mostly are not captured in a typical frequency-domain approach—have a significant influence on the results. It also proves that the frequency-domain analysis where the whole system is assumed rigid is not enough to compute appropriate natural frequencies that a time-domain analysis is necessary.

Besides the position of the resonance peaks, the magnitudes of the natural frequency responses also shown some difference, which may be explained that damping provided by nonlinearities is not included in the HydroGen calculations. And the coupling effects with the turbine rotation, the gyroscopic motion can also make some difference to the time-simulation RAOs, as shown in the sway RAO figure, the rotor rotation keeps a very small sway offset at high frequencies, and the high peaks in transverse motions are caused by the gyroscopic moment on wind turbine. Since the

trends of the RAOs in the dominant modes are quite consistent, and the magnitudes of the transverse sway-roll-yaw motions are relatively small compared to surge-heave-pitch, the differences shown in these modes are therefore very small and ignorable.

The experience dealing with this problem also indicate that it is not straightforward to calculate accurate RAOs in FAST, since the output oscillations do not have constant amplitudes for all wave frequencies in all modes, even after the solution has converged. This adds the difficulties in recording RAOs, which may contribute significantly to the deviations in response magnitudes. However, considering whether the FAST model can be trusted, the results are similar enough to provide verification for this model. The deviations occur more likely from the lack information in how to properly compute RAOs in FAST, which haven't be clarified yet.

5 MODEL MODIFICATION

The concept of the model in this work is based on the patented SWAY® system, which has already been briefly introduced in section 1.2.1. In order to simulate the most similar model as SWAY® in FAST program, certain modifications are necessary concerning the limitation of the model features in FAST.

The patent SWAY® system is based on a floating tower which extends far below the water surface. The tower consists of a floating pole with ballast in the lower end, similar to a floating bottle. The tower has its CG located far below the CB of the tower, which gives the tower sufficient stability to resist the tough loads produced by the large-scale wind turbine mounted on top of it. The mooring system of the SWAY®-type wind turbine is only a single pipe anchored to the seabed. All these general features have already been taken into consideration in the preliminary design process and the optimized model shows satisfying result as well.

Besides, the advantage of the SWAY®-concept wind turbine is its perfect solution to the challenges widely realized for large-scale FOWTs—the fatigue of the towers due to the additional motion and inertia forces compared with a fixed tower. Therefore, SWAY® gives out the solution to locate the yaw bearing, which is normally positioned at the top of the tower, at the bottom of the tower instead (subsea swivel), such that the entire tower would ‘weather-vane’ using a downwind orientated turbine and always keep the same side of the tower towards the wind. It makes the equipment of wire bracings on the tower possible, in order to dramatically increase the tower stiffness and at the same time eliminate the problem of fatigue.

However, this unique advantage is also a challenge in the present research to simulate its special system in FAST, since the mooring lines defined in HydroDyn are set to be hinged joint with the hull and the seabed by default. The following sections present the modifications applied to the original optimized model in FAST. The modified model is also compared to the original optimized model to explore the characteristics arisen from these modifications.

5.1 Downwind Simulation

In this work, the NREL 5MW baseline wind turbine was modified to be in the downwind orientation by changing the turbine configuration parameters, such as the overhang, rotor shaft tilt angle, and blade cone angles, as shown in FIGURE 5.1.

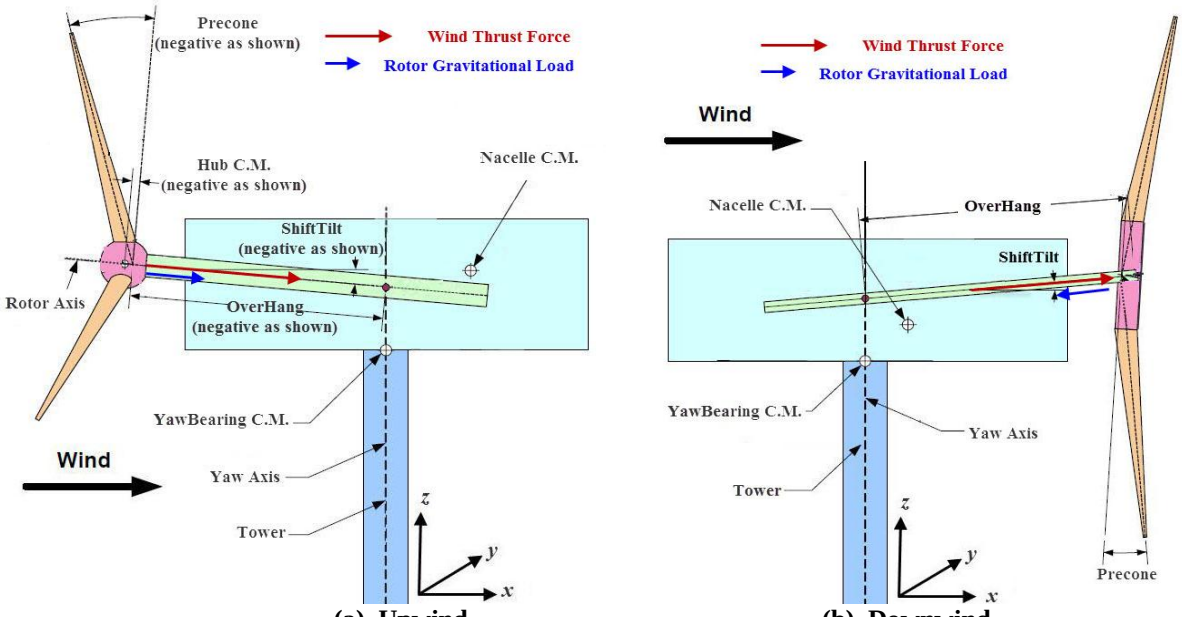

FIGURE 5.1 Layout of conventional of upwind and downwind wind turbine

Since the control system adopted in this work is still the same as the upwind case, it is necessary to check the influence of this modification to see whether the original control system still work for the downwind case. This section will discuss the effect of downwind simulation in the view of platform response, turbine performance and the aerodynamic damping.

The conventional wind turbine control system is designed such that the blades will start pitching once the incoming wind velocity exceeds the rated power speed of the wind turbine. The rotor thrust force will then decrease and the aerodynamic damping contribution becomes negative and increases the displacements of the platform. This phenomenon can be clearly observed in FIGURE 5.2, from which we can see that for both upwind and downwind case, rotor thrusts decrease when the wind speed is larger than the rated power speed, and the downwind rotor thrusts at each wind speed are nearly 194 kN less than the upwind case, except the situation that the wind speed is 18 m/s, where the rotor thrust of upwind case has a sudden drop for some reason.

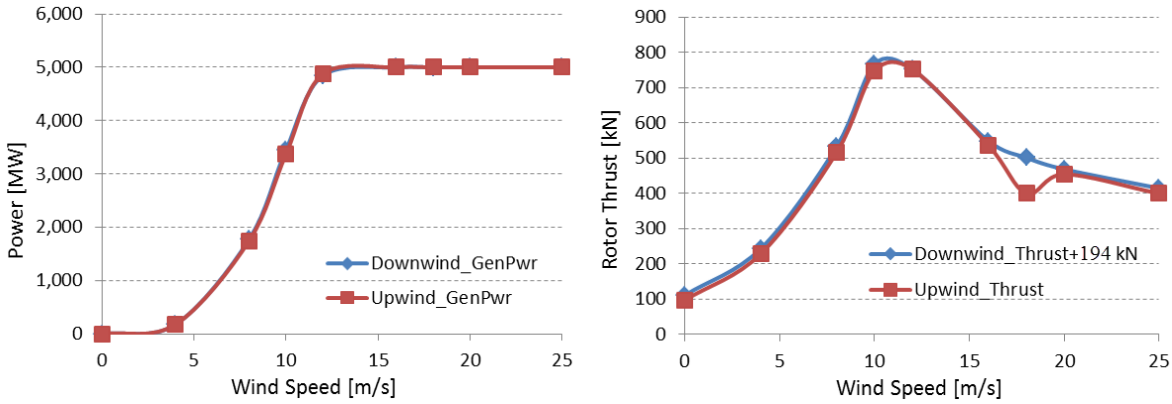

FIGURE 5.2 Power and steady rotor thrusts for upwind and downwind cases.

As shown in FIGURE 5.1, when the rotor orientation was switched from upwind to downwind, the direction of the wind thrust force on the shaft (red arrow) keeps the same while the rotor gravitational load (blue arrow, about 97 kN for the NREL 5MW wind turbine) on the shaft switches to the opposite direction, which should be the result for the 194 kN difference in the total rotor thrust force between the upwind and downwind case. And it is assumed that this difference is mainly due to the shift tilt angle, which has been changing from -5^o to 5^o. To prove it, the same upwind and downwind cases are run both with 0^o shift tilt angle, and the results show that the rotor thrust of upwind and downwind cases are the same. However, for the downwind-orientation model, more complicated problems, such as the tower shadow, vortices shed off of the tower would be arisen, together with series of coupled vibrations, see the spectrum of the platform and turbine performance in FIGURE 5.3.

It is worth mention here that the wind conditions defined for the preliminary design process are all steady wind with no shear. However, in order to see the influence of the control system for the downwind simulation when the wind speed oscillated around the rated power speed, turbulent wind is necessary to be simulated. More detail information about the turbulent wind simulation will be discussed in the following chapter 6. Here, as the results shown in FIGURE 5.3, the turbulent wind is with mean speed of 11.2 m/s in *x*-direction at the hub height 90 m.

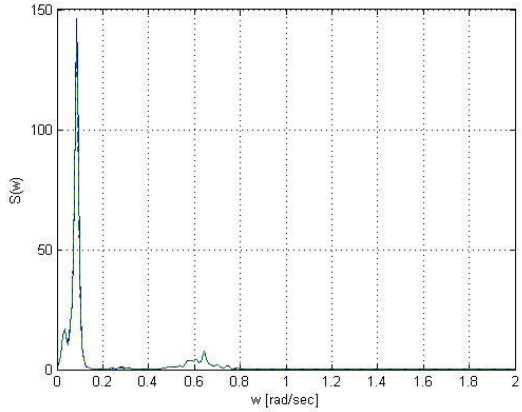

(a) Spectrum of Surge

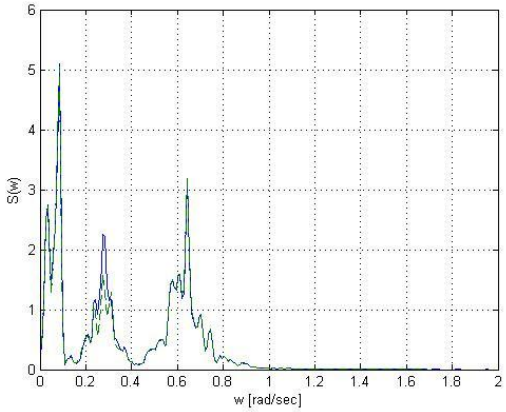

(b) Spectrum of Pitch

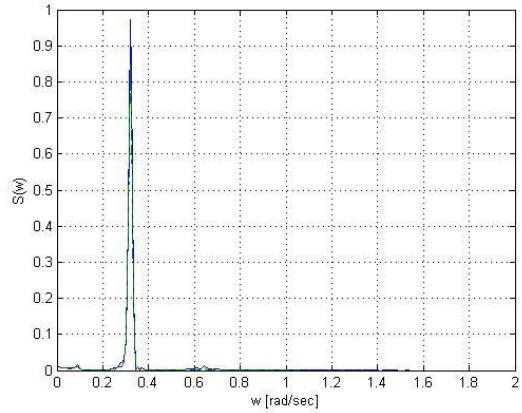

(c) Spectrum of Roll

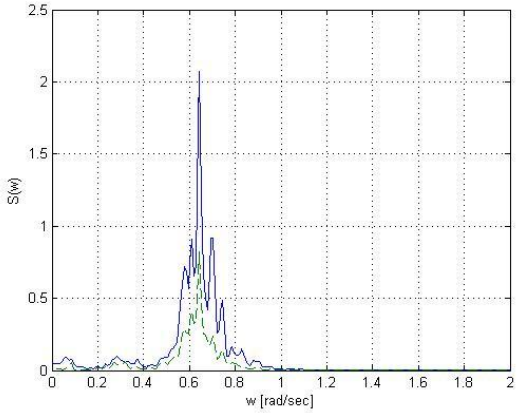

(d) Spectrum of Yaw

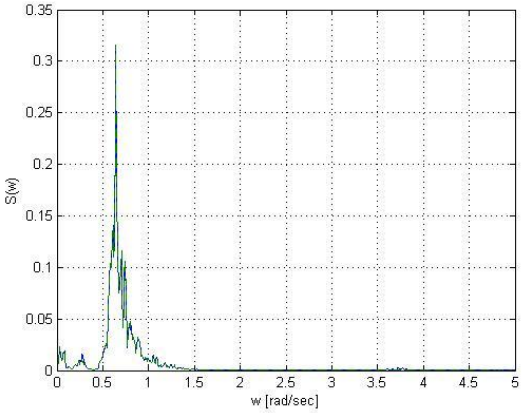

(e) Spectrum of Tower fore-aft Displacement

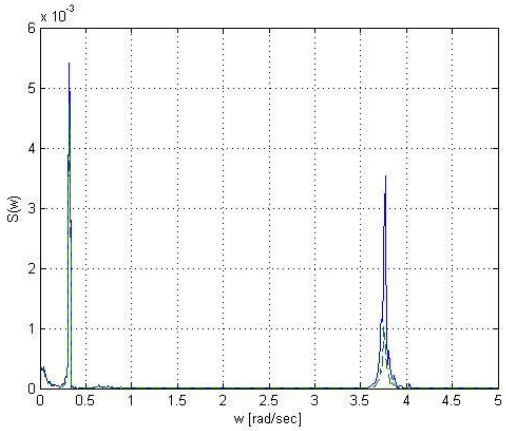

(f) Spectrum of Tower side-to-side Displacement

FIGURE 5.3 Response spectra of platform and tower top displacements Case 2.
(Solid Blue: Downwind; Dash Green: Upwind)

In FIGURE 5.3, the downwind simulation almost has no influence in the surge and pitch displacement, as well as the tower top inline displacement since the same wind thrusts. However, the dynamic coupling resonance in the pitch mode becomes greater. As for the roll and yaw motions, it is obvious that the downwind case causes larger oscillations due to the complex problems figured out above, such as the tower shadow, and vortices shedding. Since the wind and wave loads are both giving in *x*-direction only, these vibrations in roll and yaw are still relatively small compared to the dominant surge/pitch motions. In FIGURE 5.3 (f), it is also evident that the downwind tower top side-to-side displacement is suffering from more serious resonance at the blade passing frequency 3P, which equals 3.801 rad/sec when the rotor speed is 12.1 rpm.

The steady rotor thrust figure also tells that for both downwind and upwind model, the rotor thrust presents the same trend after the wind speed has exceeded the rated speed 11.4 m/s. Not surprisingly, the negative aerodynamic damping is an issue for both cases. FIGURE 5.4 and FIGURE 5.5 have identified the instability in surge and aerodynamic damping for both upwind and downwind model (see orange markers). At turbulent rated wind speed the control system will pitch the blades quite often to adjust the power production. When the wind turbine surges and pitches (motions that will change the plane of rotor rotation) the system will experience even higher fluctuations.

More detail explanation is that when the wind turbine is moving upwind, the relative velocity increases (above the rated wind speed) and the control system will pitch the blades to adjust the power production, whereas when the wind turbine is moving downwind the relative wind velocity decrease (below the rated wind speed) and the

blade pitch angle will return to initial zero. The blade-pitch control strategy above rated wind speed will lead the wind-induced loads to amplify the wave-induced motions of the wind turbine and result in larger resonance. Therefore, the negative aerodynamic damping issue, as figured out in many articles, is a potential design challenge for a FOWT. The mutual influence between the wind turbulence, blade-pitch control system and the instability surge motion, as well as the improvement of the offshore control system, are more complicated and tedious than what have been shown above, which would not be further discussed in the present thesis.

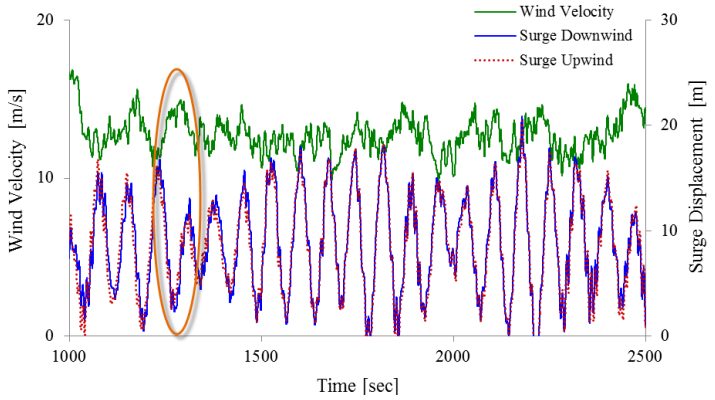

FIGURE 5.4 Surge instability for downwind and upwind model in U_{mean} = 13 m/s.

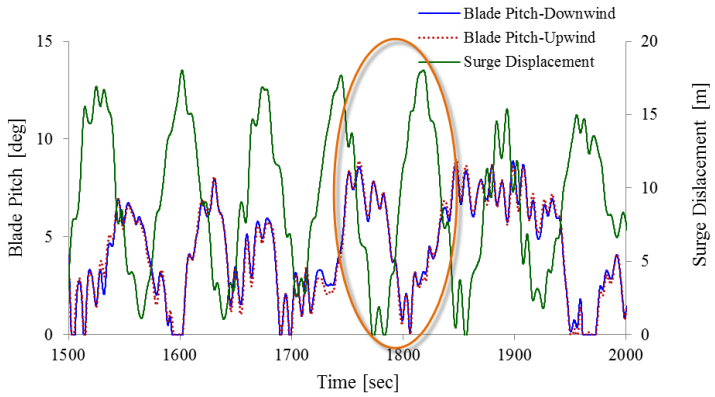

FIGURE 5.5 Time series of blade pitch and surge displacement in U_{mean} = 13 m/s.

5.2 Subsea-Swivel Simulation

Both swivel and hinged connections allow the tower system to rotate freely in the yaw mode. However, certain yaw mechanism is still necessary such that the yaw motion would not violate the platform-small-rotation assumptions in FAST. Meanwhile, the yaw natural frequency is decreased with smaller yaw stiffness such that the significant resonance problem figured out in section 4.4.3 is also avoided. However, the swivel connection differs from the hinged connection for its additional restriction on the roll and pitch rotational motions. In this case, an equilibrium model which can be modeled in FAST has been illustrated in the following FIGURE 5.6.

In this swivel model, the single tether has been treated as part of the hull, and the yaw bearing point is thereby further lowered near to the seabed, which is also the fairlead point for the mooring lines, a very similar model with the articulated loading platform (ALP) case. Considering the great set-down effect due to short tether, the single tether is replaced with three short mooring lines to constrain the fairlead displacement.

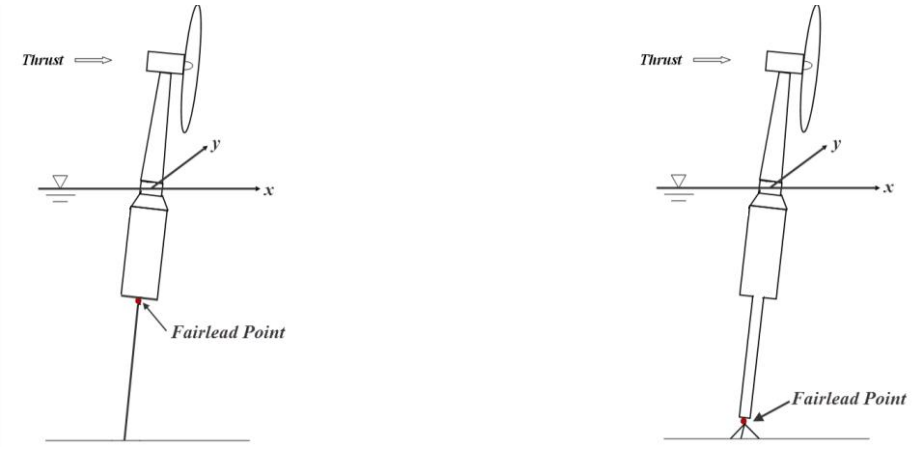

(a) Reference Model **(b) Modified Swivel Model**

FIGURE 5.6 Model configurations.

Ahead of comparing the time simulation results between the modified model (downwind, subsea swivel) and the reference model (downwind, hinged) in FAST, it is necessary to check the natural frequencies of the modified model. The natural frequencies of the platform's 6DOFs motions can be obtained by running the free decay test in FAST. For the translational modes, the free decay tests cannot be conducted by simply placing the platform some deflections from its rest position and then release it, since the fairlead of the model in this case is fixed by three short mooring lines near the seabed that FAST would be confused about these initial offsets. Therefore, the free decay tests are conducted separated for each mode by offering an initial wind load that drive the platform away from its rest position and then remove the load. No waves are simulated during these tests. The damping mechanisms in the system include the aerodynamic damping, radiation damping, viscous damping and structural damping. See Withee (2004) for more information about the decay test for single- or multi-mode. The single-mode free decay test results in the present work are illustrated in FIGURE 5.7.

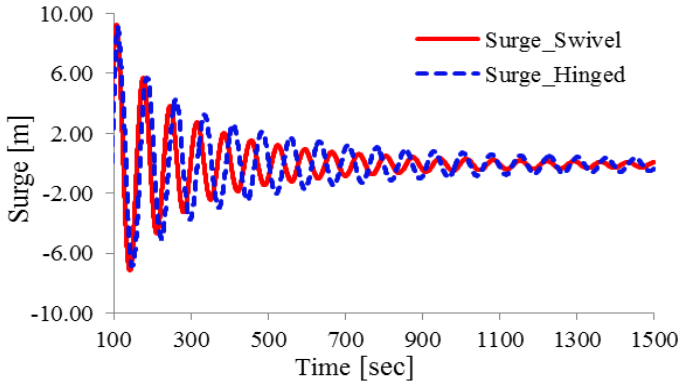

(a) Surge Free Decay

FIGURE 5.7 Free decay test for modified swivel model.

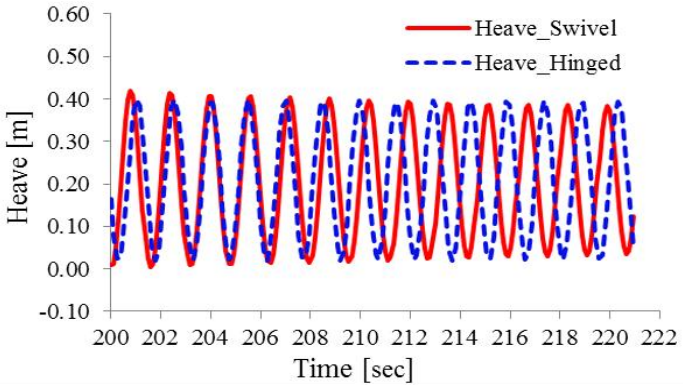

(b) Heave Free Decay

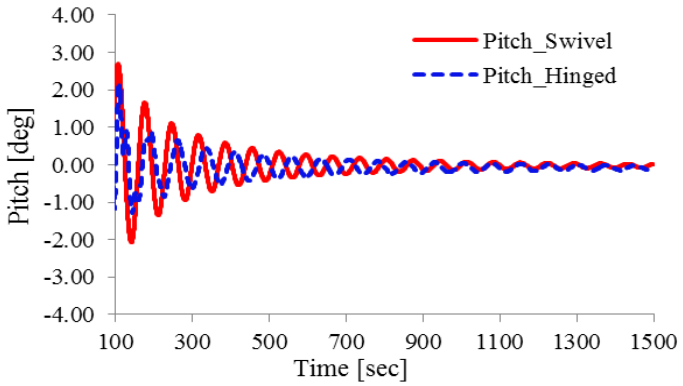

(c) Pitch Free Decay

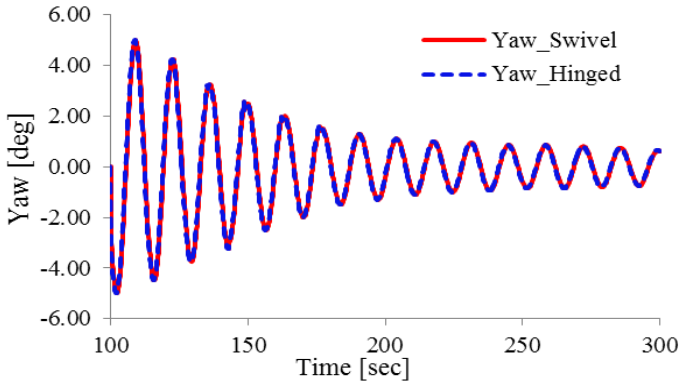

(d) Yaw Free Decay

FIGURE 5.7 Continued.

Due to the symmetry of the hull and the symmetric distribution of the mooring lines, the natural frequencies of sway and roll equal the surge and pitch natural frequency respectively. Therefore, the sway and roll free decay tests have not been

conducted. For the yaw free decay test, it is not easy to find out the yaw natural frequency since the whole system does not simply oscillate in the yaw mode after the load is released. Therefore, both models are isolated in the yaw free decay test so that systems can only move in yaw mode of motion. This can be accomplished by directly attaching the hull to the ground through a joint in the bottom of the hull which only allows yaw motion. As a result of it, the yaw natural frequency should be the same for two systems, which has been proved in the figures. See TABLE 5.1 for the summary of the natural frequencies for both models. The small reduce of the heave natural frequency is mainly due to the three-short-tether mooring system.

Natural Freuqencis (rad/sec)	Modified Model	Reference Model
Surge/Sway	0.093	0.082
Heave	3.930	4.060
Roll/Pitch	0.093	0.082
Yaw	0.418	0.418

TABLE 5.1 Summary of natural frequencies.

The hinged model and swivel model are run in FAST under the second environment loading case defined in section 6.1. Both wind and wave loads are applied in *x*-direction only. The time-simulation results are shown in the following figures. The spectra are plotted after the system is steady such that the significant transient effect due to the mooring system for the modified swivel model shown in time history have been ignored.

As shown in the time series and spectra in FIGURE 5.8, FIGURE 5.9 and FIGURE 5.10, the modified model is mainly oscillating at its natural frequencies in 6DOFs. The resonant responses due to dynamic interaction between the hull and the turbine, as well as the wave frequency responses have decreased a lot for the modified model. The reduced yaw natural frequency has also avoided the significant responses in yaw and other coupled modes, such as pitch mode, at the range of the wave excitation frequencies. However, the only problem is the high-frequency resonance of the heave motion at its natural frequency 3.93 rad/sec, which is due to its unique mooring system.

Since the single-tether mooring system in the modified model is treated as part of the hull, FAST automatically regards it as a rigid body such that its elasticity and dynamic characteristics have been ignored, which still has some distance from the actual SWAY® model and this mooring system has also caused significant heave resonances. However, the reference model and the modified model in this work can actually be regarded as two extreme cases for the simulation of the SWAY® wind turbine, such that the actual dynamic responses of the SWAY® wind turbine can be found somewhere between these two cases. The results obtained in this work therefore still meaningful for the coupled dynamic analysis of this special type of FOWT.

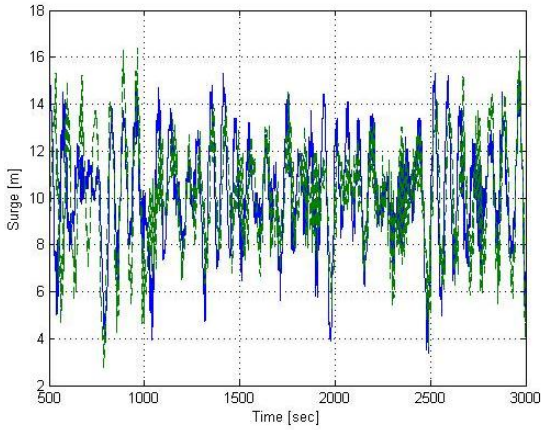

(a) Time-Series of Surge

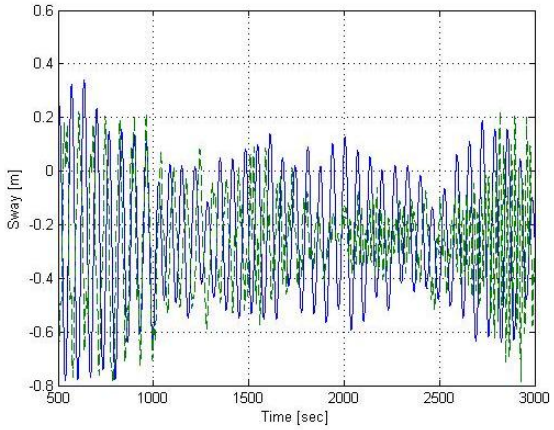

(b) Time-Series of Sway

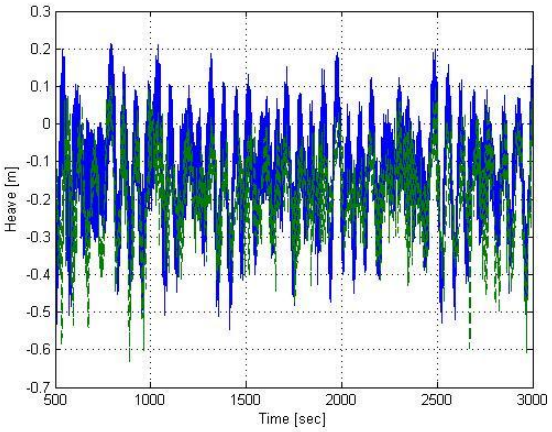

(c) Time-Series of Heave

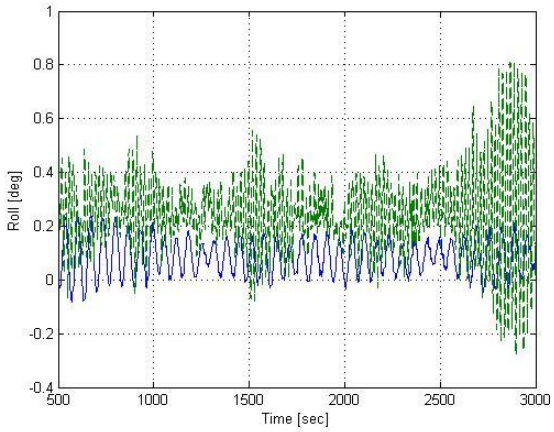

(d) Time-Series of Roll

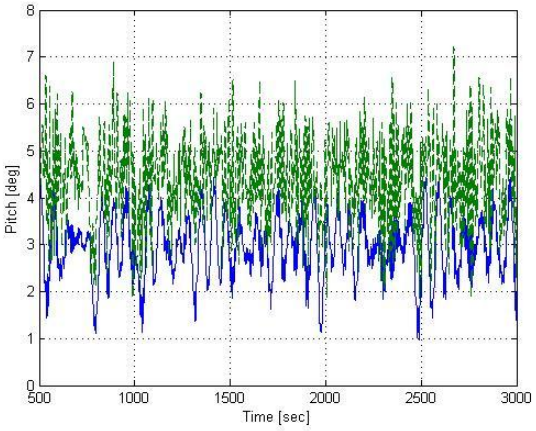

(e) Time-Series of Pitch

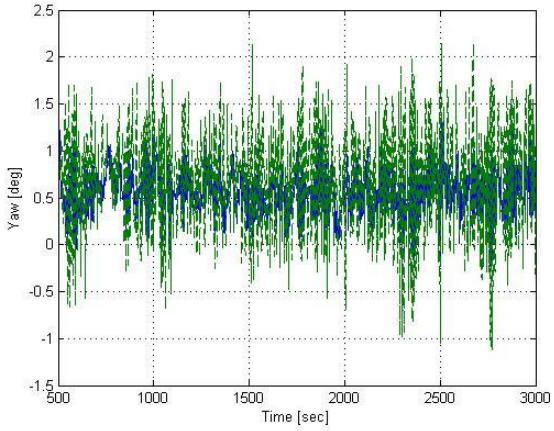

(f) Time-Series of Yaw

FIGURE 5.8 Platform responses time series of modified & reference model Case 2. (2500 sec. Solid Blue: Modified swivel model; Dash Green: Reference hinged model)

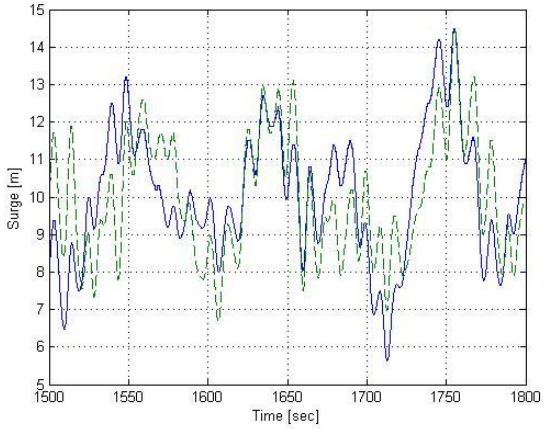

(a) Time-Series of Surge

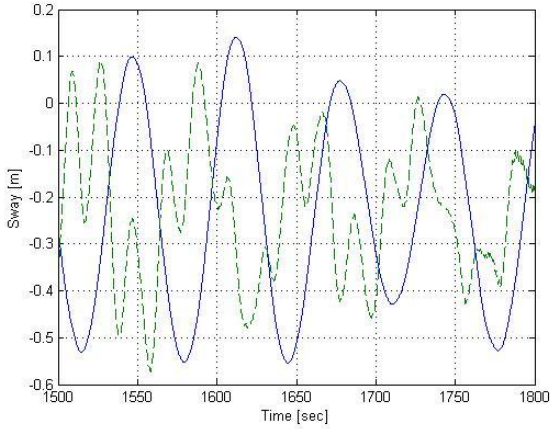

(b) Time-Series of Sway

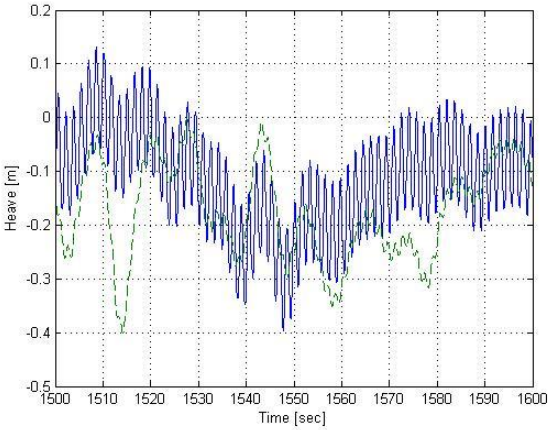

(c) Time-Series of Heave

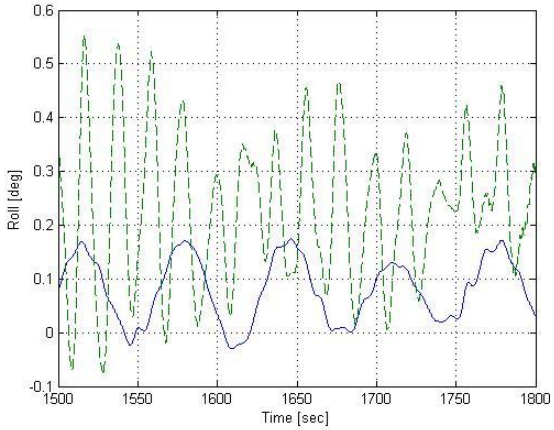

(d) Time-Series of Roll

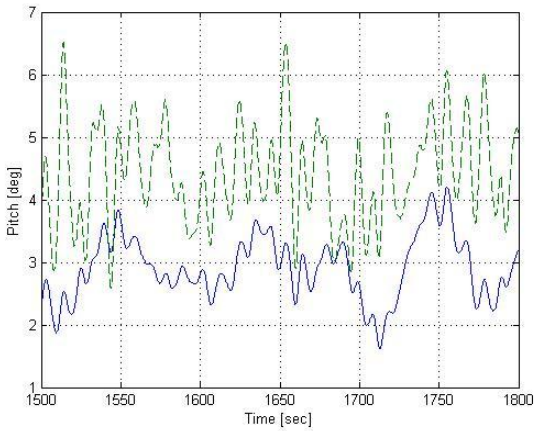

(e) Time-Series of Pitch

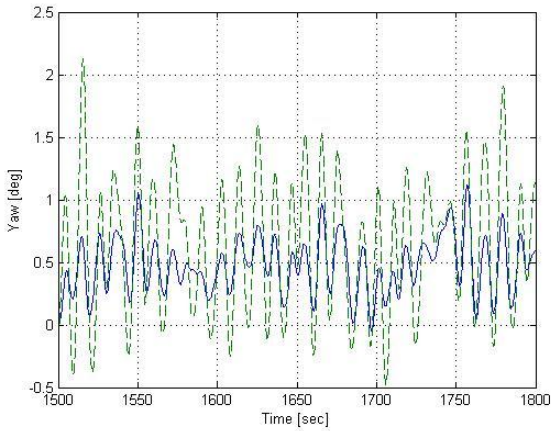

(f) Time-Series of Yaw

FIGURE 5.9 Platform responses time series of modified & reference model Case 2. (300 sec. Solid Blue: Modified swivel model; Dash Green: Reference hinged model)

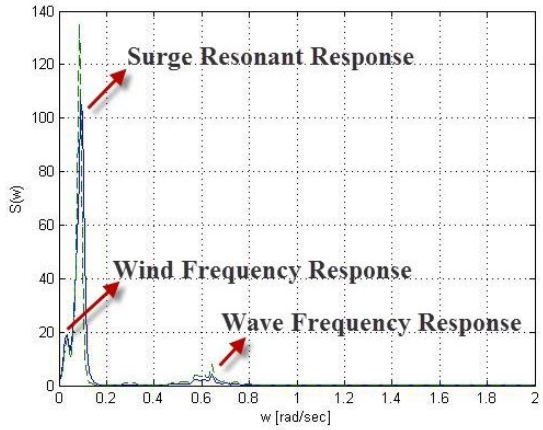

(a) Spectrum of Surge

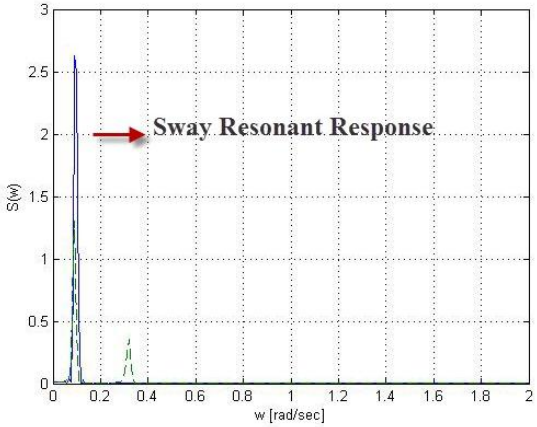

(b) Spectrum of Sway

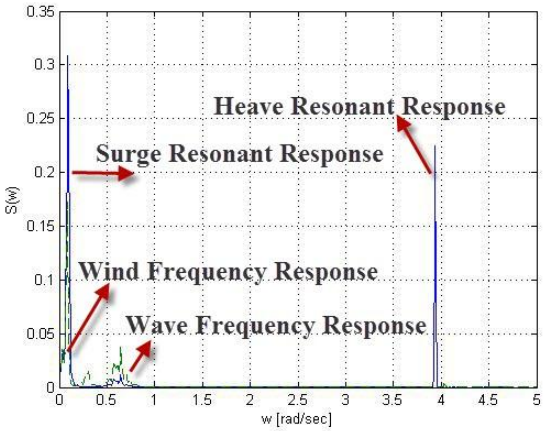

(c) Spectrum of Heave

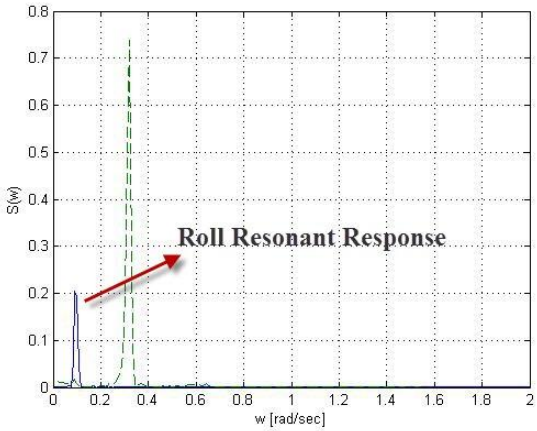

(d) Spectrum of Roll

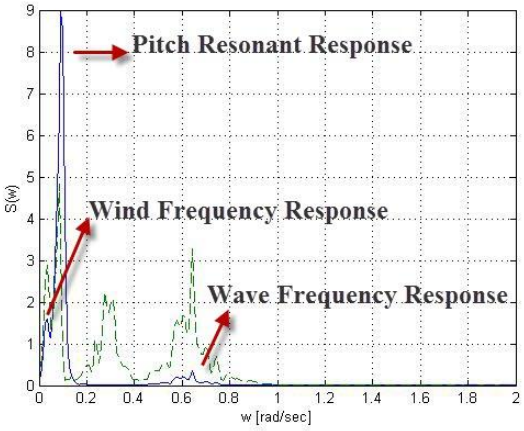

(e) Spectrum of Pitch

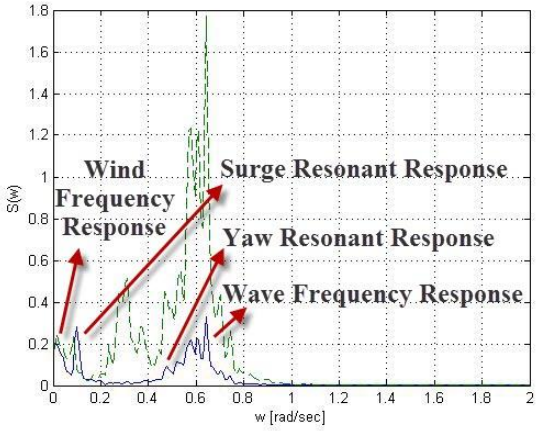

(f) Spectrum of Yaw

FIGURE 5.10 Platform response spectra of modified & reference model Case 2.
(Solid Blue: Modified swivel model; Dash Green: Reference hinged model)

5.3 Wind Turbine Performance

The tower fore-aft and side-to-side displacements, the velocity and acceleration along the *x*- and *y*-direction of the nacelle as a result of the platform displacement of the modified and reference model are given in the following FIGURE 5.11, which are the important parameters to measure the performance of wind turbine.

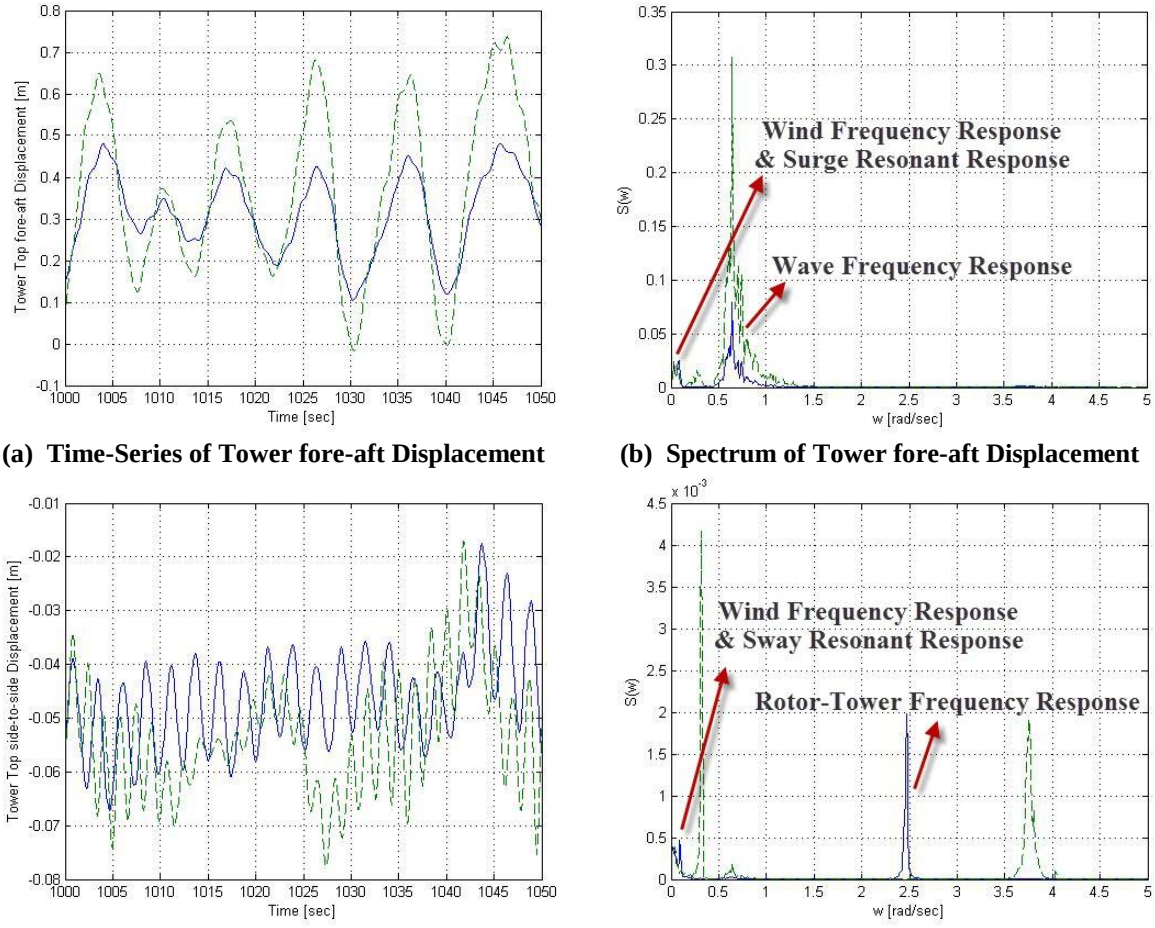

(a) Time-Series of Tower fore-aft Displacement **(b) Spectrum of Tower fore-aft Displacement**

(c) Time-Series of Tower side-side Displacement **(d) Spectrum of Tower side-side Displacement**

FIGURE 5.11 Tower top displacements of modified & reference model case 2.
(Solid Blue: Modified swivel model; Dash Green: Reference hinged model)

As shown in FIGURE 5.11, the tower top displacement shows the same characteristics as the supported platform. Fortunately, the tower top experiences obviously smaller fore-aft displacement in the modified model. However, in FIGURE 5.11(d), the blade passing frequency or tower flexibility frequency (3P) resonance for the modified model has been shifted from the original 3.801 rad/sec to about 2.44 rad/sec. To further explore the reason for this resonant peak shift, some parameters are guessed to be related to it, such as the tower flexibility, rotor rotation or the mooring system. Therefore, some test cases are run through simulating a rigid tower, defining a different rotor speed of 6.2 rpm, or modeling a four-tether mooring system. The results are shown in FIGURE 5.12 as follows.

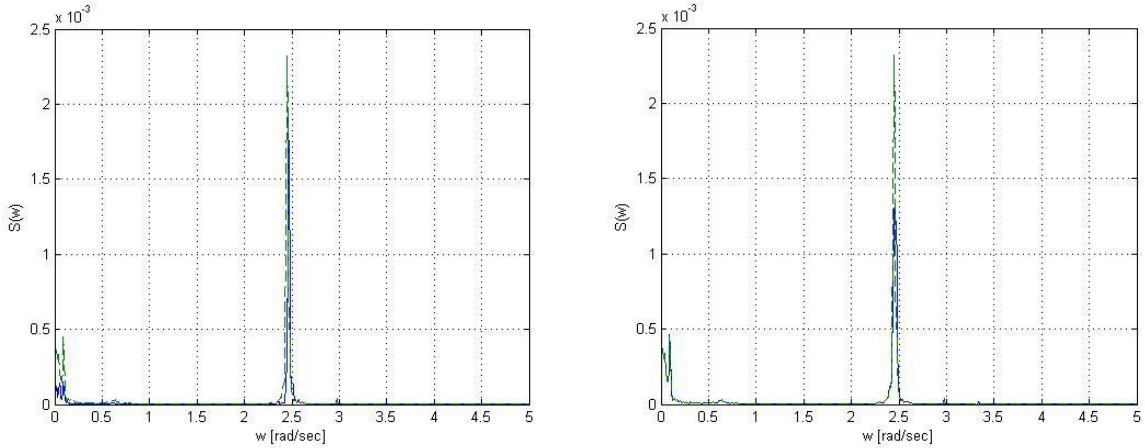

(a) Rigid Tower **(b) 6.1 rpm Rotor Speed and 4-tether Mooring**

FIGURE 5.12 Spectrum of tower top side-to-side displacement for test cases. (Solid Blue: test cases; Dash Green: Modified swivel model)

As these results shown, the guess parameters would only influence the magnitude of the resonant response at the blade passing frequency, but not the dominant element

determining the shifted frequency. Since the whole system is rather complicated, the author assumes the reason is that FAST treats the whole submerged body between free surface and the near-seabed fairlead point as hull, which is rather close to a bottom-fixed platform model. In order to verify this assumption, the modified model is redefined as bottom-fixed case, and the tower top side-to-side displacement spectrum is presented below in FIGURE 5.13, from which we find that the 3P is around 2.36 rad/sec.

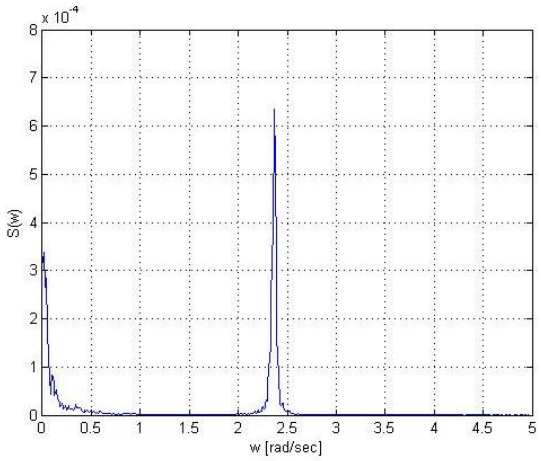

FIGURE 5.13 Spectrum of tower top side-to-side displacement for fixed-bottom case.

Wind Turbine Parameters	Mean		SD	
	Modified	Reference	Modified	Reference
Tower fore-aft Displacement [m]	0.39598	0.43608	0.09837	0.18412
Tower side-to-side Displacement [m]	-0.0420	-0.0474	0.00982	0.01589
x-dir Nacelle Velocity [m/sec]	-0.0015	-0.0007	0.67605	1.25932
x-dir Nacelle Acceleration [m/sec^2]	0.00035	-0.0017	0.48011	0.86069
y-dir Nacelle Velocity [m/sec]	0.00141	0.00890	0.03280	0.06797
y-dir Nacelle Acceleration [m/sec^2]	0.00073	0.00352	0.04588	0.08119

TABLE 5.2 Turbine performance statistics of modified & reference model Case 2.

TABLE 5.2 above presents the summary of the statistics of the wind turbine performance. In order to find certain reference data for these statistic values, the conclusion in Tracy (2007) is adopted. In Tracy's thesis, a large amount of platform designs were compared at 200 m water depth and six-meter sea state, and the standard deviations of nacelle accelerations for the TLP with taut catenary moorings mostly range from 0.1 to 0.5 m/sec^2. In the present design, we can find out that the modified model owns smaller turbine responses than the reference model, and the nacelle acceleration of the swivel design is among the range as pointed out by Tracy (2007).

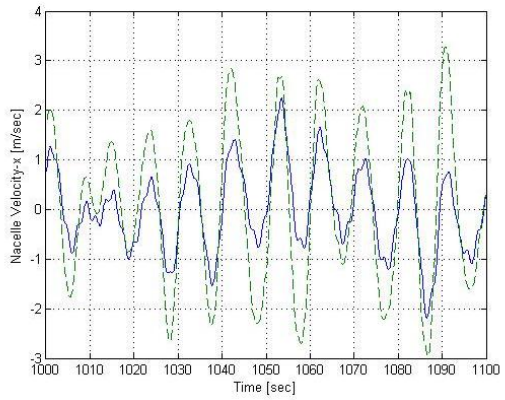

(a) Time-Series of x-dir Nacelle Velocity

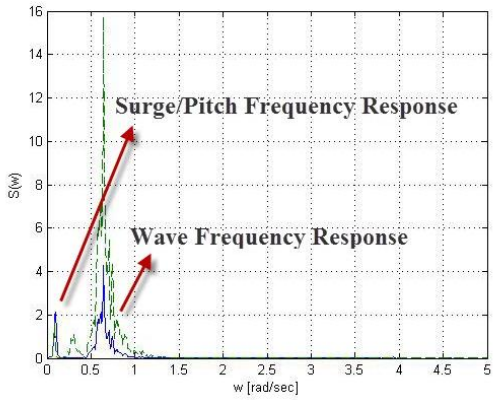

(b) Spectrum of x-dir Nacelle Velocity

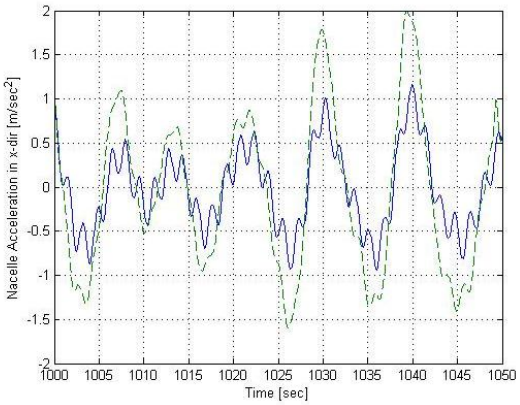

(c) Time-Series of x-dir Nacelle Acceleration

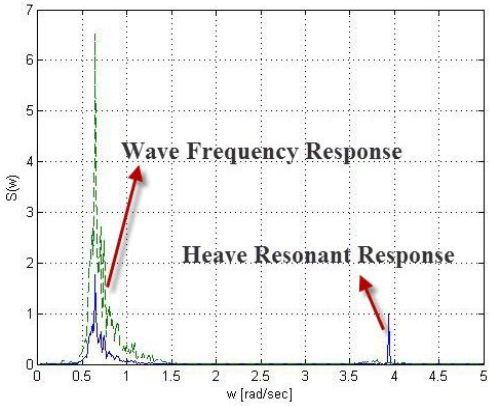

(d) Spectrum of x-dir Nacelle Acceleration

FIGURE 5.14 Nacelle velocity/acceleration for modified & reference model Case 2. (Solid Blue: Modified swivel model; Dash Green: Reference hinged model)

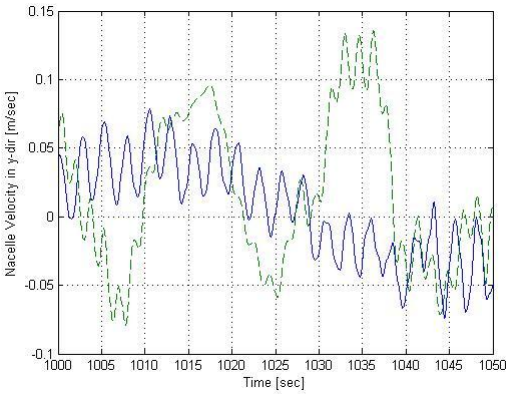

(e) Time-Series of y-dir Nacelle Velocity

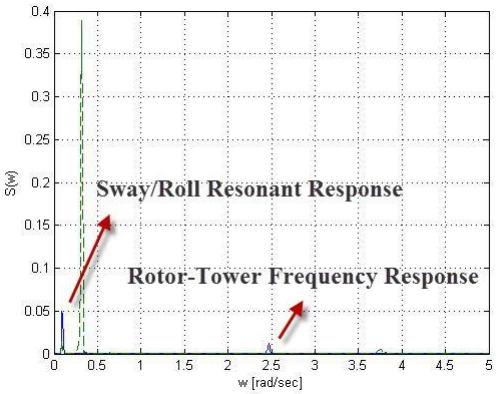

(f) Spectrum of y-dir Nacelle Velocity

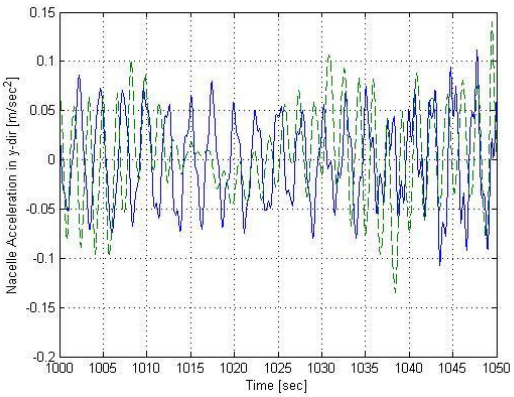

(g) Time-Series of y-dir Nacelle Acceleration

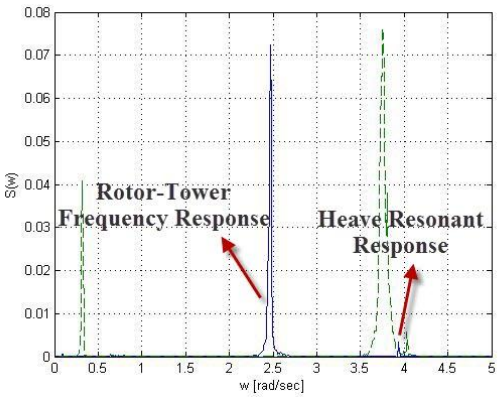

(h) Spectrum of y-dir Nacelle Acceleration

FIGURE 5.14 Continued.

FIGURE 5.14 also suggests that the fore-aft resonant response of the nacelle occur at the range of wave frequencies because of the strong coupling to the platform pitch response, which again is coupled to the roll and yaw modes. This is as well a fact that supports the decision to design for a yaw natural frequency out of the wave excitation frequency range. A unique characteristic of the nacelle acceleration in the modified models is the resonant response at the heave natural frequency, which may cause some problems concerning the life of the machines inside the nacelle. For the *y*-

direction nacelle response, the resonances are mainly due to the roll natural frequency and the blade passing frequency as shown in figures.

The rotor speed, thrust, torque and the generated power during 1500-second simulations are illustrated as well in FIGURE 5.15 for both modified and reference model. These parameters are highly correlated that vary in a similar manner. And it is fortunate to find that the modified model is not fluctuating more than the reference model. As all comparisons made above, these modifications leading the design closer to the SWAY®-type wind turbine are promising.

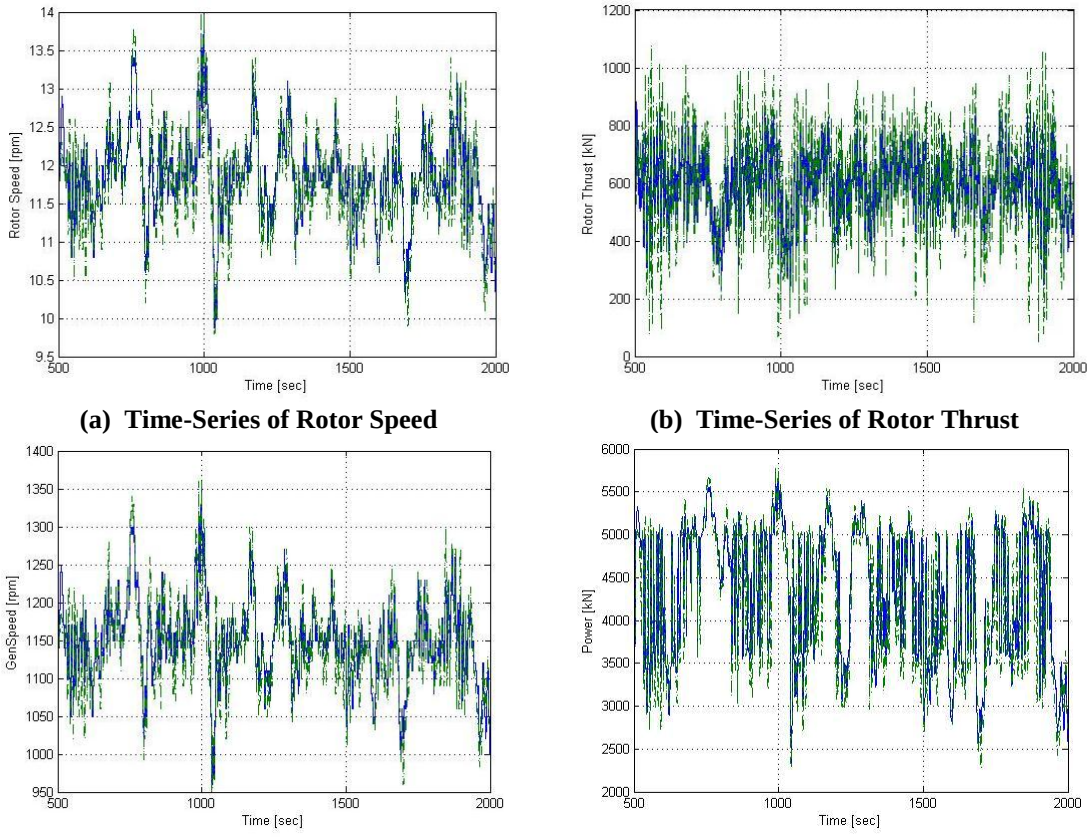

(a) Time-Series of Rotor Speed **(b) Time-Series of Rotor Thrust**

(c) Time-Series of Generator Speed **(d) Time-Series of Generator Power**

FIGURE 5.15 Wind turbine parameters for modified and reference model Case 2. (Solid Blue: Modified swivel model; Dash Green: Reference hinged model)

6 DYNAMIC ANALYSIS AND SIMULATION RESULTS

The Fully coupled dynamic models for the modified and reference design have already been established and verified, and the models are also compared by time-domain simulation under general conditions. However, it is still necessary to simulate the models in a number of design load cases in order to verify the structural integrity of an offshore wind turbine design. Due to the limitation of resources and time, the operational load cases used in the thesis are selected from the normal operational load cases in Crozier (2011) and Wayman & Sclavounos (2006). Program TurbSim, following IEC 61400-3 standard, is adopted for the generation of long-term joint-probability distribution turbulent wind spectrums.

6.1 Load Cases

	Wave: H_s = 6 m, T_p = 10s		Wind: U_{mean} = 11.2 [m/s]	
Case	Wind: U_{mean} [m/s]	Case	Wave: H_s [m]	T_p [s]
1	9	7	2.44	8.1
2	11.2	8	3.66	9.7
3	13	9	8	12.5
4	15	10	10	14
5	18			
6	25			

TABLE 6.1 Load cases conditions.

The turbulent wind conditions in TABLE 6.1 are generated with certain mean wind velocity at the reference height 90m, with the lowest turbulence intensity C in TurbSim. The stochastic wave conditions are generated within HydroDyn by choosing

JONSWAP/Pierson-Moskowitz spectra as the incident wave kinematics models, with respective significant wave heights and peak periods. The time series and spectra of the wind velocity and wave elevation can be viewed in FIGURE 6.1 for load case 2. It can be seen that the wind velocity fluctuates rapidly during the one-hour simulation and its high-energy concentration is in the range of 0.02 and 0.2 rad/s, as shown in FIGURE 6.1(a-2). These wind excitation frequencies differ from the high-energy part of the wave excitation which is in the range of 0.5 to 1.2 rad/s.

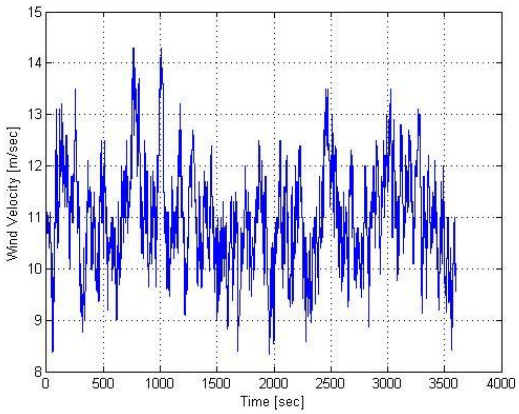

(a_1) Time-Series of Wind Velocity

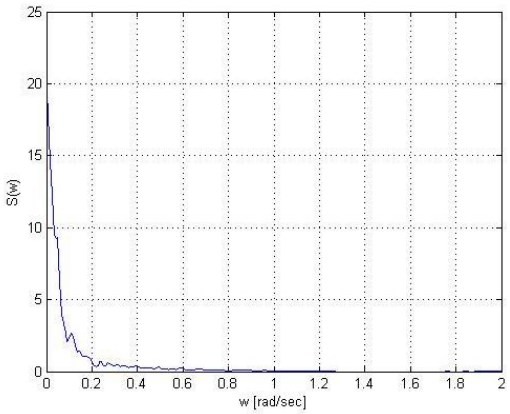

(a_2) Spectra of Wind Velocity

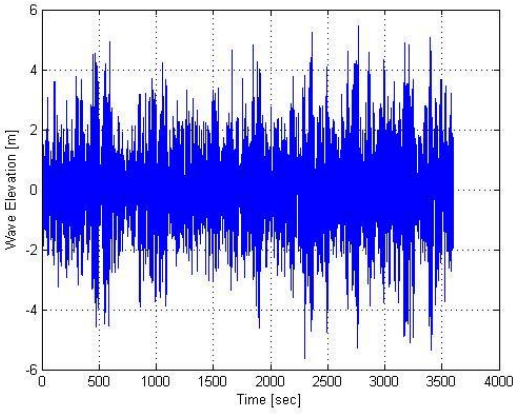

(b_1) Time-Series of Wave Elevation

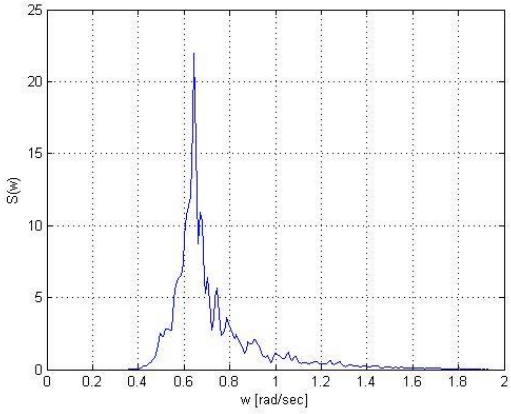

(b_2) Spectra of Wave Elevation

FIGURE 6.1 Environmental load time series and spectra.
(Case 2: U_{mean} = 11.2m/s, H_s = 6m, T_p = 10s)

6.2 Normal-Operation Conditions Simulation Results

This section presents a summary of the simulation results of both modified and reference model under the operational load cases listed in TABLE 6.1. Since the main loads are only applied in *x*-direction, the surge and pitch displacements are selected as the main parameters for examination and comparison between the platform designs. The inline nacelle velocity and acceleration are also discussed and compared for the range of operational load cases. Therefore, the effects of wind speed, sea states and water depth on the system's performance are explored.

6.2.1 Effect of Wind Speed

FIGURE 6.2 (a), (b) present the surge and pitch displacement for the range of wind speeds applied in the operational load cases for the modified swivel model and the reference hinged model. The main conclusions that can be drawn from these figures are that the mean displacement for both surge and pitch motions are dependent on the thrust force. And the decreased steady-state surge/pitch displacements after the wind speed above the rated also due to the decrease of rotor thrust on the system. It is also obvious that the surge displacements for both models are very similar, but the mean and standard deviations in pitch motion of the modified model are much smaller. Besides, the system oscillates greatly at the mean wind speed of 13 m/s, where the rotor power first exceeds its rated power. The tower top displacements in FIGURE 6.2 (c), (d) shows the same trend as the platform surge motion, with smaller mean fore-aft displacement and standard deviations in the modified swivel model.

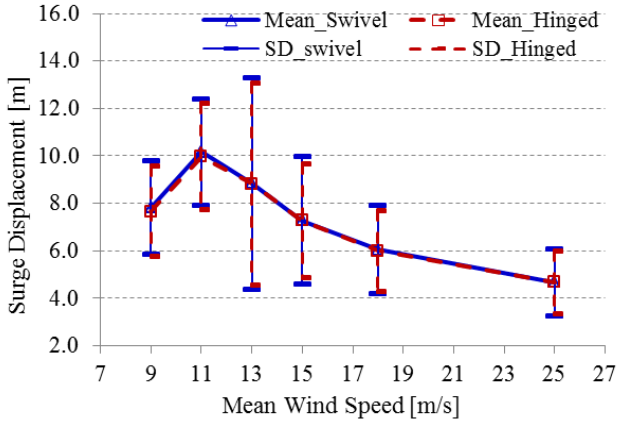

(a) Surge Displacement

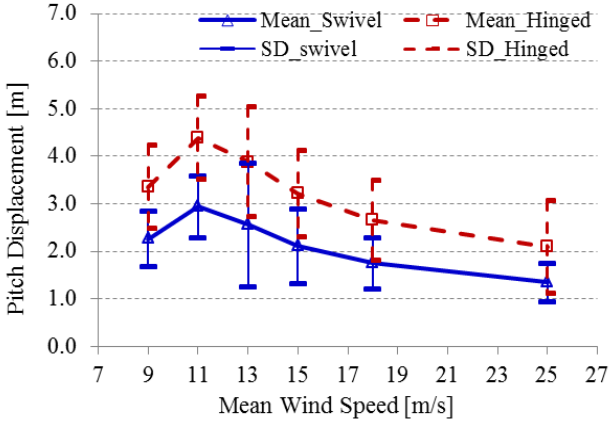

(b) Pitch Displacement

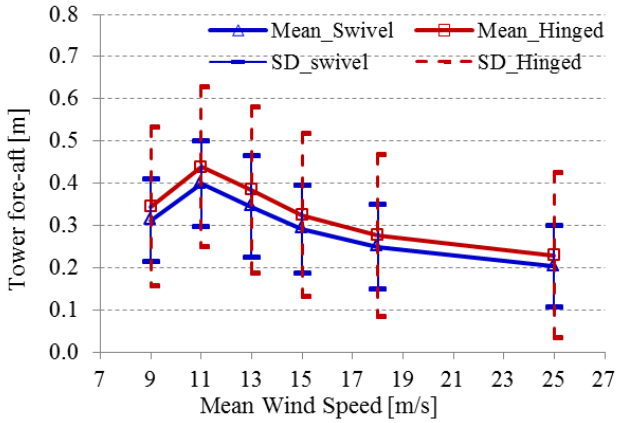

(c) Tower fore-aft Displacement

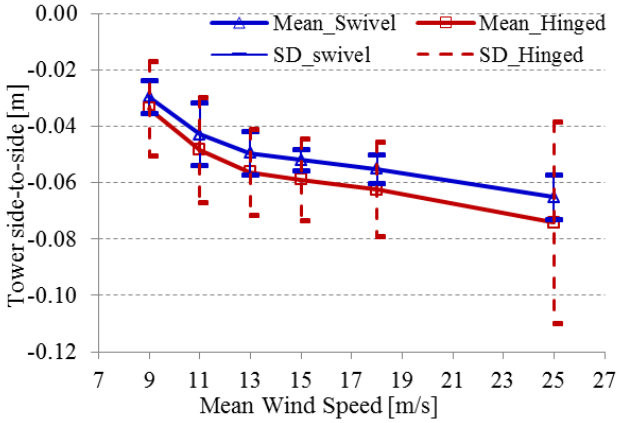

(d) Tower side-to-side Displacement

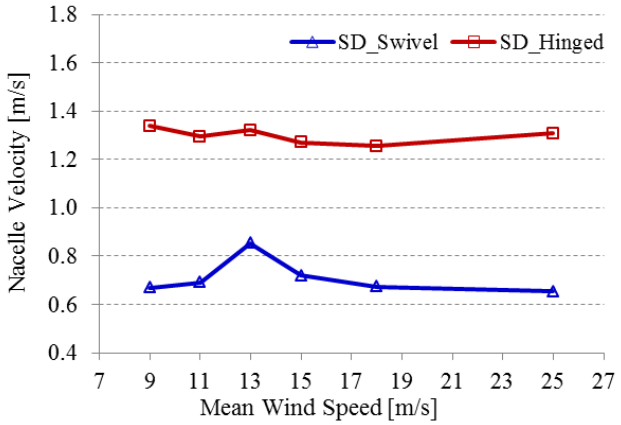

(e) Nacelle Velocity

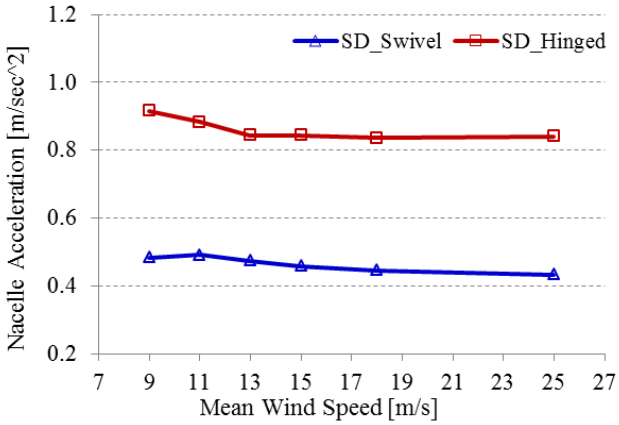

(f) Nacelle Acceleration

FIGURE 6.2 Wind effect on surge/pitch motions and turbine performances.
(H_s = 6m, T_p = 10s)

The standard deviations of the nacelle velocity and accelerations are close to constant for the range of operating wind speeds, except for a small increase of the nacelle velocity in the modified model with U_{mean} = 13 m/s, where the oscillation of the whole system is quite large. In FIGURE 6.2 (e), (f), the swivel model yet again shows an advantage in performance compared to the hinged model, and its standard deviations of nacelle acceleration are all below the limit of 0.5 m/sec^2.

6.2.2 Effect of Sea States

FIGURE 6.3 (a), (b), (c) and (d) present the surge and pitch displacements, as well as the tower top displacement for a range of significant wave heights applied in the operational load cases (peak period vary along the significant wave height) for both modified and reference model. The mean displacement values for these parameters are close to constant for the range of the significant wave heights. The conclusion therefore can be made from these results are that the standard deviation of surge and pitch displacements are dominated by the significant wave height. Larger waves will result in larger. The same characteristics are shown in tower top motions. And it can also be found that the sea state effects on the standard deviations of surge/pitch motions, as well as the tower top displacements are much smaller in the modified model.

The standard deviations of the nacelle velocity and accelerations are almost linearly increasing for the range of significant wave heights. And FIGURE 6.3 (e), (f) again proves better performance of the swivel model. However, in this case, the nacelle acceleration standard deviations will go out of the range of 0.1 to 0.5 m/sec^2 with the increasing of the severity of the sea state (when H_s is larger than 6 m).

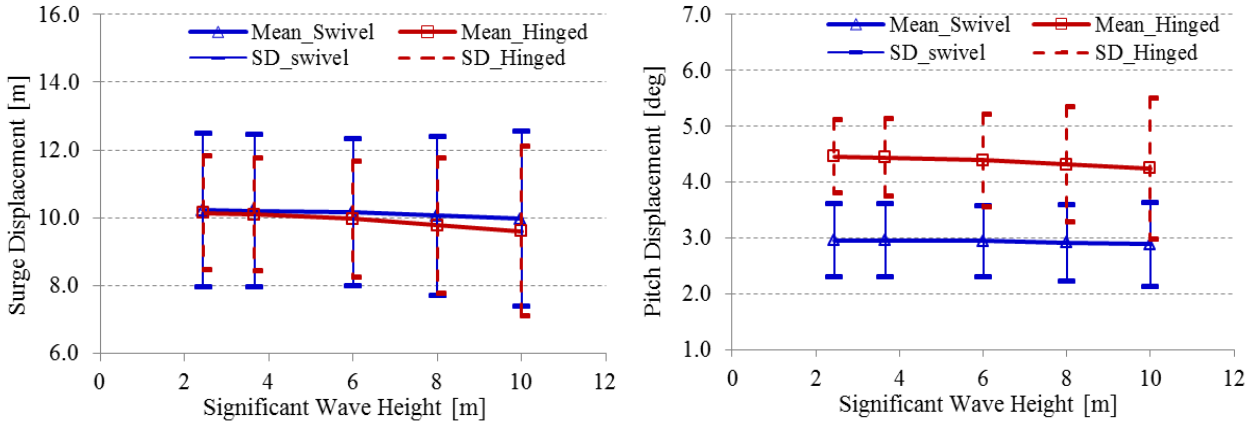

(a) Surge Displacement

(b) Pitch Displacement

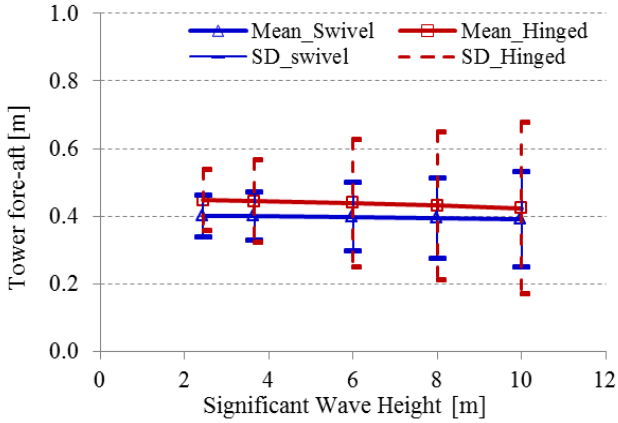

(c) Tower fore-aft Displacement

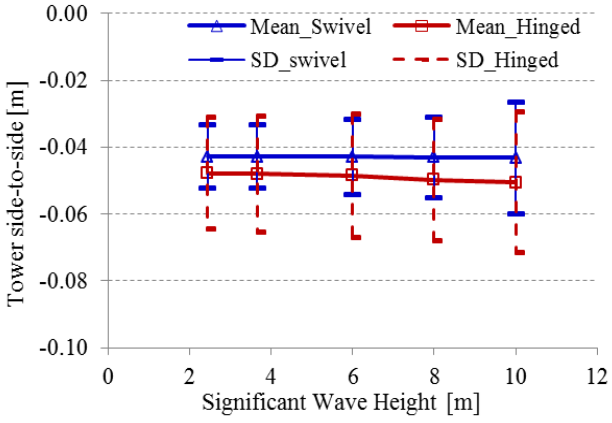

(d) Tower side-to-side Displacement

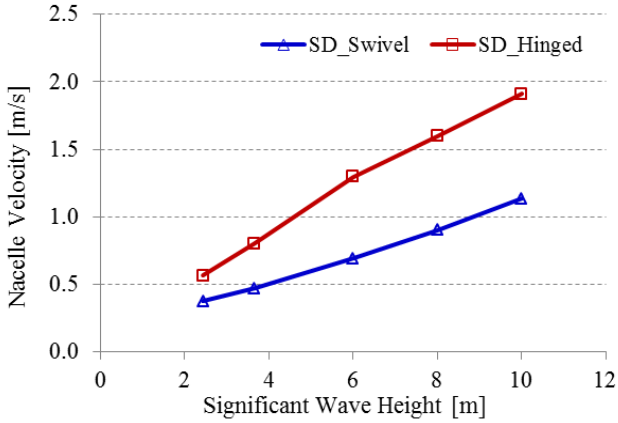

(e) Nacelle Velocity

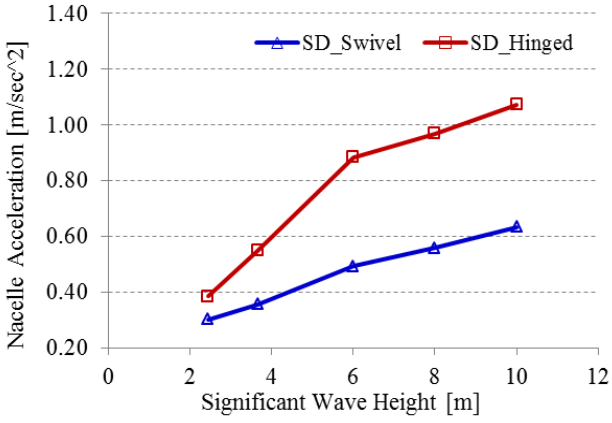

(f) Nacelle Acceleration

FIGURE 6.3 Wave effect on surge/pitch motions and turbine performances.
(U_{mean}= *11.2 m/s*)

6.2.3 Extreme Events

Previously only mean values and standard deviations have been discussed for both models. In order to determine the integrity of the derived designs, it is also important to investigate the maximum and minimum values of the extreme events that occur during the operational load cases, which are listed in TABLE 6.2.

Parameters	Modified Model		Reference Model	
Operational Load Cases	Case 3	Case 10	Case 3	Case 10
Max. Surge Displacement [m]	21.36	17.58	20.62	17.33
Max. Pitch Displacement [deg]	6.22	5.10	7.71	8.73
Max. Tower fore-aft Motion [m]	0.75	0.88	1.09	1.27
Max. Tower side-to-side Motion [m]	-0.014	0.012	-0.009	0.036
Max. Nacelle Velocity [m/sec]	3.19	4.16	3.97	7.09
Max. Nacelle Acceleration [m/sec^2]	1.66	2.79	2.84	4.28
Max. Tether Tension [kN]	-	-	2.35E+04	2.37E+04
Min. Tether Tension [kN]	-	-	1.15E+04	1.17E+04

TABLE 6.2 Extreme events for modified & reference model.

For the reference model, a minimum limit for the surge-restoring coefficient was applied intending to ensure that the angles the tethers from the vertical plane do not exceed 5 degrees during operational conditions in the preliminary design process. Since the preliminary design process is based on the static analysis, where the pitch displacement is near to zero, the surge displacement is limited to be 11.156 m, see Equation 4.1. However, in dynamic simulation process, the maximum allowed surge displacement at SWL (where the platform reference point is located) should be extended to be 17.5 m due to the coupling effect of the pitch motion. In FIGURE 6.2 and FIGURE 6.3, these limits haven't been exceeded, but in TABLE 6.2 the maximum surges are

larger than 17.5 m for both designs. This does not indicate that the preliminary design process was flawed since only steady-state displacement and thrust force were considered. And the above figures have also proven that the steady-state displacements do not exceed the given limits for the range of operational load cases. Therefore, the pretension of both designs can be increase to enhance the surge restoring coefficient such that the above requirements can be satisfied.

Another very important parameter that needs to be checked is the tether tension. Due to the specification of the swivel model mooring system, the tether tension has not been examined or compared in the view of mean value and standard deviation. However, as one extreme design case, the tether tensions of the hinged model for the range of operational load cases have been compared to ensure that the single tether do not experience a loss in pretension or an excess in the maximum allowable tension, 3.48E+04 kN. Furthermore, the maximum nacelle accelerations are rather large in these extreme cases, but due to the lack of exact information on the upper limits these values are assumed to be acceptable.

6.2.4 100m & 300m Water Depth Cases

Since the SWAY® system is patented floating wind turbine for deep water offshore locations in 100 ~ 400 m + water depths, two more cases with 100 m and 300 m water depths are modeled and examined to explore the platform response as well as the wind turbine performance under the effect of water depth.

Due to the effect of water depth on the length of tether, the restoring from tethers will shift the natural frequencies to lower frequencies with increasing water depth, see TABLE 6.3 as follows.

Model		Modified Swivel Model			Reference Hinged Model		
Water Depth		100 m	200 m	300 m	100 m	200 m	300 m
Surge/Sway	[rad/sec]	0.167	0.093	0.071	0.161	0.082	0.066
Heave	[rad/sec]	8.92	3.93	2.90	9.03	4.06	3.04
Roll/Pitch	[rad/sec]	0.167	0.093	0.071	0.161	0.082	0.066

TABLE 6.3 Modified & reference model natural frequency in various water depths.

Load Cases	H_s [m]	2.44	3.66	6	8	10
	T_p [sec]	8.1	9.7	10	12.5	14
Surge [m]	100 m	1.124	1.168	1.328	1.856	2.317
	200 m	2.410	2.354	2.240	2.348	2.618
	300 m	3.323	3.331	3.322	3.436	3.483
Pitch [deg]	100 m	0.654	0.680	0.780	1.080	1.544
	200 m	0.670	0.683	0.650	0.681	0.760
	300 m	0.612	0.644	0.642	0.664	0.673
Nacelle Acceleration [m/sec^2]	100 m	0.314	0.482	0.821	0.871	0.951
	200 m	0.302	0.355	0.491	0.557	0.633
	300 m	0.195	0.247	0.368	0.426	0.489

TABLE 6.4 Standard deviations of the modified model in various water depths. (U_{mean} = 11.2 m/s)

The following FIGURE 6.4 and 6.5 present the platform surge and pitch displacements, as well as the nacelle accelerations with 100 m and 300 m water depths, whose standard deviations are also summarized and compared with the 200 m water depth case in TABLE 6.4 above.

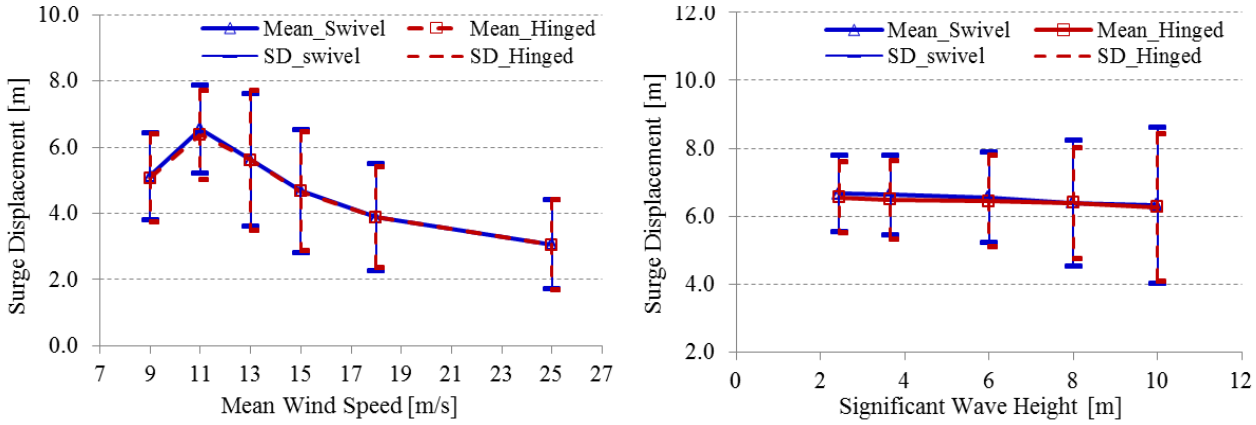

(a) Surge Displacement (100m water depth)

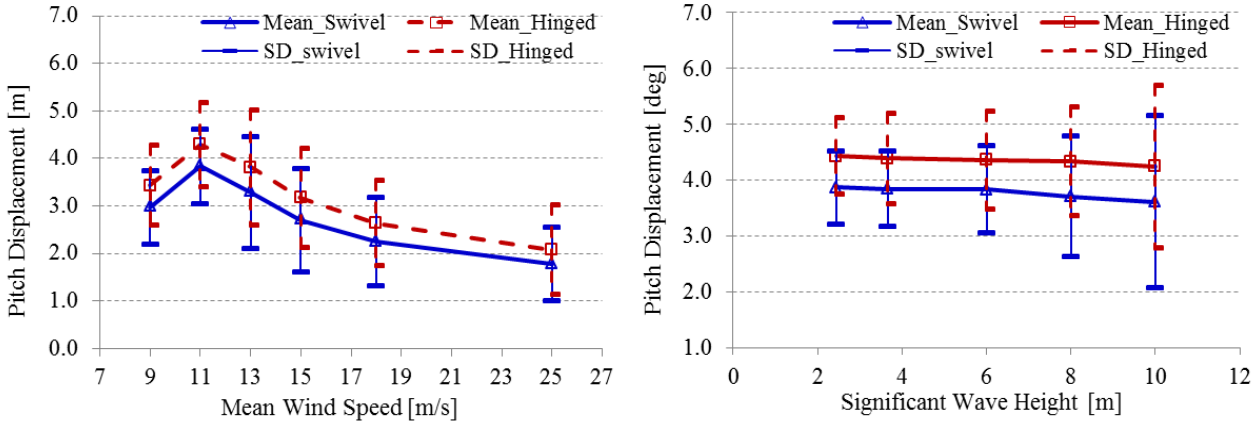

(b) Pitch Displacement (100m water depth)

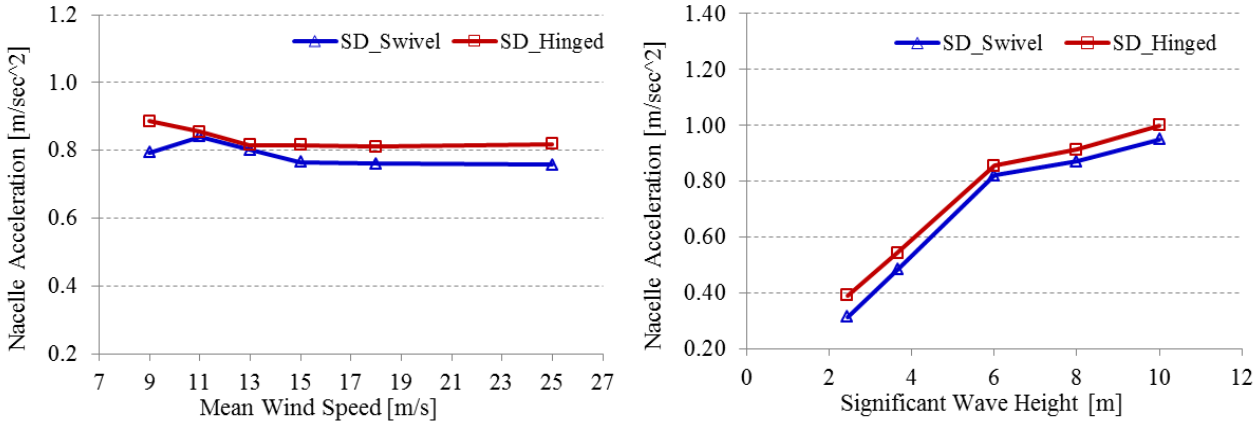

(c) Nacelle Acceleration (100m water depth)

FIGURE 6.4 Surge/pitch motions and nacelle accelerations (100 m water depth).

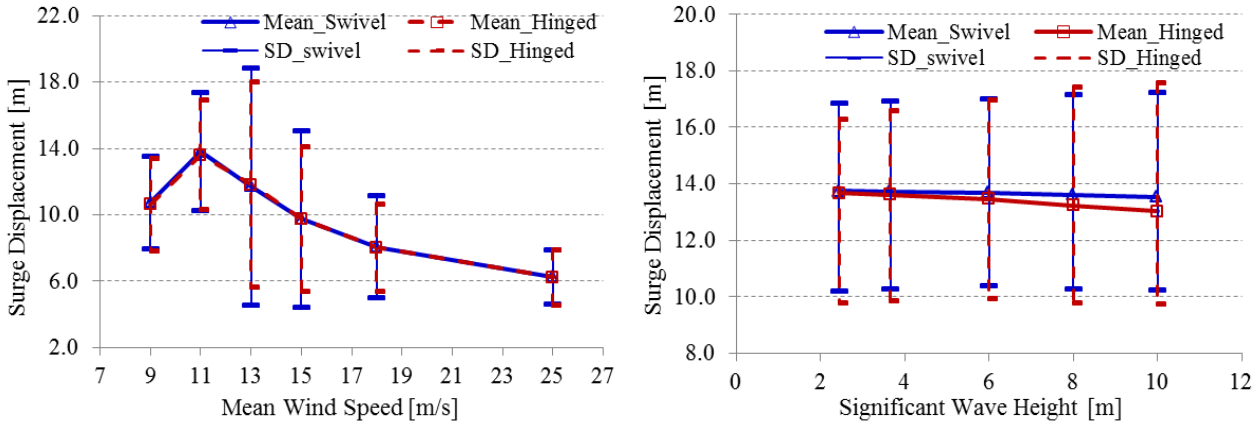

(a) Surge Displacement (300m water depth)

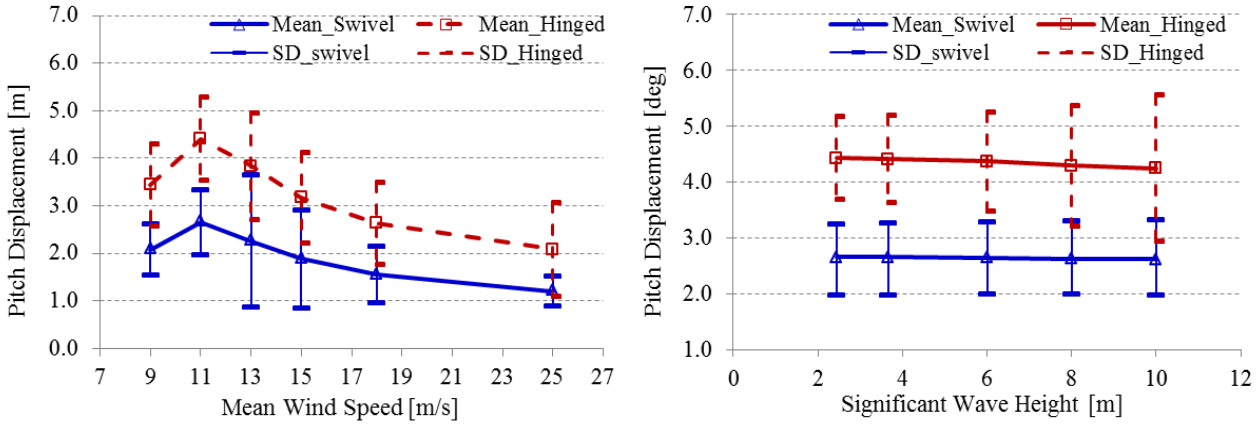

(b) Pitch Displacement (300m water depth)

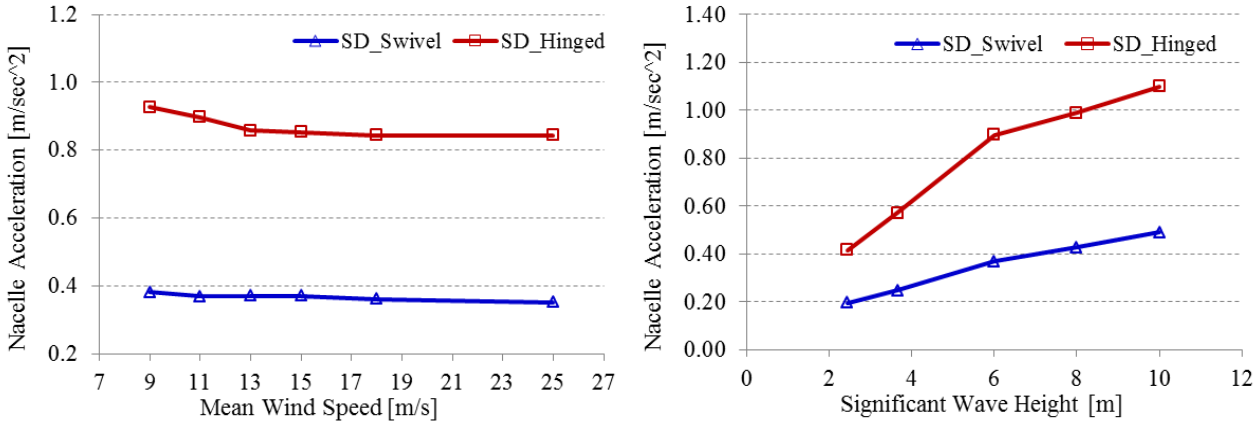

(c) Nacelle Acceleration (300m water depth)

FIGURE 6.5 Surge/pitch motions and nacelle accelerations (300m water depth).

The above table and figures show that the surge motion increases with increasing water depth while the pitch motion and the nacelle accelerations decrease in deeper water. It is also obvious to find that the nacelle accelerations in 300 m water depth are all below 0.5 m/sec^2 with various significant wave heights. In the cases with 100 m and 300 m water depth, the maximum allowable surge displacement turn out to be 8.75m and 26.25 m, respectively. And it is fortunately to find that the maximum allowable surge has not been exceeded in 300 m water depth under all operational load cases. Therefore, we can conclude that the designed swivel model is a good candidate for deep-water deployment.

7 CONCLUSION AND FUTURE WORKS

The thesis focused on the dynamic analysis of the SWAY®-concept FOWT. Since wind and wave are the principal environment loads, the analysis was therefore conducted to explore the system response to wind and wave excitations. Due to the limitation of the public-available data about this specific floating wind turbine as well as the features of the simulation tool, FAST, adopted, the work has been divided to four steps to process.

The first goal of the work was to design a support platform including the mooring systems that is close to the SWAY®-concept design, and can also be established in FAST. This was a spar-buoy support platform with concrete ballast at the bottom and single-tether mooring system hinged to seabed. The properties about the large-scale wind turbine mounted on the top were the same as the NREL 5 MW baseline wind turbine in the Hywind-OC3 project, a spar-buoy case as well.

During the design process, certain performance requirements and cost drivers are considered applying a static analysis. And the platform size and shape therefore have to be adjusted such that sufficient stability was fulfilled. These considerations in static-analysis stage include:

- Center of gravity is much lower than the center of buoyancy;
- The steady-state pitch angle of the platform is less than the maximum of 10 degrees;
- The angle the tether forms with the vertical axis was limited to 5 degrees.

Based on the above considerations, the maximum surge displacement in certain water depth, as well as the minimum surge and pitch restoring can be achieved, which then were used as an initial limit for the tether tension. The dynamics of the design have also been discussed in terms of important criteria:

- Platform natural frequencies are out of the peak frequencies of the dynamic wave loading and do not overlap the wind turbine's operating frequencies (1P, NP);
- The dynamic tether tension during operation does not experience a loss in pretension or an excess in the maximum allowable tension.

The steel, concrete ballast and the vertical anchor load were considered the main cost drivers for this design and the optimized steel and concrete mass to tether tension ratios have been presented in order to minimize the cost. The economic feasibility was taken into account on the base of maintaining the integrity of the whole system.

The second goal was to verify the design by establishing a fully coupled time-domain aero-hydro-servo-elastic model in FAST to allow for the safe operation in realistic wind and wave environment, and this time-domain model was verified as well by comparing the RAOs obtained in FAST and frequency-domain calculations. These results have shown desirable platform dynamic performance in time-simulation satisfying all above requirements. The low frequencies of surge/sway, roll/pitch modes around 0.82 rad/sec have greatly avoided the resonance from wave excitation and the coupled motion from yaw displacement. The RAO comparison have also proven the FAST model was trustable, since the differences are explainable, such as the smaller

resonant response in FAST due to damping arisen from nonlinearities and the extra dynamic responses provided from rotor rotation, gyroscopic effects, and tower flexibility.

The third goal of the thesis was the modification of the preliminary design such that the model is more similar to the SWAY®-concept wind turbine. The main modifications include switching the rotor orientation from upwind to downwind, simulating a subsea swivel connection in FAST and its corresponding yaw mechanism. During the process, the relationship between the control system, surge instability and negative aerodynamic damping were discussed and helped a lot for better understanding the characteristics of the modified design.

Since HydroDyn cannot simulate subsea swivel for the mooring system, a unique way adopted in the thesis dealing with this problem was to treat the single tether as part of the hull, and lower the yaw bearing from the tower top to the tether bottom fixed by three short lines. In this case, the tether was treated as a rigid body same as the platform, and the whole model was close to a bottom-fixed platform. More accurate natural frequencies of the modified swivel model were obtained by performing free decay test in FAST.

The work has treated the modified model and the reference model as two extreme cases and assumed that the actual response of the SWAY®-concept wind turbine could be found among the results of these two cases. The main finding was that the modified swivel model was performing mainly at its natural frequencies and the wave excitation frequencies, and the rotor- and tower-induced dynamic responses were ignorable.

Compared to the reference model, the modified one has less performance especially in pitch and yaw modes and its wind turbine performance were smaller as well.

The final goal was to simulate both the modified and reference model under various water depths with a number of operational environmental conditions: unidirectional turbulent wind and stochastic wave excitations. The simulation results mainly focused on the support structure displacements, the tether tension, and additional nacelle velocity and acceleration standard deviations, and extremes.

The mono-column platform designs with swivel or hinged connected single tether in this work have both proven their capability of supporting large-scale wind turbine and providing sufficient stability during a number of normal operational conditions. The responses of both models were within reasonable limits, and the modified swivel model showed lesser performance compared with that of the reference model. The single tether has not experience loosing tension or exceeding the maximum allowable tension under all operational conditions. This FOWT design has proven itself a good choice for deep-water deployment.

As for the future work for this topic, there are a lot of things need to be improved in the present work. The most important among them listed as follows:

- FAST program coding to enable user-defined fairlead and anchor point connections.
- Modifying the control system and the tower properties, such as the tower stiffness and mode shapes, to avoid the negative aerodynamic damping

and the dynamic resonant response due to the tower flexibility, the dynamic interaction between the hull and the turbine;

- Performing the fatigue analysis, life time estimation for the whole system, especially the fatigue of the tower, or do the economic assessment of the design by deploying it in different ocean areas;
- Improving the model design by adjusting the variables, such as the deck clearance, draft, which treated as constant inputs in the present work, for better outcomes.

REFERENCES

BAE, Y.H. & KIM, M.H. 2011 Aero-elastic-control-floater-mooring coupled dynamic analysis of floating offshore wind turbines. *21th Annual Conference for International Society of Offshore and Polar Engineers,* June 19-24, 2011, Maui, Hawaii, USA.

BAE, Y.H., KIM, M.H. & SHIN, Y.S. 2010 Roter-floater-mooring coupled dynamic analysis of mini TLP-type offshore floating wind turbine. 29th *International Conference on Ocean, Offshore & Arctic Engineering,* June 6-11, Shanghai, China.

BUTTERFIELD, S., MUSIAL, W., JONKMAN, J.M. & SCLAVOUNOS, P.D. 2005 Engineering challenges for floating offshore wind turbines. *1st Annual Copenhagen Offshore Wind Conference,* Oct. 26-28, Copenhagen, Denmark, NREL/CP-500-38776.

CROZIER, A. 2011 Design and dynamic modeling of the support structure for a 10 MW offshore wind turbines. M.S. thesis, Norwegian University of Science and Technology, Norwegian.

EYSTEIN B. 2011 Floating wind power in deep water: competitive with shallow: water wind farms. *33rd Annual Offshore Technology Conference,* Houston, Texas, USA.

FALTINSEN, O. 1998 *Sea Loads on Ships and Offshore Structures*. Cambridge University Press.

JONKMAN, J.M. 2007 Dynamics modeling and loads analysis of an offshore floating wind Turbine. *Tech. Rep.* NREL/TP-500-41958, National Renewable Energy Laboratory, Washington, D.C., USA.

JONKMAN, J.M. 2009 Definition of the floating system for Phase IV of OC3. *Tech. Rep.* NREL/TP-500-47535, National Renewable Energy Laboratory, Washington, D.C., USA.

JONKMAN, J.M. 2009 *Dynamics of Offshore Floating Wind Turbines: Model Development and Verification.* Wind Energy, Wiley Interscience.

JONKMAN, J.M. & BUHL M.L. 2007 Load analysis of a floating offshore wind turbine using fully coupled simulation. *Wind Power Conference & Exhibition*, Los Angeles, California.

JONKMAN, J.M., BUTTERFIELD, S., MUSIAL, W. & SCOTT, G. 2009 Definition of a 5-MW reference wind turbine for offshore system development. *Tech. Rep.* NREL/TP-500-38060, National Renewable Energy Laboratory, Washington, D.C., USA.

JONKMAN, J.M. & MATHA, D. 2009 A Quantitative Comparison of the Response of Three Floating Platforms. *Tech. Rep.* National Renewable Energy Laboratory, NREL/CP-46726.

JONKMAN, J.M. & SCLAVOUNOS, P.D. 2006 Development of fully coupled aeroelastic and hydrodynamic models for offshore wind turbines. *Tech. Rep.* NREL/CP-500-39066, National Renewable Energy Laboratory, Washington, D.C., USA.

JONKMAN, J.M. 2010 Index of /public/jjonkman/NRELOffshrBsline5MW. http://wind.nrel.gov/public/jjonkman/NRELOffshrBsline5MW/.

LARSEN, T.J. & HANSEN, A.M. 2007 *How 2 HAWC3, the User's Manual.* Delft University of Technology, Delft, Netherlands.

MANWELL, J. & McGOWAN, R. 2002 *Wind Energy Explained: Theory, Design and Application*. Wiley, Chichester, New York.

MASCIOLA, M., ROBERTSON, A., JONKMAN, J.M. & DRISCOLL, F., 2011 Investigation of a FAST-OrcaFlex coupling module for integration turbine and mooring dynamics of offshore floating wind turbines. *1st International Conference on Offshore Wind Energy and Ocean Energy,* Beijing, China.

MATHA, D. 2010 Model development and loads analysis of an offshore wind turbine on a tension leg platform, with a comparison to other floating turbine concepts. *Tech. Rep.* NREL/SR-500-45891, National Renewable Energy Laboratory, Washington, D.C., USA.

PIPELINE STANDARDS，2010 API 5L, Pipe dimensions and weight. http://www.ussteel.com/corp/tubular/linepipe-seamless.asp. http://www.worldsteelprice.com

SKAARE, B., HANSON, T.D. & NIELSEN, F.G. 2006a Integrated dynamic analysis of floating offshore wind turbine. *25th International Cconference on Ocean, Offshore & Arctic Engineering),* Hamburg, Germany.

SKAARE, B., HANSON, T.D. & NIELSON, F.G. 2006b Integrated dynamic analysis of floating offshore wind turbine. *20th* Annual *European Wind Energy Association (EWEC)*, Athens, Greece.

TRACY C. 2007 Parametric design of floating wind turbine. S.M. Thesis, Department of Mechanical Engineering, Massachusetts Institution of Technology, Cambridge, MA.

WAYMAN, E.N. & SCLAVOUNOS, P.D. 2006 Coupled dynamic and economic analysis of floating wind turbine systems. *Tech. Rep.* NREL/CP-500-39481, National Renewable Energy Laboratory, Washington, D.C., USA.

WITHEE, J.E. 2004 Fully coupled dynamic analysis of a floating wind turbine system. Ph.D. dissertation, Department of Ocean Engineering, Massachusetts Institution of Technology, Cambridge, MA.

APPENDIX A

SEA STATE PRESENTATION

By the small wave-amplitude assumption, the first-order wave kinematics theory, Airy wave theory, also known as regular wave theory, can be applied. Regular wave theory is valid by assuming a horizontal sea bottom and a free-surface of infinite horizontal extent. The governing equations for finite and infinite water depths can be derived from potential flow theory, by assuming sea water to be inviscid, incompressible, irrotational, and only subject to conservative body forces. The following equations give the velocity potential (ϕ) and elevation (η) for a wave of amplitude A and direction β with infinite water depth, where the wave number $k = \omega^2/g$ in deep water and ω is frequency.

$$\phi(x, y, z, t) = \mathrm{Re}\left\{ \frac{igA}{\omega} e^{kz - ik(x\cos\beta + y\sin\beta) + i\omega t} \right\} \tag{A.1}$$

$$\eta(x, y, t) = \mathrm{Re}\left\{ Ae^{-ik(x\cos\beta + y\sin\beta) + i\omega t} \right\} \tag{A.2}$$

Regular wave theory is based on potential flow theory, which is only valid when there is no separation in the flow. In the concern of the hydrodynamic loads that associated with excitation from incident wave and radiation of outgoing waves from platform motion depend on whether flow separation occurs, since different formulations for the hydrodynamic loads apply to separate and non-separate flows. The factors, Keulegan-Carpenter number, *KC*, the oscillatory Reynolds number, *Re*, defined in equation A.3, as well as the diameter to wavelength ratio, D/λ, which can be regarded as the scatter parameter, are important to determine the proper formulation for cylinders.

$$KC = \frac{VT}{D}; \qquad \mathrm{Re} = \frac{VD}{\nu} \tag{A.3}$$

where D is the cylinder diameter, ν is the kinematic viscosity of the fluid, $10^{-6}\ m^2/s$, and V is the amplitude of the fluid velocity normal to the cylinder. Based on the linear regular wave theory, the wave velocity amplitude is given in equation A.2, where the wave number k can be found through the implicit dispersion relationship.

$$V = \frac{\pi H}{T} \frac{\cosh\left[k\left(Z+h\right)\right]}{\sinh\left(kh\right)} \tag{A.4}$$

Flow separation occurs when the KC number exceeds 2. For the value less than 2, potential flow theory applies. The diffraction effects are important when the ratio of cylinder diameter to the wavelength exceeds 0.2 and are unimportant for smaller ratios. Thereby, when processing the parametric design of the mono-column model of this thesis, the above considerations should be taken into account to avoid large hydrodynamic loads from wave excitation, diffraction and radiation.

In view of the validity of potential-flow theory across many conditions, the linear potential-flow problem was solved using the indoor HydroGen computer program, which is similar to the commercial code WAMIT, solving the linearized potential-flow hydrodynamic problems for the wave-body interaction in frequency domain. The solution to the wave-induced and platform-induced problems is given in terms of wave-frequency and direction-dependent vectors, $A_{ij}(\omega)$, $B_{ij}(\omega)$, $X_i(\omega,\beta)$.

The statistical description of waves is to use linear theory to simulate irregular sea and to obtain statistical estimates. For instance, the wave elevation of an irregular sea propagating in the positive x-axis can be written as the sum of a great number of wave

components j, with specific wave amplitude A_j, circular frequencies ω_j and random phase angles ε_j, in equation A.5.

$$\eta = \sum_{j=1}^{N} A_j \sin\left(\omega_j t - k_j x + \varepsilon_j\right) \tag{A.5}$$

The frequency decomposition of the sea state can be presented by a wave spectrum, $S_\eta(\omega)$.The relationship between the wave amplitude A_j and the wave spectrum is given in equation A.6.

$$\frac{1}{2} A_j^2 = S_\eta\left(\omega_j\right)\Delta\omega \tag{A.6}$$

where, the $\Delta\omega$ is the bandwidth of the spectrum. The instantaneous wave elevation is Gaussian distributed with zero mean and variance $\sigma^2 = \sum_{j=1}^{N} A_j^2 / 2$, which is equal to $\int_0^\infty S_\eta(\omega)\, d\omega$ when $N \to \infty$ and $\Delta\omega \to 0$.

The shape of the wave spectrum needs to be fitted by a curve, the covariance fuction, and among them, the most commonly used spectral density representations are the Pierson-Moskowitz (P-M) and JONSWAP (Joint North Sea Wave Project) spectra, based on Gaussian and Rayleigh distributions, which are also included in HydroDyn in FAST. Refer to equation A.7 and A.8 for the one-side JONSWAP and P-M spectrum equation, and the typical figures for both spectra are given in FIGURE A.1.

$$S_\eta(\omega) = \frac{1}{2\pi}\frac{5}{16} H_s^2 T_p \left(\frac{\omega T_p}{2\pi}\right)^{-5} \exp\left[-\frac{5}{4}\left(\frac{\omega T_p}{2\pi}\right)^{-4}\right]\left(1 - 0.287\ln\gamma\right)\gamma^{\exp\left[-0.5\left[\frac{\frac{\omega T_p}{2\pi}-1}{\sigma(\omega)}\right]^{-2}\right]} \tag{A.7}$$

$$S_\eta(\omega) = \frac{1}{2\pi}\frac{5}{16}H_s^2 T_p \left(\frac{\omega T_p}{2\pi}\right)^{-5} \exp\left[-\frac{5}{4}\left(\frac{\omega T_p}{2\pi}\right)^{-4}\right] \quad \text{(A.8)}$$

where H_s is the significant wave height, which is equivalent to *4* times the standard deviation σ (σ^2 equals zero spectrum moment m_0). T_p is the peak period at which the wave spectrum $S_\eta(\omega)$ is the maximum, and γ is the peak shape parameter.

The P-M wave spectrum originated from Atlantic Ocean measurements is used for fully developed seas. JONSWAP spectrum is an extension of P-M spectrum, or in other words, the P-M spectrum is the specific case when the peak shape parameter of the JONSWAP spectrum equals unity. The JONSWAP wave spectrum is used to represent the unfully developed sea states under certain wind condition. Its shape is therefore characterized by a higher and narrower peak and controlled by the peak shape parameter γ as shown in the figure.

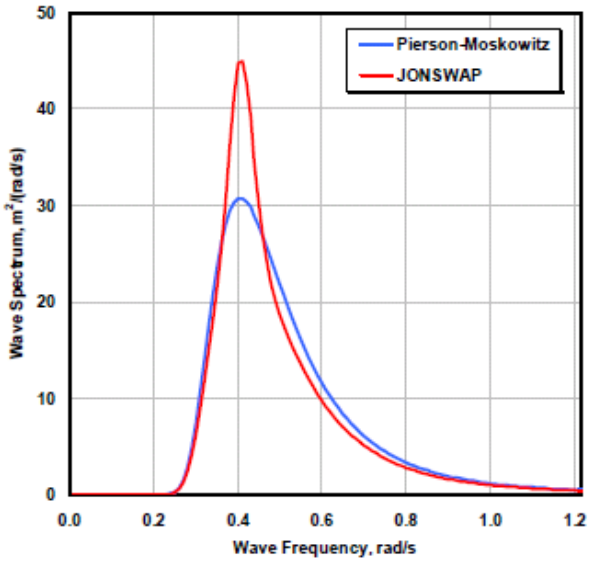

FIGURE A.1 Pierson-Moskowitz and JONSWAP spectrum.
(Hs = 11.8 m, Tp = 15.5 s, and γ = 1.75)

APPENDIX B

HYDRODYN LINEAR HYDRODYNAMIC MODEL

The equilibrium equation of the total external load acting on the support platform was given by equation A.9 from Jonkman (2007).

$$F_i^{platform} = -A_{ij}\ddot{q}_j + F_i^{lines} + F_i^{hydrostatic} + F_i^{waves} - \int_0^t K_{ij}(t-\tau)\dot{q}_j d\tau \qquad (A.9)$$

This $F_i^{platform}$ does not include the transmitted loads from turbine. The impulsive hydrodynamic-added-mass matrix A_{ij} in the first term has included the mass matrix M_{ij} from the complete nonlinear equations of motion in order to fully couple the dynamics of the system. The third term $F_i^{hydrostatic}$ is the i^{th} component of the hydrostatic restoring forces and moments, and the next two terms represent the hydrodynamic loading result from incident wave scattering and linear drag (radiation), respectively.

Term, F_i^{waves}, is the total incident wave excitation on the platform and is closely related to the wave elevation, η. The equation for wave elevation in irregular sea given in equation A.5 and A.6 above can be rewritten and extended at any location in the inertial reference coordinate (X,Y) on the SWL plane along the wave-propagation direction β as Jonkman (2007).

$$\eta(t,X,Y) = \frac{1}{2\pi}\int_{-\infty}^{\infty} W(\omega)\sqrt{2\pi S_\eta^{2-side}(\omega)}e^{-jk(\omega)[X\cos\beta + Y\sin\beta]}e^{-j\omega t}d\omega \qquad (A.10)$$

where $k(\omega)$ is the wave number for a finite water depth h, which can be found by the implicit dispersion relationship shown in equation A.6; $W(\omega)$ is the Fourier transform of a white Gaussian noise (WGN) time-series realization, which is used to ensure a random phase for each wave component and the Gaussian distribution also ensure the

instantaneous wave elevation has zero mean and unit variance. The total excitation load on the platform is then given in equation A.13.

$$F_i^{waves} = \eta(t)\, X_i(\omega, \beta) \tag{A.11}$$

where, $X_i\ (\omega, \beta)$ is a complex-valued wave-excitation force RAO associated with DOF *i*; the imaginary components allows for the situation that the excitation force is out of the wave elevation phase.

The last term $-\int_0^t K_{ij}(t-\tau)\dot{q}_j(\tau)d\tau$ written in convolution form, represents the load contribution from radiation damping and additional added mass that is not included in A_{ij} in the first term. The K_{ij} matrix, known as the wave-radiation-retardation kernel, is due to the memory effects of free surface (radiation retardation), meaning that the actual wave-radiation loads at time, *t*, depends on the impulse of the platform motions before. In general, the memory effect decays to zero after about 20-second lapsed time for instance as mentioned in Jonkman (2007). Therefore, in HydroDyn, the numerical convolution can be truncated by a user-specified amount of time. From Jonkman (2007), the equations below show the relationship between the radiation kernel and the added mass and damping solutions from frequency-domain calculation.

$$K_{ij}(t) = -\frac{2}{\pi}\int_0^\infty \omega\left[A_{ij}(\omega) - A_{ij}(\infty)\right]\sin(\omega t)\, d\omega \tag{A.12}$$

$$K_{ij}(t) = \frac{2}{\pi}\int_0^\infty B_{ij}(\omega)\cos(\omega t)\, d\omega \tag{A.13}$$

Since the mooring system in HydroDyn is assumed to be quasi-static, the inertia and damping of the mooring system can be ignored. Therefore, the total load given by

mooring lines on the support platform F_i^{lines} is given by equation A.14, where C_{ij}^{Lines} is the linearized restoring matrix and $F_{ij}^{Lines,\,0}$ represents the pretension at the fairleads.

$$F_i^{lines} = F_i^{lines,0} - C_{ij}^{lines} q_j \tag{A.14}$$

The quasi-static module developed in FAST can model an array of homogenous catenary mooring lines, but neglects the individual line bending stiffness. User can specify the fairlead and anchor points, the total unstretched length L, apparent weight density in fluid, ω, extensional stiffness, EA, and the seabed static-friction drag, C_B. The equation relates the apparent weight and the mass density, μ_c, is as follows:

$$\omega = \left(\mu_c - \rho \frac{\pi D_c^2}{4} \right) g \tag{A.15}$$

The module is based on the analytical formulation for an elastic cable problem, which suspends itself between two points and hangs under its own weight in fluid. The analytical formulations for the case with a single taut tether are given by equation A.16, A.17, to calculate the actual location of all parts of the tether. Here x_f and z_f are each fairlead position relative to the anchor; H_F and V_F are the horizontal and vertical components of the effective tension in the mooring line at the fairlead.

$$x_f\left(H_F, V_F\right) = \frac{H_F}{\omega} \ln\left[\frac{V_F}{H_F} + \sqrt{1 + \left(\frac{V_F}{H_F} \right)^2} \right] - \frac{H_F}{\omega} \ln\left[\frac{V_F - \omega L}{H_F} + \sqrt{1 + \left(\frac{V_F - \omega L}{H_F} \right)^2} \right] + \frac{H_F L}{EA} \tag{A.16}$$

$$z_f\left(H_F, V_F\right) = \frac{H_F}{\omega} \left\{ \sqrt{1 + \left(\frac{V_F}{H_F} \right)^2} - \sqrt{1 + \left(\frac{V_F - \omega L}{H_F} \right)^2} \right\} + \frac{H_F L}{EA} \left(V_F L - \frac{\omega L^2}{2} \right) \tag{A.17}$$

The detailed mooring system calculation procedures are summarized in FIGURE A.2 from Jonkman (2009). And the most remarkable feature of the quasi-static model is that the individual lines are in static equilibrium at each instant by neglecting the inertia effects. When facing large wind and waves, the inertia effect due to acceleration and deceleration of the line becomes significant that cause sudden change of the lines tension, which in reality probably would lead to buckling or breaking of the lines.

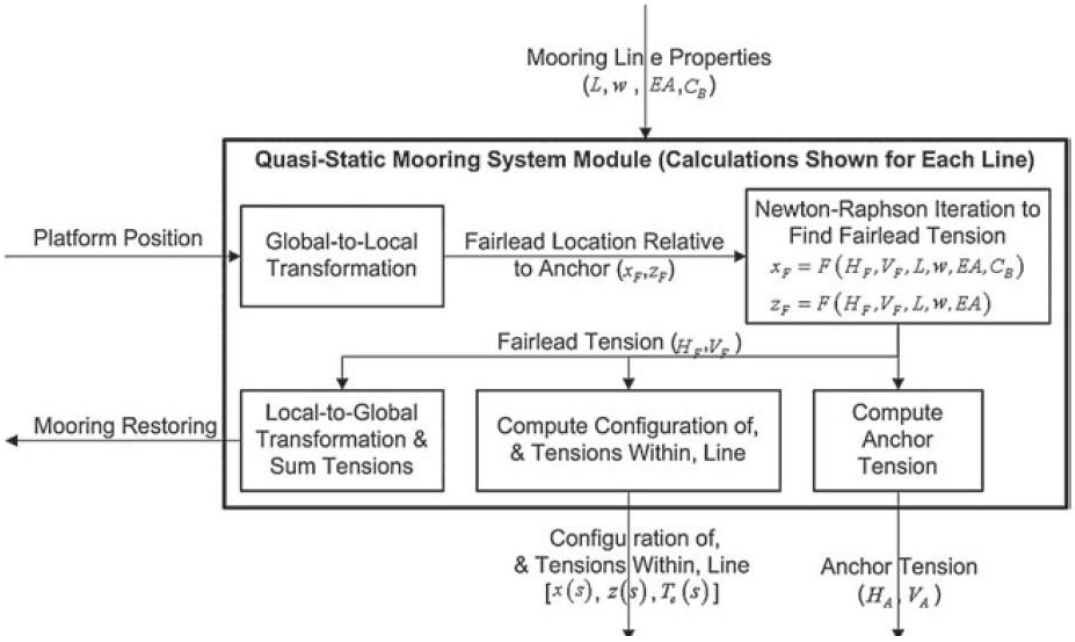

FIGURE A.2 Summary of the mooring system module calculation procedure.

The frequency-domain representation and Morison's representation are the two most common time-domain hydrodynamic formulations, both of which based on the same linearization assumptions as the true linear hydrodynamics model. Here, the governing equations of the two representations are shown in equation A.18 and A.19.

$$F_i^{platform}(t) = -A_{ij}\ddot{q}_j + \mathrm{Re}\left\{AX_i(\omega,\beta)e^{j\omega t}\right\} - \left(C_{ij}^{lines} + C_{ij}^{hydrostatic}\right)q_j - B_{ij}(\omega)\dot{q}_j \qquad \text{(A.18)}$$

$$\begin{aligned} dF_i^{platform}(t,z) = &-C_A\rho\left(\frac{\pi D^2}{4}dz\right)\ddot{q}_i(z) + (1+C_A)\rho\left(\frac{\pi D^2}{4}dz\right)a_i(t,0,0,z) \\ &+\frac{1}{2}C_D\rho(Ddz)\left[v_i(t,0,0,z)-\dot{q}_i(z)\right]\left|v_i(t,0,0,z)-\dot{q}_i(z)\right| \end{aligned} \qquad \text{(A.19)}$$

In the frequency-domain representation, when the supported platform's geometry is simple, G.I.Taylor's long-wavelength approximation ($\lambda \approx T^2 + T^2/2$ where T is the wave period) can be used to simply the diffraction problem for analytical solutions for $A_{ij}(\omega)$ and $B_{ij}(\omega)$, which Morison's equation also adopts. For bodies with complex geometrical surfaces, numerical-panel method techniques are required.

The Morison's equation, gives the horizontal excitation force on the cylinder strip at z depth with diameter D, which presents the linear wave excitation the nonlinear viscous drag in a straightforward manner by water-particle velocity v_i and acceleration a_i. The strip theory, which is similar to the BEM theory for wind turbine aerodynamics, makes it possible to calculate the overall three-dimensional loading based on the two-dimensional properties in equation A.21 horizontal motions (i =1, 2).

C_A and C_D in the equation are the normalized added-mass and viscous-drag coefficients, which are determined empirically depending on many factors like KC number, *Re*, and surface roughness. In the linear hydrodynamic problem, the nonlinear drag term in equation A.21 can be neglected, and C_A theoretically approaches unity. When viscous effects become important C_A differs from *1* and the drag term needs to be accounted in Morison's equation.

The heave force and yaw moment are both zero since the Morison's equation is for bottom-fixed axisymmetric cylinders. And the expressions for the left rotational motion, roll and pitch, are given equation A.20.

$$dF_i^{\,platform}(t,z)=\begin{cases}-dF_2^{\,platform}(t,z)\,z & for \quad i=4\\ dF_1^{\,platform}(t,z)\,z & for \quad i=5\end{cases} \tag{A.20}$$

APPENDIX C

PRIMARY FAST INPUT

```
------- FAST INPUT FILE -------------------------------------------------------
NREL 5.0 MW Baseline Wind Turbine for Use in Offshore Analysis.
Properties from Dutch Offshore Wind Energy Converter (DOWEC) 6MW Pre-Design (10046_009.pdf) and REpower 5M 5MW (5m_uk.pdf); Compatible with FAST v6.0.
---------------------- SIMULATION CONTROL --------------------------------------
False       Echo        - Echo input data to "echo.out" (flag)
   3        ADAMSPrep   - ADAMS preprocessor mode {1: Run FAST, 2: use FAST as a preprocessor to create an ADAMS model, 3: do both} (switch)
   1        AnalMode    - Analysis mode {1: Run a time-marching simulation, 2: create a periodic linearized model} (switch)
   3        NumBl       - Number of blades (-)
 3600.0     TMax        - Total run time (s)
   0.0125   DT          - Integration time step (s)
---------------------- TURBINE CONTROL -----------------------------------------
   0        YCMode      - Yaw control mode {0: none, 1: user-defined from routine UserYawCont, 2: user-defined from Simulink} (switch)
9999.9      TYCOn       - Time to enable active yaw control (s) [unused when YCMode=0]
   1        PCMode      - Pitch control mode {0: none, 1: user-defined from routine PitchCntrl, 2: user-defined from Simulink} (switch)
   0.0      TPCOn       - Time to enable active pitch control (s) [unused when PCMode=0]
   2        VSContrl    - Variable-speed control mode {0: none, 1: simple VS, 2: user-defined from routine UserVSCont, 3: user-defined from Simulink} (switch)
9999.9      VS_RtGnSp   - Rated generator speed for simple variable-speed generator control (HSS side) (rpm) [used only when VSContrl=1]
9999.9      VS_RtTq     - Rated generator torque/constant generator torque in Region 3 for simple variable-speed generator control (HSS side) (N-m) [used only when VSContrl=1]
9999.9      VS_Rgn2K    - Generator torque constant in Region 2 for simple variable-speed generator control (HSS side) (N-m/rpm^2) [used only when VSContrl=1]
9999.9      VS_SlPc     - Rated generator slip percentage in Region 2 1/2 for simple variable-speed generator control (%) [used only when VSContrl=1]
   2        GenModel    - Generator model {1: simple, 2: Thevenin, 3: user-defined from routine UserGen} (switch) [used only when VSContrl=0]
True        GenTiStr    - Method to start the generator {T: timed using TimGenOn, F: generator speed using SpdGenOn} (flag)
True        GenTiStp    - Method to stop the generator {T: timed using TimGenOf, F: when generator power = 0} (flag)
9999.9      SpdGenOn    - Generator speed to turn on the generator for a startup (HSS speed) (rpm) [used only when GenTiStr=False]
   0.0      TimGenOn    - Time to turn on the generator for a startup (s) [used only when GenTiStr=True]
9999.9      TimGenOf    - Time to turn off the generator (s) [used only when GenTiStp=True]
   1        HSSBrMode   - HSS brake model {1: simple, 2: user-defined from routine UserHSSBr} (switch)
9999.9      THSSBrDp    - Time to initiate deployment of the HSS brake (s)
9999.9      TiDynBrk    - Time to initiate deployment of the dynamic generator brake [CURRENTLY IGNORED] (s)
9999.9      TTpBrDp(1)  - Time to initiate deployment of tip brake 1 (s)
9999.9      TTpBrDp(2)  - Time to initiate deployment of tip brake 2 (s)
9999.9      TTpBrDp(3)  - Time to initiate deployment of tip brake 3 (s) [unused for 2 blades]
9999.9      TBDepISp(1) - Deployment-initiation speed for the tip brake on blade 1 (rpm)
9999.9      TBDepISp(2) - Deployment-initiation speed for the tip brake on blade 2 (rpm)
9999.9      TBDepISp(3) - Deployment-initiation speed for the tip brake on blade 3 (rpm) [unused for 2 blades]
9999.9      TYawManS    - Time to start override yaw maneuver and end standard yaw control (s)
9999.9      TYawManE    - Time at which override yaw maneuver reaches final yaw angle (s)
   0.0      NacYawF     - Final yaw angle for yaw maneuvers (degrees)
9999.9      TPitManS(1) - Time to start override pitch maneuver for blade 1 and end standard pitch control (s)
9999.9      TPitManS(2) - Time to start override pitch maneuver for blade 2 and end standard pitch control (s)
9999.9      TPitManS(3) - Time to start override pitch maneuver for blade 3 and end standard pitch control (s) [unused for 2 blades]
9999.9      TPitManE(1) - Time at which override pitch maneuver for blade 1 reaches final pitch (s)
9999.9      TPitManE(2) - Time at which override pitch maneuver for blade 2 reaches final pitch (s)
9999.9      TPitManE(3) - Time at which override pitch maneuver for blade 3 reaches final pitch (s) [unused for 2 blades]
   0.0      BlPitch(1)  - Blade 1 initial pitch (degrees)
   0.0      BlPitch(2)  - Blade 2 initial pitch (degrees)
   0.0      BlPitch(3)  - Blade 3 initial pitch (degrees) [unused for 2 blades]
   0.0      B1PitchF(1) - Blade 1 final pitch for pitch maneuvers (degrees)
   0.0      B1PitchF(2) - Blade 2 final pitch for pitch maneuvers (degrees)
   0.0      B1PitchF(3) - Blade 3 final pitch for pitch maneuvers (degrees) [unused for 2 blades]
---------------------- ENVIRONMENTAL CONDITIONS --------------------------------
   9.80665  Gravity     - Gravitational acceleration (m/s^2)
---------------------- FEATURE FLAGS -------------------------------------------
True        FlapDOF1    - First flapwise blade mode DOF (flag)
True        FlapDOF2    - Second flapwise blade mode DOF (flag)
True        EdgeDOF     - First edgewise blade mode DOF (flag)
False       TeetDOF     - Rotor-teeter DOF (flag) [unused for 3 blades]
True        DrTrDOF     - Drivetrain rotational-flexibility DOF (flag)
True        GenDOF      - Generator DOF (flag)
False        YawDOF      - Yaw DOF (flag)
True        TwFADOF1    - First fore-aft tower bending-mode DOF (flag)
```

```
True        TwFADOF2    - Second fore-aft tower bending-mode DOF (flag)
True        TwSSDOF1    - First side-to-side tower bending-mode DOF (flag)
True        TwSSDOF2    - Second side-to-side tower bending-mode DOF (flag)
True        CompAero    - Compute aerodynamic forces (flag)
False       CompNoise   - Compute aerodynamic noise (flag)
---------------------- INITIAL CONDITIONS -------------------------------------
   0.0      OoPDefl     - Initial out-of-plane blade-tip displacement (meters)
   0.0      IPDefl      - Initial in-plane blade-tip deflection (meters)
   0.0      TeetDefl    - Initial or fixed teeter angle (degrees) [unused for 3 blades]
   0.0      Azimuth     - Initial azimuth angle for blade 1 (degrees)
  12.1      RotSpeed    - Initial or fixed rotor speed (rpm)
   0.0      NacYaw      - Initial or fixed nacelle-yaw angle (degrees)
   0.0      TTDspFA     - Initial fore-aft tower-top displacement (meters)
   0.0      TTDspSS     - Initial side-to-side tower-top displacement (meters)
---------------------- TURBINE CONFIGURATION ----------------------------------
  63.0      TipRad      - The distance from the rotor apex to the blade tip (meters)
   1.5      HubRad      - The distance from the rotor apex to the blade root (meters)
   1        PSpnElN     - Number of the innermost blade element which is still part of the pitchable portion of the blade for partial-span pitch control
   0.0      UndSling    - Undersling length [distance from teeter pin to the rotor apex] (meters) [unused for 3 blades]
   0.0      HubCM       - Distance from rotor apex to hub mass [positive downwind] (meters)
  5.01910   OverHang    - Distance from yaw axis to rotor apex [3 blades] or teeter pin [2 blades] (meters)
  -1.9       NacCMxn     - Downwind distance from the tower-top to the nacelle CM (meters)
   0.0      NacCMyn     - Lateral  distance from the tower-top to the nacelle CM (meters)
   1.75     NacCMzn     - Vertical distance from the tower-top to the nacelle CM (meters)
  87.6      TowerHt     - Height of tower above ground level [onshore] or MSL [offshore] (meters)
  1.96256   Twr2Shft    - Vertical distance from the tower-top to the rotor shaft (meters)
   0.0      TwrRBHt     - Tower rigid base height (meters)
  5.0       ShftTilt    - Rotor shaft tilt angle (degrees)
   0.0       Delta3      - Delta-3 angle for teetering rotors (degrees) [unused for 3 blades]
  2.5       PreCone(1)  - Blade 1 cone angle (degrees)
  2.5       PreCone(2)  - Blade 2 cone angle (degrees)
  2.5       PreCone(3)  - Blade 3 cone angle (degrees) [unused for 2 blades]
   0.0      AzimB1Up    - Azimuth value to use for I/O when blade 1 points up (degrees)
---------------------- MASS AND INERTIA ---------------------------------------
   0.0      YawBrMass   - Yaw bearing mass (kg)
 240.00E3   NacMass     - Nacelle mass (kg)
  56.78E3   HubMass     - Hub mass (kg)
   0.0      TipMass(1)  - Tip-brake mass, blade 1 (kg)
   0.0      TipMass(2)  - Tip-brake mass, blade 2 (kg)
   0.0      TipMass(3)  - Tip-brake mass, blade 3 (kg) [unused for 2 blades]
2607.89E3   NacYIner    - Nacelle inertia about yaw axis (kg m^2)
 534.116    GenIner     - Generator inertia about HSS (kg m^2)
 115.926E3  HubIner     - Hub inertia about rotor axis [3 blades] or teeter axis [2 blades] (kg m^2)
---------------------- DRIVETRAIN ---------------------------------------------
 100.0      GBoxEff     - Gearbox efficiency (%)
  94.4      GenEff      - Generator efficiency [ignored by the Thevenin and user-defined generator models] (%)
  97.0      GBRatio     - Gearbox ratio (-)
False       GBRevers    - Gearbox reversal {T: if rotor and generator rotate in opposite directions} (flag)
  28.1162E3 HSSBrTqF    - Fully deployed HSS-brake torque (N-m)
   0.6      HSSBrDT     - Time for HSS-brake to reach full deployment once initiated (sec) [used only when HSSBrMode=1]
            DynBrkFi    - File containing a mech-gen-torque vs HSS-speed curve for a dynamic brake [CURRENTLY IGNORED] (quoted string)
 867.637E6  DTTorSpr    - Drivetrain torsional spring (N-m/rad)
   6.215E6  DTTorDmp    - Drivetrain torsional damper (N-m/(rad/s))
---------------------- SIMPLE INDUCTION GENERATOR -----------------------------
9999.9      SIG_SlPc    - Rated generator slip percentage (%) [used only when VSContrl=0 and GenModel=1]
9999.9      SIG_SySp    - Synchronous (zero-torque) generator speed (rpm) [used only when VSContrl=0 and GenModel=1]
9999.9      SIG_RtTq    - Rated torque (N-m) [used only when VSContrl=0 and GenModel=1]
9999.9      SIG_PORt    - Pull-out ratio (Tpullout/Trated) (-) [used only when VSContrl=0 and GenModel=1]
---------------------- THEVENIN-EQUIVALENT INDUCTION GENERATOR ----------------
9999.9      TEC_Freq    - Line frequency [50 or 60] (Hz) [used only when VSContrl=0 and GenModel=2]
9998        TEC_NPol    - Number of poles [even integer > 0] (-) [used only when VSContrl=0 and GenModel=2]
```

```
9999.9      TEC_SRes    - Stator resistance (ohms) [used only when VSContrl=0 and GenModel=2]
9999.9      TEC_RRes    - Rotor resistance (ohms) [used only when VSContrl=0 and GenModel=2]
9999.9      TEC_VLL     - Line-to-line RMS voltage (volts) [used only when VSContrl=0 and GenModel=2]
9999.9      TEC_SLR     - Stator leakage reactance (ohms) [used only when VSContrl=0 and GenModel=2]
9999.9      TEC_RLR     - Rotor leakage reactance (ohms) [used only when VSContrl=0 and GenModel=2]
9999.9      TEC_MR      - Magnetizing reactance (ohms) [used only when VSContrl=0 and GenModel=2]
---------------------- PLATFORM -----------------------------------------------
   3        PtfmModel   - Platform model {0: none, 1: onshore, 2: fixed bottom offshore, 3: floating offshore} (switch)
"NRELOffshrBsline5MW_Platform_OC3Hywind.dat"     PtfmFile    - Name of file containing platform properties (quoted string) [unused when PtfmModel=0]
---------------------- TOWER --------------------------------------------------
  20        TwrNodes    - Number of tower nodes used for analysis (-)
"NRELOffshrBsline5MW_Tower_OC3Hywind.dat"        TwrFile     - Name of file containing tower properties (quoted string)
---------------------- NACELLE-YAW --------------------------------------------
9028.32E6   YawSpr      - Nacelle-yaw spring constant (N-m/rad)
 19.16E6    YawDamp     - Nacelle-yaw damping constant (N-m/(rad/s))
   0.0      YawNeut     - Neutral yaw position--yaw spring force is zero at this yaw (degrees)
---------------------- FURLING ------------------------------------------------
False       Furling     - Read in additional model properties for furling turbine (flag)
            FurlFile    - Name of file containing furling properties (quoted string) [unused when Furling=False]
---------------------- ROTOR-TEETER -------------------------------------------
   0        TeetMod     - Rotor-teeter spring/damper model {0: none, 1: standard, 2: user-defined from routine UserTeet} (switch) [unused for 3 blades]
   0.0      TeetDmpP    - Rotor-teeter damper position (degrees) [used only for 2 blades and when TeetMod=1]
   0.0      TeetDmp     - Rotor-teeter damping constant (N-m/(rad/s)) [used only for 2 blades and when TeetMod=1]
   0.0      TeetCDmp    - Rotor-teeter rate-independent Coulomb-damping moment (N-m) [used only for 2 blades and when TeetMod=1]
   0.0      TeetSStP    - Rotor-teeter soft-stop position (degrees) [used only for 2 blades and when TeetMod=1]
   0.0      TeetHStP    - Rotor-teeter hard-stop position (degrees) [used only for 2 blades and when TeetMod=1]
   0.0      TeetSSSp    - Rotor-teeter soft-stop linear-spring constant (N-m/rad) [used only for 2 blades and when TeetMod=1]
   0.0      TeetHSSp    - Rotor-teeter hard-stop linear-spring constant (N-m/rad) [used only for 2 blades and when TeetMod=1]
---------------------- TIP-BRAKE ----------------------------------------------
   0.0      TBDrConN    - Tip-brake drag constant during normal operation, Cd*Area (m^2)
   0.0      TBDrConD    - Tip-brake drag constant during fully-deployed operation, Cd*Area (m^2)
   0.0      TpBrDT      - Time for tip-brake to reach full deployment once released (sec)
---------------------- BLADE --------------------------------------------------
"NRELOffshrBsline5MW_Blade.dat"                  BldFile(1)  - Name of file containing properties for blade 1 (quoted string)
"NRELOffshrBsline5MW_Blade.dat"                  BldFile(2)  - Name of file containing properties for blade 2 (quoted string)
"NRELOffshrBsline5MW_Blade.dat"                  BldFile(3)  - Name of file containing properties for blade 3 (quoted string) [unused for 2 blades]
---------------------- AERODYN ------------------------------------------------
"NRELOffshrBsline5MW_AeroDyn.ipt"                ADFile      - Name of file containing AeroDyn input parameters (quoted string)
---------------------- NOISE --------------------------------------------------
            NoiseFile   - Name of file containing aerodynamic noise input parameters (quoted string) [used only when CompNoise=True]
---------------------- ADAMS --------------------------------------------------
"NRELOffshrBsline5MW_ADAMSSpecific.dat"          ADAMSFile   - Name of file containing ADAMS-specific input parameters (quoted string) [unused when ADAMSPrep=1]
---------------------- LINEARIZATION CONTROL ----------------------------------
"NRELOffshrBsline5MW_Linear.dat"                 LinFile     - Name of file containing FAST linearization parameters (quoted string) [unused when AnalMode=1]
---------------------- OUTPUT -------------------------------------------------
True        SumPrint    - Print summary data to "<RootName>.fsm" (flag)
True        TabDelim    - Generate a tab-delimited tabular output file. (flag)
"ES10.3E2"  OutFmt      - Format used for tabular output except time.  Resulting field should be 10 characters. (quoted string)  [not checked for validity!]
   0.0      TStart      - Time to begin tabular output (s)
   10       DecFact     - Decimation factor for tabular output {1: output every time step} (-)
   1.0      SttsTime    - Amount of time between screen status messages (sec)
 3.09528    NcIMUxn     - Downwind distance from the tower-top to the nacelle IMU (meters)
   0.0      NcIMUyn     - Lateral  distance from the tower-top to the nacelle IMU (meters)
  2.23336   NcIMUzn     - Vertical distance from the tower-top to the nacelle IMU (meters)
  -1.912     ShftGagL    - Distance from rotor apex [3 blades] or teeter pin [2 blades] to shaft strain gages [positive for upwind rotors] (meters)
   1        NTwGages    - Number of tower nodes that have strain gages for output [0 to 9] (-)
  10        TwrGagNd    - List of tower nodes that have strain gages [1 to TwrNodes] (-) [unused if NTwGages=0]
   1        NBlGages    - Number of blade nodes that have strain gages for output [0 to 9] (-)
   9        BldGagNd    - List of blade nodes that have strain gages [1 to BldNodes] (-) [unused if NBlGages=0]
            OutList     - The next line(s) contains a list of output parameters.  See OutList.txt for a listing of available output channels, (-)
```

```
 WindVx1   , WindVy1   , WindVz1                    - Longitudinal, lateral, and vertical wind speeds
"WaveElev"                                          - Wave elevation at the platform reference point
"NacYaw    , NacYawErr"                             - Nacelle yaw angle and nacelle yaw error estimate
"RotSpeed , GenSpeed"                               - Low-speed shaft and high-speed shaft speeds
"RotThrust"                                         - Rotor thrust and low-speed shaft 0- and 90-rotating shear forces at the main bearing
"GenPwr    , GenTq"                                 - Electrical generator power and torque
"BldPitch1, BldPitch2, BldPitch3"                   - Pitch angles for blades 1, 2, and 3
"PtfmSurge, PtfmSway , PtfmHeave"                   - Platform translational surge, sway, and heave displacements
"PtfmRoll , PtfmPitch, PtfmYaw"                     - Platform rotational roll, pitch and yaw displacements
"Fair1Ten , Fair1Ang , Anch1Ten , Anch1Ang"         - Line 1 fairlead and anchor effective tensions and vertical angles
"YawBrFxp  , YawBrFyp  , YawBrFzp"                  - Fore-aft shear, side-to-side shear, and vertical forces at the top of the tower (not rotating with nacelle yaw)
"YawBrMxp  , YawBrMyp  , YawBrMzp"                  - Side-to-side bending, fore-aft bending, and yaw moments at the top of the tower (not rotating with nacelle yaw)
"YawBrTDxp      YawBrTDyp       YawBrTDzp"          - Tower-top/yaw bearing deflection relative to the undeflected position)
"YawBrTAxp      YawBrTAyp       YawBrTAzp"          - Tower-top/yaw bearing fore-aft/side-to-side/axial acceleration
"YawBrRAxp      YawBrRAyp       YawBrRAzp"          - Tower-top/yaw bearing angular roll/pitch/torsion acceleration
"TipSpdRat, RotCp    , RotCt    , RotCq"            - Rotor tip speed ratio and power, thrust, and torque coefficients
"NcIMUTvxs, NcIMUTvys, NcIMUTvzs"                   - Nacelle IMU translational accelerations (absolute) in the nonrotating, shaft coordinate system
"NcIMUTAxs, NcIMUTAys, NcIMUTAzs"                   - Nacelle IMU translational accelerations (absolute) in the nonrotating, shaft coordinate system
"NcIMURvxs, NcIMURvys, NcIMURvzs"                   - Nacelle IMU translational accelerations (absolute) in the nonrotating, shaft coordinate system
"NcIMURAxs, NcIMURAys, NcIMURAzs"                   - Nacelle IMU translational accelerations (absolute) in the nonrotating, shaft coordinate system
"TTDspFA   , TTDspSS   , TTDspTwst"                 - Tower fore-aft and side-to-side displacements and top twist
END of FAST input file (the word "END" must appear in the first 3 columns of this last line).
---------------------------------------------------------------------------------
```

VITA

Name: Jieyan Chen

Address: Zachry Department of Civil Engineering

Texas A&M University, 3136 TAMU

College Station, Texas, 77843-3136, USA

Email Address: jychen.jane@gmail.com

Education: B.E., Naval Architecture & Ocean Engineering

Shanghai Jiao Tong University, 2010

M.S., Ocean Engineering

Texas A&M University, 2012